NUMERICAL SIMULATIONS OF HYDRODYNAMICS OF MULTIPLE WATER JETS IMPINGING OVER A HORIZONTAL MOVING PLATE

by

Sultan Ibrahim Alqash

B.Sc., Tiabah University, Saudi Arabia, 2010

A THESIS SUBMITTED IN PARTIAL FULFILLMENT OF

THE REQUIREMENTS FOR THE DEGREE OF

MASTER OF APPLIED SCIENCE

in

THE FACULTY OF GRADUATE AND POSTDOCTORAL STUDIES

(Mechanical Engineering)

THE UNIVERSITY OF BRITISH COLUMBIA

(Vancouver)

September 2015

Abstract

The use and control of water jet impingement in the run-out table (ROT) are crucial in the steel plate cooling phase. Because of the complexity of the involved heat transfer process, the industries still mostly rely on a trial-and-error method for controlling the ROT cooling process. Although there are some experimental and numerical studies of the jet impingement cooling on ROT, the process is not fully understood. The analysis of hydrodynamics of water jet impingement is a key to understanding the process better. This aspect has received little attention in literature and it is the objective of this research.

At first, Computational Fluid Dynamics (CFD) axisymmetric simulation of water jet was considered to explore wetting front propagation on stationary surface. In the case of a moving plate, there are different zones over the plate surface and appropriate three-dimensional geometry and model must be built in order to have a complete analysis and realistic outcomes. Nine cases (namely three distinct jet flow rates of 15, 22, and 30 L/min impinging on different plate speeds of 0.6, 1.0, and 1.5 m/s) were numerically investigated. Two main regions were carefully inspected; the propagations of water fronts in wetting zones and the interactions of wall jets in interaction zones.

The realizable k-ε turbulent model (RKE) was utilized with the aid of a non-equilibrium wall function treatment and it showed good performance. The numerical results were validated with the experimental data obtained by other members of the UBC ROT group and showed reasonable agreement in terms of wetting front spreading and wall jets interaction type. Higher plate speeds and/or lower jet flow rates require dense mesh near the target surface to avoid water flow intermittency and capture the wetting front propagation as well as the hydraulic jump configuration. A huge air backflow was depicted when the plate was at the highest speed. Due to the plate movement, the symmetric wetting zone was distorted and became noncircular. According to the flow rate amount and the plate speed, different water wall jet interaction type and a corresponding bulge of water ahead of interaction zone (Int-Z) were captured.

Preface

This thesis is an original, unpublished, independent work by the author, Sultan Ibrahim Alqash.

Table of Contents

List of Tables

List of Figures

List of Symbols

A	Area of nozzle (m^2)
B	Dimensionless gradient of radial velocity
d	Nozzle diameter (m)
d_{imp}	Impingement diameter(m)
d_h	Jet diameter at distance h (m)
h	Heat transfer coefficient (W/m^2K)
h	Distance from nozzle outlet (m)
H	Nozzle-to-plate distance (m)
$Fr = u / \sqrt{gS}$	Froude number (h is flow layer thickness)
f	Volume fraction of the fluid
g	Gravity acceleration (m/s^2)
k	Turbulent kinetic energy (m^2/s^2)
$Nu = hd/k$	Nusselt number
$Pr = \nu / \alpha$	Prandtl number
p	Pressure (N/m^2)
p_o	Ambient pressure (N/m^2)
p_{stgn}	Stagnation pressure (N/m^2)
Q	Jet flow rate (m^3/s or L/min)
r	Radial distance from impingement point (m)
R	Radial distance of wetting front (m)
$Re = Vd/\nu$	Jet Reynolds number
$Re_{imp} = V_{imp}d_{imp}/\nu$	Impingement Reynolds number
S	jet-to-set space (m)
t	Time (s)
V	Exit velocity or axial velocity (m/s)
V_c	adjusted velocity (m/s)
V_{imp}	Impingement velocity(m/s)
V_h	Jet velocity at distance h (m/s)
V_p	Plate velocity (m/s)

V_y	Velocity in Y direction (m/s)
u	Velocity in radial direction (m/s)
u'	Velocity fluctuation (m/s)
U_i	Velocity components (m/s)
$We = \rho V^2 d/\sigma$	Weber Number
X	x-coordinate
Y	y-coordinate
Z	z-coordinate
z	Distance above the surface in vertical direction(m)
ρ	Density (kg/m^3)
ν	Kinematic viscosity (m^2/s)
μ	Viscosity ($N\ s/m^2$)
μ_t	Eddy viscosity
$\alpha = k / \rho C_p$	Thermal diffusivity (m^2/s)
τ	Shear stress (N/m^2)
τ_t	Turbulent shear stress
σ	Surface tension (N/m)
κ	Karman's constant
θ	Inlet angle at different height
ϕ	Obliquity angle of jet
ε	Dissipation rate of turbulent kinetic energy (m^2/s^3)
ω	Specific dissipation rate (1/s)
δ_{ij}	Kronecker delta

List of Abbreviations

ROT	Run-out table
HJ	Hydraulic jump
CHJ	Circular Hydraulic jump
CFD	Computational Fluid Dynamics
CV	Control Volume
PDE	Partial Deferential Equation
N-S Equation	Navier-Stokes Equations
RANS Equation	Reynolds-Averaged Navier-Stokes Equations
Int-Z	Interaction Zone
SST	Shear-Stress Transport k-ω turbulent model
RKE	Realizable k-ε turbulent model
VOF	Volume of Fluid Method
1-D	One-dimensional
2-D	Two-dimensional
3-D	Three-dimensional

Acknowledgements

First and foremost, all thanks to God for his endless blessings and for this successful completion. I would like to express my deep gratitude to my supervisor, Professor Mohamed S. Gadala for his academic guidance and endless support. His significant revisions greatly contributed to prepare this thesis to its final stage.

I would also like to record my appreciation to Dr. Mohammad M. Seraj and Dr. Taher Halawa who have provided me with significant help during my studies. Thanks also to my friends at the FE-lab for sharing their knowledge and experiences.

Special gratefulness is given to my father, my mother, my wife, and my little daughter. They provided me with their persistent encouragement throughout my studies. This work was not possible without their unlimited patience, cooperation, motivation, and love.

Last but not least, I want to express my deepest appreciation to the Saudi government for granting a valuable scholarship in order to pursue my higher education.

Dedication

To My Respected Parents

To My Lovely Wife

To My Little Daughter

Chapter 1: Introduction

1.1 Background

Steel products are important and numerous, making steel the most used material in industry. Steel has been used in most applications in our lives ranging from small things like drinking cans to major ones such as automobiles, cranes, bridges, ships, high-rise buildings, etc. According to the World Steel Association, the total crude steel production for 2013 only was as high as of about 1.6 billion tons [1]. Also, with the rapid development of technology, many steelmaking industries work very hard to cope with this improvement and increase their production. However, this massive productivity needs much attention in controlling the quality of outcome, which is the main purpose and priority to satisfy the customers and fulfill their needs. For instance, a high inspection and controllability during the design process are implemented in order to produce robust steels (i.e., advanced high-strength steel, AHSS) which have a high level of mechanical properties (strength, toughness, and formability, etc.) and metallurgical properties (microstructure and hardness, etc.). In particular, the hot-rolling process, which is a well-known manufacturing method of steel strips, requires great management since it has a crucial influence on the properties of the final product.

During the hot-rolling process (see Figure 1.1), the already-casted steel slab or plate with thickness around 220 mm is reheated up 800-900^{o}C. Next, it passes through the roughing mill to roughly reduce the slap's thickness. Then, it goes to the cleansing stage to get rid of the impurities. After that, it passes under the finishing mills to reduce its thickness further up to about 2 mm (strip). Then, it goes through a Run-out Table (ROT) cooling stage to reduce the temperature of the strip. Finally, it is coiled up when the temperature reaches to 500-650^{o}C according to the final desired thickness [2].

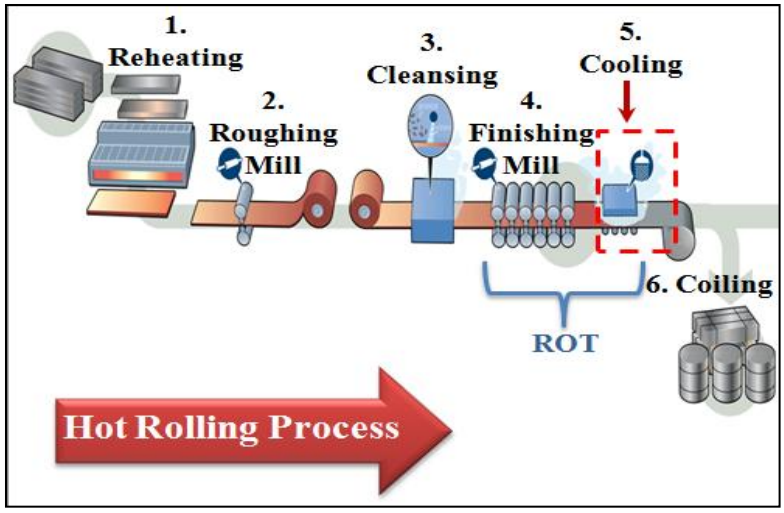

Figure 1.1 Hot Rolling Mill Process (Modified from [2])

The decreasing of hot steel slab temperature from 900^{o}C to 500^{o}C is achieved by a control accelerated cooling system at the ROT where the properties of the manufactured steel can be manipulated. Consequently, the amount of heat that will be removed or extracted from the steel strip surface during this step is dependent on some factors such as the supplied coolant temperature and cooling method.

Water impingement jets have been widely used as a coolant medium because of their capability in rapidly decreasing the high temperature of the steel strip. There are three cooling methods namely: laminar cooling, curtain cooling, and spray cooling (see Figure 1.2) [3]. All of them are located vertically on top of the steel strip at a certain height according to the industry's layout standard. Also, there is a cooling system underneath the strip which is mostly cooled by a water spray jet.

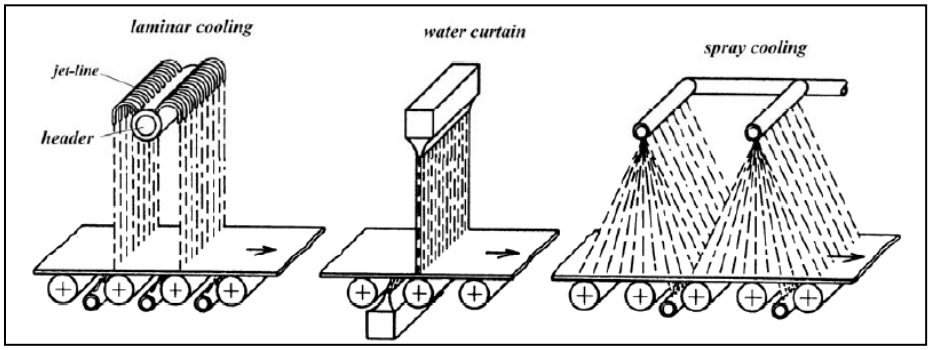

Figure 1.2 Run-out Table Cooling Systems [3]

Each one of those cooling systems has a different ability in achieving the task of extracting heat from the horizontal surface of the steel strip which passes beneath those systems. In Figure 1.2, the laminar cooling technique has the greatest ability of heat removal followed by water curtain and, lastly, the spray system. In the laminar cooling method, the water issued from in-line circular tube nozzles contacts the steel heated surface to create round areas which have highly local cooling rates, especially at the zones right beneath the incoming jets. This zone is known as the impingement zone that is characterized by a high local stagnant pressure due to the increase of contact time. As soon as the jet touches the hot surface of steel, it immediately turns into vapor which acts as a barrier and increases the turbulence. Also in this kind of cooling, the nozzles should be closed to each other as much as possible in order to perform an even heat transfer coverage along the strip width. During the water curtain process, the heat transfer is even because the water exiting the slot nozzle makes a line configuration when it contacts the hot surfaces. Therefore, this is intended to adjust the uniformity of the transported energy [4]. The last system of cooling is the spray cooling and it has the lowest heat removal rate although it covers a large area of the hot steel surface. The laminar cooling method has been employed extensively since it extracts considerable heat flux from the strip surface and, at times, followed by curtain cooling to adjust the heat transfer uniformity.

There are many operating parameters in ROT cooling in industrial scales involved in determining the cooling rate. The main operational parameters include strip speed, strip temperature, and water jets configuration parameters (e.g., jet-to-jet distance and jet-to-plate height, and water flow rate). Changes in these parameters may significantly change the cooling pattern and rate. To give an idea about the industrial scale parameters involved in the process, consider a case of: strip temperature is approximately 900^{o}C just after the finishing mill and the required temperature at the last stage (i.e., coiling process) is 500-600^{o}C. Therefore, when the maximum speed of the strip is about (9.4 m/s), then the strip passes the cooling zone of length around (92 m) in less than 10 seconds and this implies a huge heat removal rate [5].

1.2 Why Hydrodynamics?

A different boiling regime occurs in accordance with the temperature of the strip which influences the heat transfer process at the ROT cooling. Meanwhile, the flow field structure on the plate surface is always linked to the heat transfer. Therefore, adequate and reliable knowledge in both aspects is of high necessity to tackle the problem and accomplish the desirable final product with reasonable mechanical and metallurgical properties. However, this is not an easy task since it involves simulation of complex heat transfer and boiling phenomena as well as complicated CFD and interaction between jets. For example, due to the high temperature of the flat steel, as soon as the water impinges, the surface instantaneously turns the water into vapor which leads to a more complicated flow and multi-scale heat transfer phenomena.

Most of the studies in the literature concentrate only on one field, either the CFD or the heat transfer and boiling phenomena [6, 7]. The heat transfer aspect was extensively studied by experiments with laboratories, rather than industrial, conditions (e.g., scaled-down single jet impinged on stationary plate). Also, the objective in these studies was to examine and investigate the boiling regimes with different parameters such as water flow rate, jet-to-plate height, water and plate temperatures, etc. [6, 7]. As indicated above, many of these experiments were conducted on a small scale that did not reflect the real industrial problem. Therefore, the metal-making industries still rely on unrealistic correlations and the problem has not been completely understood. Also, most of the existing correlations rely on jet hydrodynamics on cold plates [8-10]. The number one priority practically is achieving a uniform and rapid heat transfer cooling rate in order to ensure the high quality of the final product. Accomplishing this objective requires an accurate control of the thermal characteristics in the entire manufacturing process [11]. On the other hand, studying the multiple water jets with respect to a moving plate is of high importance in industrial applications. Unfortunately, this is seldom considered and much of the work only considers single jet impingement over a stationary plate for two main reasons: the difficulties in handling of the real problem with the industrial conditions and the high complexity in investigating the flow structure phenomena when it is combined with a complex heat transfer problem. Also, the majority of the experiments on ROT were conducted to only investigate the heat transfer part without involving the effect of the hydrodynamics of the flow structure. However, the flow field should also be studied since it has a direct effect on the heat transfer

analysis. In particular, the impingement zone plays a very important role in determining the overall cooling rate where the localized high pressure has direct impact on the cooling water saturation temperature [12]. In addition, the radial velocity gradient of the flow at the impingement zone is considered as another factor that directly influences the local heat transfer coefficient and, in turn, alters the overall extracted heat fluxes [13]. Thus, a high heat transfer coefficient is obtained at the impingement region because it is characterized by a very thin boundary layer that maintains the surface at low temperature. Many theoretical and experimental studies [14-16] confirmed that at the impingement zone, the heat transfer was directly affected by the mean radial velocity gradient that depends on the flow structure. For example to these dependencies, the following equation for Nusselt number is widely used in jet impingement analysis [6, 12]:

$$Nu = \frac{hd}{k} = f(Pr, \dots) Re^{1/2} \sqrt{B} \tag{1.1}$$

where h and k are the heat transfer coefficient and thermal conductivity, respectively, Pr is the dimensionless Prandtl number ($Pr = \nu/\alpha$, where ν is kinematic viscosity and α is thermal diffusivity) and Re is the Reynolds number ($Re = Vd/\nu$). The last dimensionless number B is the radial velocity gradient.

As mentioned above, most of the experimental studies were conducted with a small scale, single nozzle impinging on stationary cold or hot (non-boiling regime) plates. For instance, during Stevens and Webb's experimental studies [17], the nozzle-to-plate distance was $z/d = 1$. In this experiment, the jet is too close to the target surface (short jet) which maintains the flow at laminar regime. However, in steel industries, long and turbulent jets are always used where the nozzles are located at a higher vertical distance (many times more than nozzle diameter) from the moving surface. This elevation enhances the falling water to develop turbulent flow characteristics. For that reason, the heat transfer relies on both Re and B (as indicated in Eqn. 1.1 above). In the next section, we shall discuss the variation of the B factor for different studies in accordance with the jet parameters. Relying on a single water jet does not provide the desirable cooling rate and resolve the heat transfer uniformity. However, in case of multiple water jets impingement, the entire strip's width is ensured to be mostly covered. In addition, the water wall jets interaction increases the mixing and enhances the removal of heat at this zone. There are many factors that affect the flow structure during multiple impinging jets such as: jet-to-jet

spacing and nozzle geometry [18, 19], jet-to-plate height and wall jets interaction [20]. Existing literature mostly consider single jet with non-industrial parameters. Single jet hydrodynamics on cold plates has been considered by many authors [8-10, 21] whereas the heat transfer of single jets has been also studied [6, 12, 22]. However, combined multi-phase heat transfer and Computational Fluid Dynamics (CFD) analysis of single jet is seldom considered and is currently being investigated in our group at UBC. Needless to say that multiple jets interaction has not been considered neither on cold or hot plates.

From the above discussion, one can realize the importance for studying the multiple jets impinging on a moving surface in order to extend the fundamental understanding of this industrial problem. Certainly, the outcomes of studying the CFD of the multiple jet interaction on cold plates will change for hot plates. Nevertheless, such study will enhance our fundamental understanding, provide higher level of accuracy for existing correlations that are based on single jet-cold plate, and pave the way for more detailed coupled and multiphase simulations. The intended research will consider industrial parameters and moving plate. At the University of British Columbia (UBC), many experiments were conducted at a special lab (pilot-industrial-scale ROT facility, see Appendix A) that are designed to reflect the industrial scale parameters [23-26]. Most of the results highly contributed to direct and better guide the industries to increase the accuracy and the controllability of the process and, eventually, best tailor the final products with great mechanical and metallurgical properties. Thus, in this research, the previous studies of ROT cooling, particularly the hydrodynamics of water jets impingement over a moving plate are numerically studied and simulated based on ROT UBC experimental conditions and then the results were compared and validated.

1.3 Literature Review

The cooling process becomes an essential stage whenever heat is absorbed by the device and causes problems. Industrially, jet impingement is distinguishably considered as a first option in dissipating a huge amount of excessive heat. Due to the capability of the jet impinging to extract heat, it has been widely utilized in many distinct industries such as glass making processes, paper producing, turbine blade manufacturing, electronic devices cooling [27, 28], etc. In metal making processes, the water jet impingement cooling method is recognized as a

distinguishable approach in removing the heat from the strip surfaces [6, 26]. Thus, many studies have been conducted focusing, in particular, on the heat transfer aspect by experiments of only one jet and a non-moving plate in simple laboratory conditions, but not representing the complex nature of the problem at hand [6, 22]. The jets impingement classifications depend on some parameters such as nozzle types and geometries (round or slot, orifice or tube), arrangements (in-line, staggered, etc.), working fluid (gas or liquid), and if the jet impinges over a dry surface (free-surface jet), discharges into the same fluid (submerged jet), or plunges over the accumulated pool of water (plunging jet) [29]. At the ROT cooling stage, the water first exits the circular nozzle and impinges over the dry heated plate surface (free-surface jet), followed next by arrays which collide with the left water over the surface (plunging jet). In fact, these two types are mostly treated as free-surface jets in comparison with the submerged jet.

This literature review is devoted to solely consider the hydrodynamics of circular jets impingement over the moving plate according to the experiments conducted at UBC ROT facility. The following hierarchy, as shown in Figure 1.3, explains the problematic progress in considering the hydrodynamics of water jet/jets impingement over a horizontal fixed/moving plate. As shown in Figure 1.3, a 3-D model is the only adequate method in the case of a moving surface in order to simulate the problem in a reasonable manner that reflects the real conditions. This is one of the reasons behind the complexity of this issue. Also note that a 3-D model is also required in the case of round, multiple jets when the impinging occurs on a stationary plate (as highlighted by superscript stars).

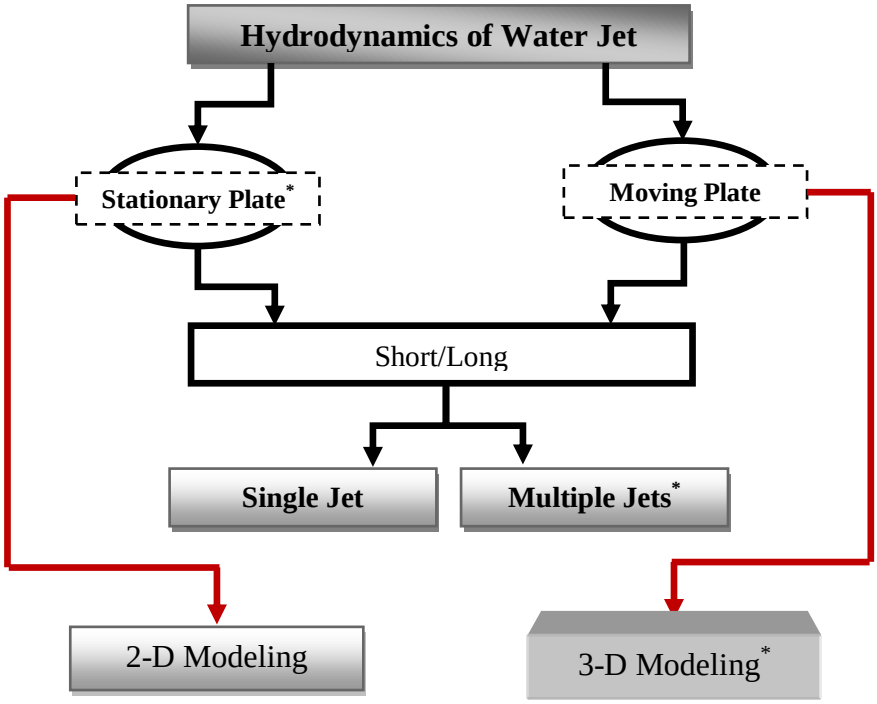

Figure 1.3 Hydrodynamics Field Point of View Possible Studies

1.3.1 Single Impinging Jet Flow Structures

When the water issues from a round nozzle that is located vertically above the target surface at a considerable height, the jet speed is increased and the jet size is contracted and this normally called a long water jet. The incoming falling water jet (*pre-impingement*) hits the target (*impingement*) and the water film forms and radially spreads over the plate and creates a circular shape in the case of the stationary plate and non-circular area in the case of a moving plate. In the case of the non-stationary plate, the problem is no longer a 2-D axisymmetric as in the stationary plate condition. Therefore, a 3-D model is required in order to properly capture what is happening when the water impinges on the horizontal surface.

As shown in Table 1.1 for the case of moving plate, the wetting front is no longer circular and due to the frictional motion between the water surface and the moving substrate, different zones will take place over the plate. The following schematics in Table 1.1 illustrate the differences between the stationery and moving plate conditions and how it will affect the circular hydraulic jump (CHJ) which, in turn, has a significant impact on the amount of heat that may be extracted from the hot plate surface [6, 22]. Basically, the HJ configuration is governed by jet parameters like *Reynolds number* (*Re=Vd/ν* where ν is kinematic viscosity), *Weber number*

(*We*= $\rho\frac{V^2 d}{\sigma}$ where σ is surface tension), and *Froude number* (*Fr*= $u/\sqrt{gS}$ where *S* is liquid depth). The first two dimensionless numbers determine the upstream conditions of flow (i.e., flow regime) and the third dimensionless number indicates the flow layer thickness downstream after the jump takes place. Interestingly, the plate movement creates the asymmetric characteristic and the upstream flow is no longer similar to the downstream flow; consequently, new zones are defined as non-wetting and wetting, respectively. At the stagnation point the axial velocity becomes stagnant and then the water film is deflected and the radial velocity, *u*(*r*), is initiated. The non-dimensional radial velocity gradient can be represented as follows [6]:

$$B = \frac{d(u/V)}{d(r/d)}\Big|_{r=0} \tag{1.2}$$

where *V* is the axial velocity, *u* indicates the radial velocity, *d* and *r* are the jet diameter and the radial displacement, respectively. The velocity in impingement zone can be defined linearly as [17]:

$$\frac{u}{V} = B\left(\frac{r}{d}\right) \qquad \text{for } r/d \leq 0.5 \tag{1.3}$$

From Bernoulli equation, the pressure at the stagnation zone is determined as follows:

$$P(r) = P_o + \frac{\rho}{2}\left(V_{imp}^2 - u(r)^2\right) \tag{1.4}$$

where P_o is the atmospheric pressure, V_{imp} is the impingement velocity, and *u*(*r*) is the inviscid free-stream velocity. Usually, by measuring the pressure distribution *P*(*r*) at the wall, the free-stream velocity can be determined. The pressure has the maximum value at the stagnation point (*r* = 0) and then decreases until reaches ambient pressure P_o as the flow spreads out radially (V_{imp} = *u*(*r*)).

Table 1.1 Single Jet impinging Flow Structure in the Case of Stationary and Moving Plate

Stationary Plate	Moving Plate
Top View: 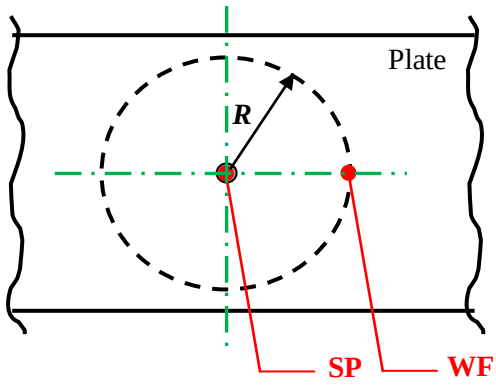	**Top View:** 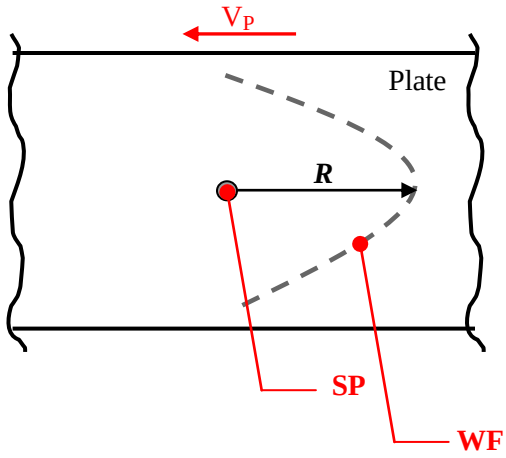
Side View: 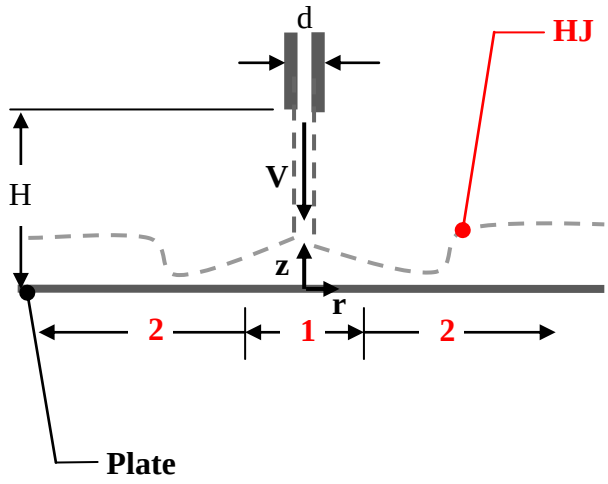	**Side View:** 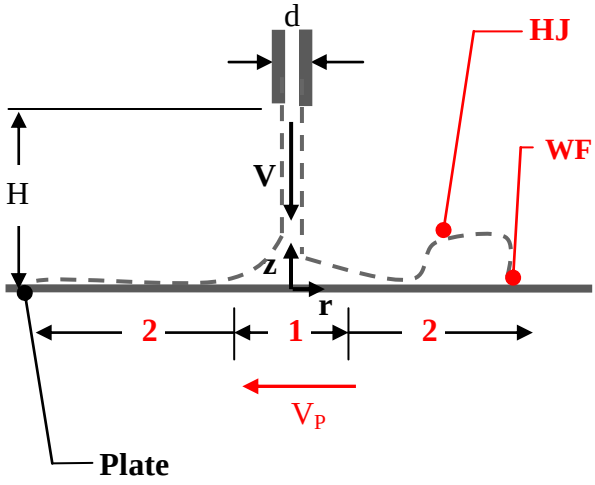

Note:

- The abbreviations SP and WF at the top and side (moving case) views indicate the stagnation point and the wetting front, respectively. However, *R* indicates the radial distance.
- Number 1 and 2 at the side views represent the impingement zone and parallel zone, respectively. Also, HJ indicates the hydraulic jump.

Steven and Webb [17] experimentally found that the velocity linearly varies at different heights above the plate and for fully-developed flows and a uniform velocity they obtained from equation (1.3) that $B \approx 1.83$. Notice that, depending on the nozzle type, different values for *B* will

be produced which, in turn, influences the amount of heat that needs to be removed [30]. However, the main factor that affects velocity variation value *B* is the profile of the velocity [22]. Liu *et al.* [12] considered the effects of the surface tension in their analytical study and found that the radial velocity becomes nearly equal to the impingement velocity when the surface tension is neglected, which makes the velocity varies almost linearly. In addition, they observed that both the pressure and the velocity at the impingement zone vary almost linearly. Similarly, Ochi *et al.* [31] conducted experiments with nozzle diameter d = 10 mm, nozzle height H = 25 mm, and the jet velocity was maintained as 3 m/s. They found similar results as the aforementioned studies [17, 30]. They then found the value of *B* was equal to about 1.56. All these studies were conducted for short jets. Determining the size of the impingement zone is very crucial since, at this region in particular, the most heat removal takes place in comparison with overall heat dissipation. Ochi *et al.* [31] estimated this region and found that it was equal to be around r/d = 1.28; whereas Stevens *et al.* [32] experimentally measured this region and found that it was equal to around r/d = 0.75. On the other hand, Liu *et al.* [14] assumed it to equal to r/d = 0.787 based on the thermal data in the case of laminar flow.

Watson [21] theoretically studied the radial propagation of a single round water jet over a horizontal stationary cold plate. He applied the momentum balance for the two regions downstream and upstream of the jump. He also assumed a uniform velocity and ignored the effect of pressure gradient and skin friction at the jump. He found that, the radius of the CHJ depended on the *Re* number and the layer thickness after the jump. After that, many researchers [8-10] were motivated to modify Watson's work and came up with some correlations. They found that, both jet flow rate *Q* and kinematic viscosity *v* are dominant in sizing the radius *R* of the CHJ. Craik *et al.* [33] noticed that during the formation of the hydraulic jump, the averaged flow velocity decreased and the flow turbulence increased. Then, the free-surface and boundary layer were mixed and then a separation and backflow with reverse velocity (negative value) resulted. Bush *et al.* [34, 35] investigated the stability of the CHJ and figured out that the surface tension plays an important role in shaping the jump but does not control the location. The CHJ structure and location were extensively investigated experimentally and numerically [36-38].

Fujimoto et al. [39] experimentally and numerically studied the flow structure of single round liquid jet over a moving surface that is covered by a film of water. By changing some

parameters such as jet velocity, nozzle-to-plate distance, and water film flow rate they observed three types of flow structures, namely, steady flow, transition, and unsteady flow, depending on the experimental conditions. They studied different type of jet that is called plunging jet. This kind of flow structure does not take place at the beginning of the cooling stage in industry, rather it appears after the moving plate passes the first array of jets where some water remains at the surface and the next array of jets impinges on wetted surface. In terms of industrial real problem, the UBC ROT group [40-43] conducted extensive experiments at a pilot-industrial-scale ROT facility of a single circular long free-surface water jet on stationary and moving plate. The experiments were conducted on unheated plates for the purpose of only examining the flow characteristics as a first step to decrease the level of complexity. In the case of the fixed plate [40, 41], for different flow rates (15, 30, and 45 L/min) they observed that the flow is totally turbulent due to the gravity effect and when the amount of the flow rate increases, the flow creates a bigger circular spot over the horizontal target. For that reason, increasing the flow rate is one way to achieve better heat dissipation since it covers more area of the plate. The water layer makes a circular hydraulic jump (CHJ) at the outer edge of the spot over the surface. As the amount of the flow rate increases, the jump becomes thicker in height and spreads further from the stagnation point. In the case of the moving plate [42, 43] with different speeds (0.3, 0.6, 1.0, 1.3, and 1.5 m/s) and different flow rates (10, 15, 30, and 45 L/min), the situation became much more difficult, where the circular hydraulic jump changed into non-circular shape with distinct zones at the upstream and downstream, non-wetted and wetted regions, respectively. This is why relying on one single jet to dissipate the heat is not sufficient, since the water does not entirely cover the whole plate width which, in turn, influences the uniformity of the heat transfer, which is not desirable. According to the observation of those experiments, they concluded that, for different plate-to-jet velocity ratios, distinct flow structure takes place. Also, when the plate speed increases, the wetting front becomes closer to the impingement zone. Out of these data, one can conclude that the single jet does not provide the complete heat removal, which makes the multiple jets approach necessary.

In order to investigate the effect of plate motion on the spreading of the impingement water and distortion of the CHJ, Kate *et al.* [44] experimentally investigated this problem on a stationary plate impinged on with a round water jet inclined with an angle ϕ from vertical

direction (i.e., oblique). This obliquity feature causes distortion of the CHJ and turns it to noncircular shape (elliptical geometry) as the case in moving plate (Table 1.1). The stagnation point becomes no longer at the center of the geometry as of stationary plate and it is shifted a bit towards the upstream side. Also, in another study, Kate *et al.* [45] examined the effect of the obliquity of a single circular water jet impinging on a moving surface. They noticed that the flow behaved similar to the non-moving case except the difference in the minor and major axes of the created elliptical spot with shifted position of the stagnation point further upstream as shown in Figure 1.4 below. The upper schematic represents the side view and the lower one shows the top view. As the plate speed increases, the major axis extends and the minor axes compresses and the HJ becomes thicker upstream and thinner downstream.

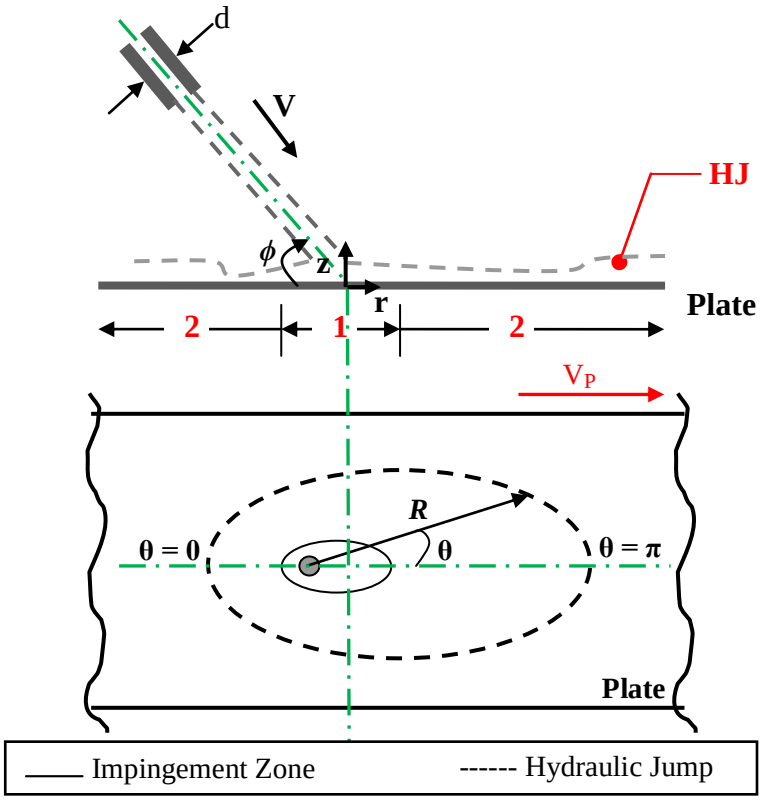

Figure 1.4 Noncircular Hydraulic Jump due to an Oblique Circular Water Jet Impingement (for Stationary Plate $V_p = 0$ and for Moving Plate $V_p \neq 0$)

1.3.2 Multiple Impinging Jet Flow Characteristics

This kind of jets arrangement (i.e. arrays) is the typical method in industries such as the steel-making industries. The multiple jets impingement method is required to dissipate a large amount of heat within less than 10 seconds. Keeping in mind that the steel strip speed is very fast which implies that the cooling rate must be extremely high. As mentioned above in the case of a single jet, the maximum heat dissipation occurs in the impingement zone which is characterized with the highest pressure value (stagnation pressure). Also, within this zone the pressure varies rapidly which, in turn, has a direct effect on the amount of heat removal. Moreover, it was also experimentally observed that the radial velocity has a rapid linear gradient which reduces the temperature much faster. The flow development and associated heat transfer in the case of the round jet impinging on a moving surface is more complicated and rather different from impinging on a non-moving surface where axisymmetric flow expansion happens. However, it is still true that the highest heat transfer takes place in the stagnation zone ($r = 0$) in comparison to overall dissipated heat even though the plate moves. Due to this motion, the upstream zone flow structure has completely distinct characteristics than the downstream zone. Consequently, a non-uniform heat transfer is developed which leads to difficulty in controlling this stage since there is no other way to keep the strip from becoming stationary, which will delay the productivity.

To overcome this problem, the method of multiple jets impingement is implemented. In the case of the multiple water jets, each jet creates its own stagnation point directly beneath the jet column which, in turn, considerably increases the heat dissipation efficiency. In addition, it was discovered that the second highest heat transfer occurs when the flow regime transfers to a turbulent which enhances the convection heat transfer [14]. In the case of a single jet when the plate moves the flow structure at the upstream, the parallel zone strongly turns to turbulent regime due to the increase of the friction forces which promotes the disturbances and vortices that cause the water film to flow chaotically. Adding other jets in-line arrangements certainly increases the heat extraction from the strip surface, especially during the collision of the jets. Figure 1.5 illustrates the case of twin jets collision over a fixed plate where the highlighted region by the dotted-red circle indicates the interaction zone (Int-Z), where the two water wall jets meet each other.

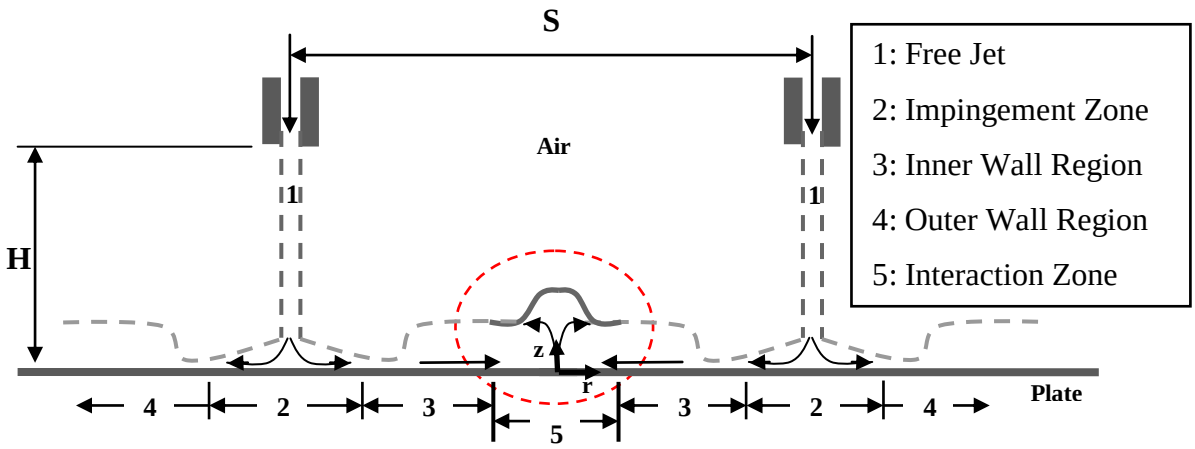

Figure 1.5 Schematic of Twin Jets Flow Structure over a Stationary Plate

According to the experimental studies of Ishigai *et al.* [46] and Kate *et al.* [44] on two round water jets with respect to a fixed plate, after the impingement as well as the collision take place, the fluid film creates four distinct regions above the horizontal surface as shown in Figure 1.5 above, namely: *Impingement Zone* (2), *Inner Wall Region* (3), *Outer Wall Region* (4), and *Interaction Zone (Int-Z)* (5). Also, zone (1) in Figure 1.5 represents the free-surface water jet which starts from the nozzle exit and extends up to just before the target surface. Although this kind of flow structure is unique for multiple jets impingement, it has some similarities with the single impinging jet such as all the regions were observed in the single jet case on a stationary substrate except zone (5) which represents the collision region between the two adjacent jets. When the water jets have the same amount of flow rate, they meet at the midway distance between them. Afterwards, the water film rises up and forms either a thick or thin fountain.

The formation and the exact position of the interaction depend on many factors like jet-to-jet distance (S), jet-to-plate height (H), and jet velocity (or flow rate, Q). Any small changes to one of these parameters significantly alter the behavior of the water film flow structure which, in turn, locates and forms a different kind of interaction [47]. During the collision, the twin wall jets become stagnant and then they jump upward (against the gravity) to balance the energies (i.e. transformation between kinetic to potential energies). At that moment, they meet at a line known as the *stagnation line*. The shape of this line is highly dependent on the momentum ratio between the parent jets [48, 49]. If the two round jets have an equal amount of flow rates and the same vertical distance above the surface, they meet at the midway distance and rise up in a straight

shape of interaction pointing in the opposite direction of the incoming water from the jets, as shown in Figure 1.4 above. In contrast, if the twin jets have different parameters (e.g. the amount of flow rate *Q*), these differences result in a different type of interaction than the previous situation. Therefore, the fountain moves toward the water jet that has a lesser amount of flow rate [50]. In other words, the location and formation of the interaction depends on the momentum ratio between the twin jets. For instance, if the momentum ratio decreases, the curvature of the interaction film increases and inclines towards the weaker jet. In the case of 2-D twin jets, the exact place of the interaction zone can be defined based on the position of the total pressure of equal values for both inner wall flows due to the collision. Analytically, for circular twin jets that have equal momentum, the following relation is valid [49]:

$$\frac{r_2}{r_1} = \left(\frac{V_2}{V_1}\right).\left(\frac{d_2}{d_1}\right) \tag{1.5}$$

where *r* is the radial displacement from the impingement point towards the interaction zone, *V* is the jet velocity, and *d* is the jet diameter. The subscripts numbers 1 and 2 refer to the two nozzles.

Pan and Webb [51] experimentally investigated the influence of jet-to-jet distance (*s/d*) in the range of $2 \leq s/d \leq 8$ for two distinct free-surface jet array configurations (in-line and staggered) in the overall heat transfer from the heated fixed surface. They found that the jet-to-jet space and the array arrangement do not directly affect the stagnation heat transfer coefficient that occurs directly below the jet column, even though different structures of interaction flow form at the midway distance between the jets. Also, they observed that the second maximum heat transfer takes place at the interaction zone since the film becomes thicker and has a characteristic of turbulent flow regime which, in turn, influences the convection heat transfer. The location of the interaction between the two jets is highly dependent on the two main factors, namely: the flow rates (*Q*) and the jet-to-plate vertical distance (*H/d*). Similarly, Womac *et al.* [52] conducted experiments to examine the heat transfer for the two different circular jet arrays (e.g. 2 × 2 and 3 × 3) between the following range of the jet-to-plate distance ($5 \leq H/d \leq 10$). They found that the vertical distance between the jets to the target surface does not have much effect on the heat transfer as the space between jets does. In addition, Pan and Webb [51] discovered that when the distance between the jets to the plate (*H/d*) was increased from 2 to 5, the jet flow characteristics

strongly changed from submerged to a free-surface type of jet. Also, they noticed that the jet-to-jet space has a great influence on the flow structure over the plate which, in turn, affects the amount of extracted heat being removed. All these studies were done on a non-boiling heat transfer regime. Moreover, Slayzak *et al.* experimentally studied the effect of the two planar water jets [53] as well as circular water jets rows [54] on the amount of removal heat from the top heated surface. They also confirmed that second high heat transfer occurs at the interaction zone at the middle space between the jets which considerably influences the cooling rate besides the primary heat transfer that takes place at the impingement zone. In addition, they experimentally showed that the interaction zone bends toward the weaker jet when the twin jets do not have the same flow rates.

The flow structure type of the interaction zone is complicated in comparison with the other flows. More difficulties are encountered when the target surface is moving. Also, this flow is turbulent and 3-D due to the recirculation and vortices. Although the problem is quite complicated, it may be simplified and modeled as a symmetric flow (in terms of mean velocity and pressure) at the middle plane of the interaction zone if the twin jets have an equal amount of flow rates [49, 52]. Moreover, the fountain that is characterized by the elevated film due to the accumulation of both wall jets were also noticed as remarkably unsteady flow and highly sensitive to any changes in the input parameters [50]. From the above discussion, one can explore that, despite the importance of the multiple water jets impingement over a moving plate, little attention is paid to this issue in regard to the two involved aspects of heat transfer and the hydrodynamics characteristics. Among those little studies, Chen *et al.* [55] experimentally investigated the effect of both fixed and moving (maximum plate velocity is 0.5 m/s and the jet velocity 2.3 m/s), unheated and heated (between 88^{o}C and 240^{o}C), and plates on the impinging of a single circular water jet. In the case of the moving and unheated plate, they found that the size of the wetted zone at the upstream is highly dependent on the jet Reynolds number. They also discovered that the water film spreads over the surface due to the balance of the water properties such as viscosity, surface tension, the gravitational force, and the velocity. For more details about the studies over a moving plate, refer to the following literature [56, 57].

However, in the case of multiple jets with regard to a heated moving surface, the ROT UBC group conducted many experiments to examine the heat transfer and then evaluate the

cooling rate [26, 58-63]. The outcomes of these experiments of a circular array of twin jets arranged in-line can be summarized into the following sentences. Firstly, the jet-to-jet space plays a very important role in determining the amount of removal heat flux from the top surface of the plate. For instance, the second maximum heat transfer takes place at the collision area (i.e. Int-Z) which is located at the middle between the twin jets if they have equal flow rates. If this distance between the adjacent jets decreases, the amount of heat removal increases. Secondly, the heat transfer coefficient at the impingement zone is not affected whether the jet-to-jet spacing increases or decreases. In fact, in the case of moving plate, the highest heat transfer is not coincident with the stagnation point [59]. Thirdly, it was explored that the uniformity of the heat transfer can be achieved when the distance between the two jets becomes as small as possible. Finally, the jets arrangement does not affect the cooling efficiency as soon as the parameters (flow rate, jet-to-jet distance, and the plate speed) are maintained without any changes. However, the type of configuration directly impacts the overall extracted heat uniformity [60]. Therefore, the jet-to-jet spacing is considered as the main factor to evenly accomplish dissipated heat, so this parameter should be wisely implemented to cover as much as the plate's width possible.

In addition, Fujimoto *et al.* [64] experimentally and numerically studied the flow structures of twin circular water jets impinging on a moving thin film of the same fluid (water) that is pre-existed on top of cold plate. They systematically changed some parameters such as jet velocity (mean velocity, V_0 varied from 0.4 to 2.0 m/s), nozzle-to-plate distance (H was set to 20 or 40 mm), nozzle-to-nozzle spacing (d_n was set to 20, 30, or 40 mm), and the flow rate of the water film in order to investigate their influence on the flow behavior. They noticed that three flow modes, namely: stable, transient, and unstable took place whenever jet velocity decreased or film velocity increased. Eventually, at the unstable mode, the flow became completely unsteady. Notice that they considered the plunging jet type; however, in this thesis, a free-surface jet type was utilized which occurs at the beginning of the cooling stage at the ROT.

1.3.3 Numerical Simulations Studies

Nowadays, with CFD capabilities, it is possible to optimize and revise the design at an early stage with reasonable cost rather than building a prototype and performing experimental testing. In addition, by simulating the real-life problem, multiple variables can be easily investigated and optimized [65, 66]. As indicated above, existing jet impinging studies are

mostly for single jet with non-industrial parameters and there is a need for multiple jet studies and interaction. One part of the complexity of the problem is that the jet impinging flow over a fixed or moving plate is turbulent in nature. To study this problem numerically, one of the turbulent models with some adjustments by taking advantage of the wall treatment method [67, 68] is required. This, in general, requires massive CPU time and memory. Not all turbulent models are validated for application in such problem. The majority of the numerical studies were basically utilized to investigate only a single submerged jet impinging on a non-moving wall while the free-surface jet type received little attention. Among the existing studies on the subject, Fujimoto *et al.* [69, 70] and Tong [71] both numerically considered the water free-surface jet with respect to a stationary plate to evaluate both the flow characteristics and the heat transfer phenomena. The numerical outcomes such as velocity and pressure variations at the impingement as well as the parallel zone were validated based on the experimental data of the follow up publications by Stevens *et al.* [13] and Liu *et al.* [12, 72]. All these studies were conducted only for a non-boiling, heat transfer condition.

The level of the complexity increases when the liquid jet impinges on the moving plate due to the involvement of the shear (friction) between the fluid and solid contact surface and the problem received little attention in literature. One study by Sharif and Banerjee [73] considered the effect of plate motion on the jet propagation. Another study was published by Huang *et al.* [74] with different considerations of jet type and fluid. They numerically investigated the thermal aspect of the planer air jet impinging over a moving wall involving a cross-flow. They discovered that the plate motion with a certain high speed can dramatically alter the value of the *Nu* number. Aldabbagh and Mohamad [75] numerically studied the flow field and heat transfer of multiple square air jets impinging on a moving heated plate. They discovered that, in the case of small nozzle-to-plate distance, the plate-to-jet velocity ratio had no effect on the *Nu* number. However, Kumar and Prasad [76] investigated the multiple circular air jets impinging on fixed plate with effusion holes. They found that, when jet-to-plate, H/D equals 2, three peaks of the *Nu* number occurred in different flow locations, namely: stagnation zone, wall jets region, and up-wash zone. Chattopadhyay and Benim [77] studied only the turbulent heat transfer aspect of slot jets impinging on a moving surface utilizing the realizable k-ε model. They found that close to the impingement surface, the level of turbulent kinetic energy affects the amount of heat transfer.

The *k*-ε and *k*-ω models are the most utilized turbulent models due to their acceptable accuracy as well as their low computational cost in comparison with Large Eddy Simulation (LES), which has an intermediate cost, and the Direct Numerical Simulation (DNS), that is considered a very costly method. As studies show [78, 79], the standard version of the *k*-ε turbulent model was used to simulate the heat transfer of jet impingement. The numerical simulations revealed that this model poorly predicted the accurate heat removal, especially at the impingement zone. However, the results improved when the wall treatment function was implemented [67, 68]. The latter *k*-ω turbulent model with recently-developed version (Shear Stress Transport SST version) was utilized [80-82] and it was concluded that this model has great accuracy in predicting the flow structure near the wall but requires a very fine mesh. Therefore, the outcomes of any turbulent models are highly dependent on the mesh size and refinement [83].

From the above discussion, one realizes that *k*-ε and *k*-ω turbulent models are widely utilized in simulating the complicated industrial flow problem of jet impingement on stationary or moving plates. For instance, Gradeck *et al.* [84] used the *k*-ε model to simulate the jet impinging on a moving surface and then examine the effect of motion on the hydraulic jump configuration. The numerical results showed good agreement with their own experimental results. Another study was done by Cho *et al.* [85] who also utilized the *k*-ε model to investigate the heat transfer aspect of the jet impingement problem and then they compared the results of the different Low Reynolds Number *k*-ε model. Passandideh-Fard *et al.* [86] numerically investigated the development of a circular hydraulic jump (CHJ) due to circular liquid jet impinging vertically on a stationary horizontal surface. They utilized the volume of fluid (VOF) method to track the free-surface propagation. It showed a good performance in predicting the CHJ location and its structure. Stark and Fritsching [87] developed a numerical model to simulate both the flow aspect and the corresponding heat transfer phenomena for the unsteady cooling process of a flat surface with a single submerged water jet. They investigated the effect of the flow rate ($10{,}800 \leq Re_d \leq 32{,}400$) and nozzle-to-plate distance ($4 \leq H/d \leq 20$) on the cooling rate. All the boiling phases that occurred during the jet cooling process could be obtained using one single model. However, Aghahani *et al.* [88] only numerically investigated the heat transfer field of a turbulent slot jet impinging on a moving substrate with respect to high plate-to-

jet velocity ratios ($0 \leq R \leq 6$) and jet Reynolds number ($3{,}000 \leq Re \leq 60{,}000$). They utilized the four equations ($v^2 - f$) turbulence model since it accurately predicts both the Nusselt number and the secondary peak place and value. They observed that, for a fixed plate-to-jet velocity ratio and only the Reynolds number was increased, the average *Nu* number altered accordingly. However, the Nusselt number decreased as the plate-to-jet velocity ration increased for each Reynolds number. Only in the case of plate-to-jet velocity ratio greater than 2.5 the average *Nu* number improved.

Recently, the UBC ROT group [89, 90] numerically investigated the flow characteristics of a single and twin axisymmetric long water jets on stationary plate. For both one and two jets simulations, the *k*-ε (RKE version) and *k*-ω (SST version) turbulent models were utilized to capture the flow development over the plate. In the case of the single jet [89], they examined the HJ configuration and compared the results with their experimental data. It was revealed that the numerical results are in agreement with the experimental data. In case of twin jets, Seraj *et al.* [90] numerically observed the interaction formation after a collision on the stationary surface. In both cases, the simulation was lengthy due to the large number of cells (around 5 million). Also, they observed some water intermittency over the plate where the film thickness was of order 0.1 mm which means the mesh should be refined near the wall in accordance with the wall y^+ value in order to have better resolution. Finally, they concluded that the *k*-ω (SST version) turbulent model has close results to the *k*-ε (RKE version) but the number of cells increased dramatically near the wall so a wall treatment function is recommended in both models.

1.4 Research Objectives

From the above literature review, one can notice the high demand to numerically study the hydrodynamics of free-surface multiple water jets impinging on a moving surface since it has not yet been considered enough with an industrial scale such as jet flow rates, jet-to-jet space, jet-to-plate distance, strip speed, and nozzle type (e.g. round nozzle). With good assumptions and some simplifications, one can make the simulations feasible and perform reasonable computational modeling. Therefore, the scope of this study is to numerically investigate the hydrodynamics of circular free-surface twin water jets and validate the results with the experimental data of the UBC ROT group. Basically, this research is intended to bridge the gap

in previous studies, contribute in understanding of the turbulent flow structure of the long twin water jets based on industrial scale, provide more accurate results for existing correlations that are based on single jet impinging, document a reasonable approach to simulate this complicated case, and finally pave the road for more complicated multi-phase studies. In order to achieve these objectives the following steps are necessary:

1. Numerically investigate the single jet over fixed plate by a 2-D model and prepare the required data to be utilized in the 3-D simulations.
2. Investigate various assumptions and simplifications to model the twin jets on a moving plate with the amount of flow rates and plate speeds realized in industry.
3. Evaluate the effect of the plate motion on the wetting front propagation as well as the interaction zone for various industrial cases.
4. Compare the numerical results (velocity and pressure profiles, wetting front contours and some plotted data) with the experimental data of the UBC ROT group.

Chapter 2: Numerical Simulations

The hydrodynamics of circular long water jets was investigated numerically with the low cost turbulent model. First, the fundamental governing equations are discussed, then the numerical modeling and procedures are mentioned in details. A 2-D model is briefly presented and a systematic strategy of the 3-D model in the case of moving surface is discussed in detail.

2.1 Governing Equations

In the numerical study, a Computational Fluid Dynamics (CFD) approach is utilized to solve the fundamental conservation laws which govern the hydrodynamics of fluid flow, namely: Continuity (mass balance) and Momentum (force balance). These equations are either in differential or integral form with nonlinear and transient terms.

2.1.1 Continuity Equation

The continuity equation is the balance of the mass that flows in and out of the domain. For simplicity, we consider a 2-D axisymmetric problem to characterize the circular long jet in 2-D layout. Also, viscosity, surface tension and gravity will be included but turbulence is neglected. Therefore, the differential form of the continuity equation can be represented as follows (in Cylindrical Coordinate) [91]:

$$\frac{\partial \rho}{\partial t} + \frac{\partial}{\partial z}(\rho u_z) + \frac{\partial}{\partial r}(\rho u_r) + \frac{\rho u_r}{r} = S_m \qquad (2.1)$$

where z is the axial coordinate, r is the radial coordinate, u_z and u_r are axial and radial velocity components, and S_m is the outside source (mass added or user-defined sources).

Generally, in concise form for incompressible transient laminar flow with constant density and viscosity and no outside source [73, 92],

$$\frac{\partial u_i}{\partial x_i} = 0 \qquad (2.1.1)$$

where u_i indicates the components of the velocity vector $\boldsymbol{u}$ and x_i represents the coordinate directions.

2.1.2 Momentum Equations

The momentum equation is a vector equation representing a force balance according to Newton's second law. In CFD analysis, these equations are known as the Navier-Stokes (N-S) Equations. In 2-D case, the momentum equation is represented by two equations in the axial component (i.e. along the vertical z-axis, Eqn. 2.2) and in the radial component which flows in the horizontal r-axis, Eqn. 2.3 [91] as follows:

Axial momentum component:

$$\frac{\partial}{\partial t}(\rho u_z) + \frac{1}{r}\frac{\partial}{\partial z}(r\rho u_z u_z) + \frac{1}{r}\frac{\partial}{\partial r}(r\rho u_r u_z) = -\frac{\partial P}{\partial z} + \frac{1}{r}\frac{\partial}{\partial z}\left[r\mu\left(2\frac{\partial u_z}{\partial z} - \frac{2}{3}(\nabla.\boldsymbol{u})\right)\right] + \frac{1}{r}\frac{\partial}{\partial r}\left[r\mu\left(\frac{\partial u_z}{\partial r} + \frac{\partial u_r}{\partial z}\right)\right] + F_z \quad (2.2)$$

Radial momentum component:

$$\frac{\partial}{\partial t}(\rho u_r) + \frac{1}{r}\frac{\partial}{\partial z}(r\rho u_z u_r) + \frac{1}{r}\frac{\partial}{\partial r}(r\rho u_r u_r) = -\frac{\partial P}{\partial r} + \frac{1}{r}\frac{\partial}{\partial z}\left[r\mu\left(\frac{\partial u_r}{\partial z} + \frac{\partial u_z}{\partial r}\right)\right] + \frac{1}{r}\frac{\partial}{\partial r}\left[r\mu\left(2\frac{\partial u_r}{\partial r} - \frac{2}{3}(\nabla.\boldsymbol{u})\right)\right] - 2\mu\frac{u_r}{r^2} + \frac{2}{3}\frac{\mu}{r}(\nabla.\boldsymbol{U}) + \rho\frac{u_z^2}{r} + F_r \quad (2.3)$$

where $\nabla.\boldsymbol{u} = \frac{\partial u_z}{\partial z} + \frac{\partial u_r}{\partial r} + \frac{u_r}{r}$, F_z and F_r are the external body force components. In general, concise form for incompressible transient laminar flow with constant density and viscosity [92] may be given by:

$$\rho\frac{\partial u_i}{\partial t} + \rho u_j\frac{\partial u_i}{\partial x_j} = -\frac{\partial P}{\partial x_i} + \frac{\partial}{\partial x_j}\left[\mu\left(\frac{\partial u_i}{\partial x_j} + \frac{\partial u_j}{\partial x_i}\right)\right] + \rho g_i \quad (2.2.1)$$

where p is pressure, ρ is density, μ is viscosity, g is body force (e.g. gravity), and xi indicates the coordinate directions. The u_i indicates the components of the velocity vector $\boldsymbol{u}$.

2.2 Turbulent Flow Modeling

Most of the flows are turbulent in nature when their Reynolds numbers (*Re*) are very high. In this study, the free-surface water jet issued from a nozzle located at a considerable height above the impingement surface which yields to significantly increase in the flow *Re* number to above 50,000. As a result, the abovementioned N-S equations are not adequate to resolve this kind of flow that transfers from laminar to the turbulent regime. When the flow is turbulent, the two main variables, velocity and pressure are fluctuating. For instance, the velocity of turbulent flow will have two terms, one indicates the mean part and the latter represents the fluctuating part (i.e. $u_i = \overline{u_i} + \acute{u}_i$ where $\overline{u_i}$ is the mean part and $\acute{u}_i$ is the fluctuating part). Therefore, the N-S equations that govern the turbulence condition will be [92, 93]:

$$\frac{\partial \bar{u}_i}{\partial x_i} = 0 \tag{2.4}$$

$$\rho \frac{\partial \bar{u}_i}{\partial t} + \rho \bar{u}_j \frac{\partial \bar{u}_i}{\partial x_j} = -\frac{\partial \bar{P}}{\partial x_i} + \frac{\partial}{\partial x_j}\left[\mu\left(\frac{\partial \bar{u}_i}{\partial x_j} + \frac{\partial \bar{u}_j}{\partial x_i}\right) - \rho\overline{\acute{u}_\iota \acute{u}_J}\right] + \rho g_i \tag{2.5}$$

where ($\bar{}$) indicates the mean magnitude of the variables (velocity and pressure) and ($\acute{}$) is their fluctuating parts. The most important term is $\rho\overline{\acute{u}_\mathrm{i}\acute{u}_\mathrm{j}}$ which is often known as *turbulent shear stress* or simply *Reynolds stress*. In fact, this is the key parameter behind the complexity since it is unknown and turbulent modeling is required in order to resolve this issue. Actually, the Newton's law can be applied to the shear stress in turbulent flow which is now the combination of the *laminar shear stress*, τ_l and the *turbulent shear stress*, τ_t. Mathematically, it can be written as follows [92]:

$$\tau_{ij} = \tau_l + \tau_t = \mu\left(\frac{\partial \bar{u}_i}{\partial x_j} + \frac{\partial \bar{u}_j}{\partial x_i}\right) - \rho\overline{\acute{u}_\iota \acute{u}_J} \tag{2.6}$$

Therefore, by substituting the last equation (2.6) into equation (2.5), the new equation becomes:

$$\rho \frac{\partial \bar{u}_i}{\partial t} + \rho \bar{u}_i \frac{\partial \bar{u}_i}{\partial x_i} = -\frac{\partial \bar{P}}{\partial x_i} + \frac{\partial \tau_{ij}}{\partial x_j} + \rho g_i \tag{2.7}$$

In the case of the 2-D turbulent flow, the *turbulent shear stress*, τ_t is simply treated as molecular shear as in the case of Newtonian viscous flow which then can be defined as follows:

$$\tau_\mathrm{t} = -\rho\overline{\acute{u}\acute{v}} = \mu_t \frac{\partial \bar{\mathrm{u}}}{\partial \mathrm{y}} \tag{2.8}$$

where μ_t is often known as the eddy viscosity. Generally, the Reynolds stresses can be found by using the Boussinesq theory [93, 94] as follows:

$$-\rho\overline{\acute{u}_\mathrm{i}\acute{u}_\mathrm{j}} = \mu_t\left(\frac{\partial \bar{u}_i}{\partial x_j} + \frac{\partial \bar{u}_j}{\partial x_i}\right) - \frac{2}{3}\rho k \delta_{ij} \tag{2.9}$$

where *k* and δ_{ij} refer to *turbulent kinetic energy* $k = \frac{1}{2}\overline{(\acute{u}_\mathrm{i}\acute{u}_\mathrm{i})}$ and Kronecker delta, respectively.

The two equations (2.4 and 2.5) can be solved and they are often called Reynolds-Averaged Navier-Stokes (RANS) equations. It is important to note that this approach does not obtain the velocity fluctuating part as well as the turbulent parameters and it is considered as a low computational cost model. There are many turbulent models that have been developed to compensate for that lacking. They are mainly based on some correlations in terms of different turbulent parameters such as kinetic energy *k*, turbulent dissipation ε, turbulence length scale, etc. When only the turbulent kinetic energy *k* is added to the governing equations, the turbulent model is named as one equation model. In fact, the name of the model depends on the number of

additional turbulent parameter equations that are coupled with the original RANS equations. For example, the two equations *k*-ε model introduces two extra equations to resolve the turbulent flow. There are many other models but they are much more complicated and costly compared with the two equation models which belong to the RANS models. In addition, the RANS models are not only inexpensive but they also provide a reliable accuracy for industrial applications [73, 93].

2.2.1 Two Equation *k*-ε Turbulent Model

This two-equation model was first proposed by Launder and Spalding [95], where another extra equation for turbulent dissipation $\varepsilon = (\mu/\rho)\overline{\left(\partial \grave{u}_\iota/\partial x_j\right)^2}$ is introduced and coupled with the turbulent kinetic energy *k*. In this case, the two extra transport equations for the two turbulent quantities *k* and ε are represented in PDE's form and can be written as follows [73, 96]:

$$\rho\frac{\partial k}{\partial t} + \rho\overline{u_j}\frac{\partial k}{\partial x_j} = \frac{\partial}{\partial x_j}\left[\left(\mu + \frac{\mu_t}{\sigma_k}\right)\frac{\partial k}{\partial x_j}\right] + P_k - \rho\varepsilon \tag{2.10}$$

$$\rho\frac{\partial \varepsilon}{\partial t} + \rho\overline{u_j}\frac{\partial \varepsilon}{\partial x_j} = \frac{\partial}{\partial x_j}\left[\left(\mu + \frac{\mu_t}{\sigma_\varepsilon}\right)\frac{\partial \varepsilon}{\partial x_j}\right] + C_1 P_k\frac{\varepsilon}{k} - C_2\rho\frac{\varepsilon^2}{k} \tag{2.11}$$

where $P_k = -\rho\overline{\acute{u}_\imath\acute{u}_\jmath}\frac{\partial \overline{u_\imath}}{\partial x_\jmath}$ determines the production of turbulence kinetic energy. These two equations rely on the empirical constants such as σ_k = 1.0, σ_ε = 1.3, C_1 = 1.44 and C_2 = 1.92; however, they might not be applicable for other problems so they need to be defined accordingly [96]. As soon as these *k* and ε are obtained from aforementioned equations (2.10 and 2.11), then the turbulent eddy viscosity can be modeled as follows:

$$\mu_t = C_\mu\rho\frac{k^2}{\varepsilon} \tag{2.12}$$

where the constant C_μ = 0.09 is empirically found. After that, the averaged momentum equation (2.7) can be solved by substituting the result of the turbulent eddy viscosity as introduced in the equation (2.12). Thereafter, this model has been validated for many engineering problems that involve turbulent flow with a high Re number. Also, it shows a good result, especially for flows far from the wall [93].

2.2.2 Wall Function Treatment

The first original version of the *k*-ε turbulent model did not account for the molecular viscosity and was only valid up to above the wall. Thus, some improvements were needed to include the wall-bounded low Re numbers into consideration. Thereafter, various eddy viscosities and new transport equations for the turbulent parameters were derived. Therefore, the need for so-called *wall function treatment* [97] is of high requirement in order to compensate for the variables at the first cells above the wall and link them to the mean velocity as well as the turbulent parameters. Indeed, this kind of treatment remarkably reduces the computational time and cost because the region at the first cells above the wall will be modeled rather than rely on the grid alone which is not capable enough to resolve it.

2.2.2.1 The Law of the Wall

If the flow spreads over a solid surface, it would be significantly affected due to the presence of the wall which enhances the adhesive forces (i.e. friction with no-slip condition mean velocity). Thus, a new empirical relationship was developed to account for this behavior (i.e. *law of the wall*) [94]. According to the measurements in both cases of internal and external flows, the velocity of the fluid streamlines varies logarithmically with the vertical distance above the wall. Consequently, the turbulent flow region near the wall is divided even further into three sub-regions vertically above the wall. At the first region, the flow is almost laminar since the viscosity is the dominant factor. In contrast, the outer layer of this near-wall region is fully-turbulent and its mean velocity behaves as a logarithmic function. In between these layers there is an interim region, the so-called buffer layer or blending region, because both the effects of the molecular viscosity and turbulence merge and become equally balanced [93, 94].

By dimensional analysis approach, one can obtain the law of the wall that is written and highlighted by the red-dotted line in Figure 2.1, as follows [94]:

$$\frac{U}{u_\tau} = \frac{1}{\kappa} ln \frac{u_\tau y}{\nu} + C \qquad (2.13)$$

where $u^+ \equiv \frac{U}{u_\tau}$ is the dimensionless velocity, $y^+ \equiv \frac{u_\tau y}{\nu}$ is the vertical distance above wall and $u_\tau \equiv \sqrt{\frac{\tau_w}{\rho}}$ is the velocity scale which is often known as the *friction velocity*. Also, the other two

constants, κ and *C*, are Karman's constant and dimensionless integration constant, respectively. Both are based on correlations in regard to the surface roughness where $\kappa \approx 0.41$ for smooth or rough surfaces, whereas $C \approx 5.0$ for only smooth surfaces according to Kline *et al.* (for more references see [94]).

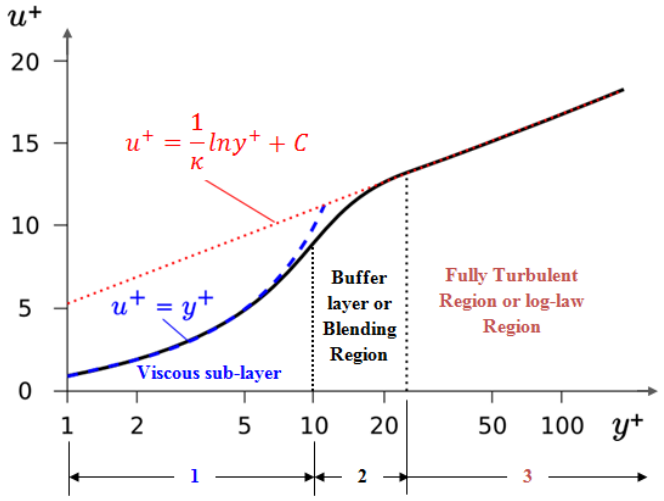

Figure 2.1 Velocity Profile for a Turbulent Boundary Layer (Modified from [98])

In fact, the appropriate wall y^+ value determines how efficient the mesh should be. For example, the value of $5 < y^+ < 10$ is recommended for examining the flow in the viscous sub-layer. However, the y^+ range might slightly change in accordance with the nature of the problem and available data. As a result, a very fine mesh above the wall is necessary to capture the flow of the very thin layer of the film and avoid spreading discontinuity. Of course, increasing the number of cells leads to an increase in the time of simulation as well as consumes too much CPU and memory resources. In this study, the non-equilibrium wall function was selected since it has a better description of the flow in comparison with the original method that is known as the standard wall function [93]. It was developed to consider the sensitivity of the mean velocity flow due to the rapid pressure gradient as exactly happens in the case of the round water jet impingement. Also, it was improved to include the effect of the production of the turbulent kinetic energy that occurs in the far cells above the wall.

2.2.3 Realizable k-ε Turbulent Model (RKE)

During the water jet impingement, both mean velocity and pressure gradients fluctuate rapidly, especially at the impingement region and, in turn, the Standard version of *k*-ε model (SKE) is not recommended [93, 99]. Thus, the realizable *k*-ε model (RKE) was selected among other *k*-ε models because it is customized to give good prediction for the liquid jet impingement, especially for circular and planer jets [97]. In addition, it shows good performance for the flows that are characterized by separation and vortices due to very strong adverse pressure gradients. Actually, the realizability of this model is satisfied by specific mathematical constraints on the Reynolds stresses. Physically, this alteration reflects the nature of the turbulent flows.

There were two main modifications to improve the performance of the model. Firstly, a new equation for the eddy viscosity was found which includes an extra constant, C_μ that relays on experimental observations conducted by Reynolds (i.e. for sub-layer flow $C_\mu \approx 0.09$). Secondly, a new transport formula was introduced for the second turbulent parameter (turbulent dissipation ε) based on the dynamic nature of the turbulent flows.

2.3 Volume of Fluid Method (VOF)

This method is used in multi-phase problems in order to trace the interface of two immiscible fluids like ocean water and the surrounding air [100]. In this particular problem, the air and water fluids cannot be immersed in each other as well. Therefore, VOF method was utilized here to construct the surface of the falling water jet before it hits the plate as well as to capture the free-surface of water film and wetting front propagation over the plate after impingement takes place. Basically, this method can be implemented by defining a volume fraction scalar parameter f for both phases in each single cell and then located them into the domain as follows:

$$\begin{cases} f = 0, & empty\ cell \\ 0 < f < 1, & \text{air and water } cell \\ f = 1, & water\ cell \end{cases}$$

Empty cell means air. In each control volume (CV) or cell, the total volume fraction of two fluids is unity. In other words, in terms of properties such as density ρ, and viscosity μ, the following equations are adjusted accordingly:

$$\rho = \rho_w f_w + \rho_a(1 - f_w) \quad (2.14)$$

$$\mu = \mu_w f_w + \mu_a(1 - f_w) \quad (2.15)$$

where the subscripts *w* and *a*, refer to water and air fluids, respectively. Now, the continuity equation needs to be adjusted accordingly as follows:

$$\frac{\partial}{\partial t}(f\rho) + \nabla.(f\rho\mathbf{u}) = 0 \quad (2.16)$$

Since the velocity vector **u** is shared between the two phases, one momentum equation must be defined for the entire domain as follows:

$$\frac{\partial}{\partial t}(\rho\mathbf{u}) + \nabla.(\rho\mathbf{u}\mathbf{u}) = -\nabla p + \nabla.[\mu(\nabla\mathbf{u} + \nabla\mathbf{u}^{\mathrm{T}})] + \rho\boldsymbol{g} \quad (2.17)$$

2.4 Problem Description

The main objective of this work was to study the twin jets impinging on a moving plate of three distinct speeds such as 0.6, 1.0, and 1.5 m/s in order to examine the effect of the plate motion on the spreading of water impingement and explore the jets interaction type after the collision. This problem needs appropriate assumptions to simplify the case and, at the same time, reflects the reality of the industrial nature and also a powerful computation for such a lengthy process. Modeling this flow field (hydrodynamics) problem is not an easy task for many reasons. The water jet issued from the nozzle located at 1500 mm above a horizontal plate. The jet flow is turbulent even at exiting the nozzle due to a very high Reynolds Number (e.g. of order 10^4) and Re number is increasing as it falls down because the jet is accelerated and contracted due to the gravity. After impingement, water flow develops over a moving surface. Therefore, starting right from the beginning with a complicated 3-D simulation is somehow not feasible according to the available facilities; but instead, a 2-D simulation of a single jet seemed to be a good start. The 2-D model can be considered for validation as well as providing necessary information. We know that the 2-D model is only valid for the case of the stationary plate since the round jet is characterized by a symmetrical flow structure before and after impingement. As soon as the impingement surface moves with a certain speed, the flow will have distinct hydrodynamics characteristics after impingement. For that reason, 3-D modeling is required in the case of moving plate involving the turbulent flow and the 2-D model was simulated and investigated first and then some data were extracted and used as inputs to 3-D simulations.

2.4.1 Numerical Simulations Methodology

Twin long water jets of 15, 22, and 30 L/min flow rates impinge on moving surface were modeled numerically based on the experimental scales of the UBC ROT group [101] by utilizing the feasible turbulent model (RKE *k*-ε model) available in the CFD package ANSYS FLUENT 14.5. The non-equilibrium wall function was utilized to enhance the modeling of the water layer near the wall. Also, the VOF method was utilized in all simulations in order to model the two-phase air/water as well as trace the wetting front propagation and jets interaction. All the models and meshes were performed using ANSYS Workbench 14.5.

2.4.1.1 Numerical Procedure for All Cases

The CFD simulations in this study are based on RANS equations (2.4 and 2.5) and were solved numerically using the finite volume method. All PDE's are replaced by a set of discrete algebraic equations (*discretization*) and the resulted governing equations integrated over all finite volumes. Then, a set of linear algebraic equations in terms of the main two variables velocity and pressure are obtained. The flow is transient so Pressure-Implicit with Splitting of Operators (PISO) scheme was utilized in order to solve for the velocity and pressure variables simultaneously (e.g. coupled). Also, the time was discretized implicitly using the first order scheme. However, a second order upwind method was selected for both momentum and turbulence equations. The VOF model was discretized using a geo-reconstruction approach. Finally, each algebraic equation was numerically solved by an iterative method in order to achieve a converged solution. Generally, the solution convergence criterion was achieved by setting the normalized residuals for continuity equation up to an order of (10^{-4}), for the momentum and the two turbulent equations up to order of (10^{-6}). For more details on setting up the solution procedures refer back to the FLUENT user's guide [93]. Also, the constant properties at atmospheric conditions are for the primary phase, air ρ = 1.225 kg/m^3 and μ = 1.7894e-05 kg/m.s and for the secondary phase, water ρ = 998.2 kg/m^3 and μ = 1.003e-03 kg/m.s and finally the surface tension between the two-phase is σ = 0.0728 N/m.

2.5 Numerical Simulation of 2-D Single Jet with respect to a Fixed Plate

2.5.1 Domain, Boundary Conditions and Meshes

2.5.1.1 Model Dimensions and Boundary Conditions

Modeling the long water jet takes a large amount of time and computer's memory so, rather than building the whole height (1500 mm), only 300 mm above the plate was considered, which is far enough from the wall. However, the velocity inlet adjustment has to be calculated for this new height. Figure 2.2 illustrates the flow domain and its boundary conditions in the case of the original height where the highlighted dotted red line represents the new consideration in order to reduce the amount of simulating time and computer memory consuming.

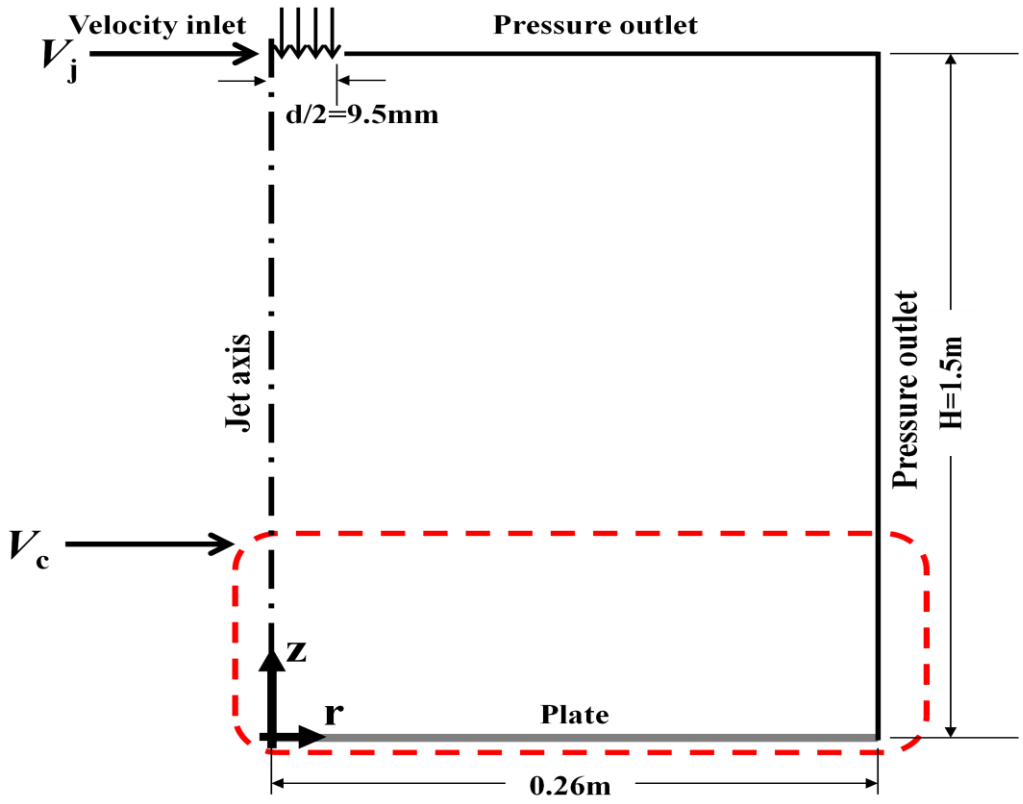

Figure 2.2 Single Long Jet Flow Domain and Boundary Conditions

Table 2.1 represents the jet parameters at the nozzle exit (H = 1.5 m) for three different flow rates (Q = 15, 22, and 30 L/min). Also, it shows the values of the velocity jet, diameter, and Reynolds number, Re = $\rho V d/\mu$, before and after impingement. The velocity jet and diameter after impingement are found based on equations 2.18 and 2.19, respectively.

Table 2.1 General Jet Parameters

		Before impingement			**After Impingement (H_{AI} = 1.5 m)**		
Q (L/min)	$Q \times 10^{-04}$ (m^3/s)	d_j (mm)	V_j (m/s)	Re_j	V_{imp} (m/s)	d_{imp} (mm)	Re_{imp}
15	2.5	19	0.882	16,667	5.496	7.61	41,666
22	3.7		1.293	24,477	5.577	9.15	50,832
30	5		1.763	33,379	5.704	10.56	60,032

The new inlet velocity, V_c including the gravity effect of the free fall body and the corresponding diameter, d_c need to be calculated using the mass and momentum conservations and written as:

$$V_c = \sqrt{V_j^2 + 2gH} \tag{2.18}$$

$$d_c = d_j \sqrt{\frac{V_j}{V_c}} \tag{2.19}$$

in which the original velocity inlet, V_j is known from the volume flow rate equation (Q = A V).

For example, in the case of the 15 L/min (2.5×10^{-04} m^3/s), V_j is equal to 0.88 m/s and the adjusted velocity V_c will become 4.93 m/s. Also, since the original jet diameter, d_j = 19 mm, and the adjusted diameter, d_c at the new height (H = 300 mm) becomes as 7.6 mm. Table 2.2 shows the jet parameters for new 2-D model. Both velocity jet and diameter before impingement are calculated using the above two equations. In order to get the values before impingement, the height, H_{BI} = 1500 – 300 = 1200 mm is used.

Table 2.2 Single Jet Parameters in the Case of the 2-D Model

		Before impingement (H_{BI} = 1.2 m)						**After Impingement (H_{AI} = 0.3 m)**		
Q, (L/min)	Q, $\times10^{-04}$ (m^3/s)	d_j (mm)	d_c (mm)	V_j (m/s)	V_c (m/s)	Re_j	Re_{jc}	V_{imp} (m/s)	d_{imp} (mm)	Re_{imp}
15	2.5	19	8.03	0.882	4.932	16,667	39,431	5.496	7.61	41,666
22	3.7		9.68	1.293	5.025	24,477	48,420	5.577	9.15	50,832
30	5		11.10	1.763	5.163	33,379	57,055	5.704	10.56	60,032

Figure 2.3 represents the adjusted flow domain and its corresponding boundary conditions. For the axisymmetric of the circular jet as shown in Figure 2.3a, only a quarter of the domain will be modeled because, when the water jet hits the stationary plate, it will spread radially and make a circular shape as shown below in Figure 2.3b (one of the UBC ROT group experimental data [101]).

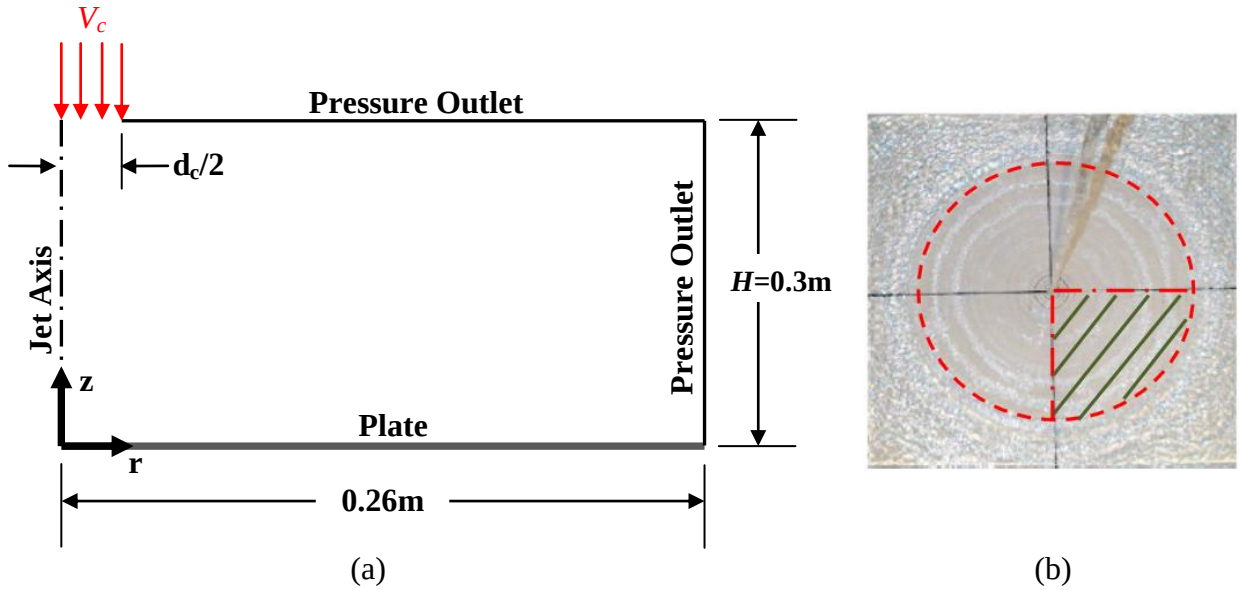

(a) (b)

Figure 2.3 (a) Adjusted Model Flow Domain and Boundary Conditions, (b) Circular Water Jet Impingement on a Fixed Plate (Modified from [101])

2.5.1.2 Generating Mesh Strategy

In Figure 2.4, only the mesh pattern without scaling is illustrated where a non-uniform structural grid of a rectangular shape was used: the mesh increases as it moves toward the target bottom surface. As a first attempt, the mesh was not adequate, especially at the two important regions: the jet downward stream space and the jet–plate interaction zone. It was noticed that the water layer flows over the plate after impingement is a very thin of order about 0.1 mm. Therefore, the mesh refinement was needed in those regions. To avoid the discontinuity of the flow propagation above the plate, an appropriate wall y^+ must be obtained to get a good mesh resolution. Overall, a 2-D model was simulated to examine the RKE turbulent model efficiency in a simple case (i.e. single jet impinging on a stationary surface). The numerical results, e.g.

axial and radial velocities at pre-impingement and after impingement, were found and compared with analytical results (above equations) and showed a good agreement with a very minor percentage of errors. Therefore, gained confidence in using the RKE turbulent model and had observed numerically the development of a very thin film of water over the surface. We will keep this part brief and will go to the next part for 3-D simulation as main goal of this study.

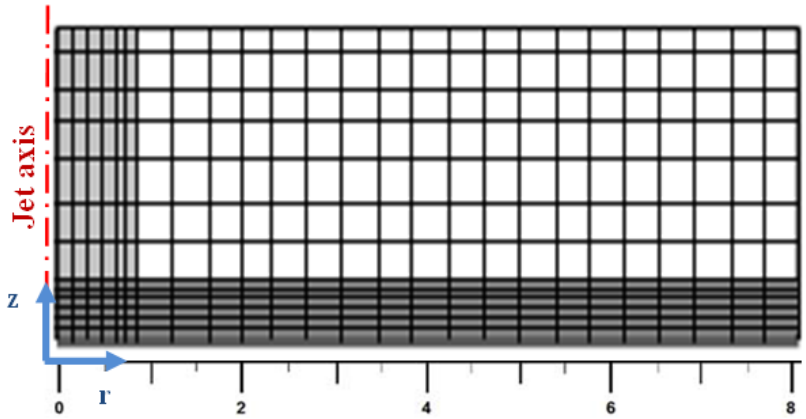

Figure 2.4 Non-uniform Structural Grid (Not to scale)

2.6 Numerical Simulation of 3-D Twin Jets with respect to a Moving Plate

2.6.1 Domain, Boundary Conditions and Meshes

The liquid flow domain for twin jets needs to be changed accordingly. The distance between the jets is S = 203.2 mm according to the UBC ROT experimental conditions [101]. When both jets with the same volume flow rate of 15L/min, for example, impinges and spreads over the moving plate, they create a non-circular wetting front and two different regions: upstream and downstream sides and dry and wetting areas. Meanwhile, the two wall jets hit and collide with each other and get raised up in *Interaction Zone* (Int-Z). Therefore, a new domain has to be built in order to capture these characteristics. Figure 2.5 shows the twin jets model with the extra zone added in the middle for the interaction zone. To use the notion of symmetry and reduce the amount of computation, half of each jet domain is considered as illustrated on the right side of Figure 2.5.

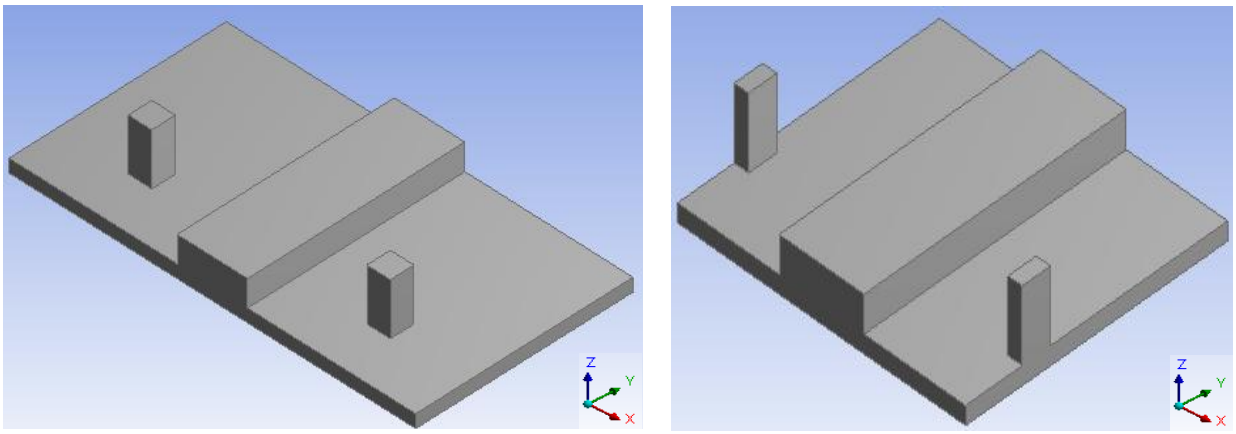

(a) Full Domain (b) Half Jets Domain

Figure 2.5 New Twin Jets Model with a Square Inlet Boundary

In addition, the twin jets issued from both nozzles were identical so only one jet can be modeled up to the middle of the interaction zone (see Figure 2.6).

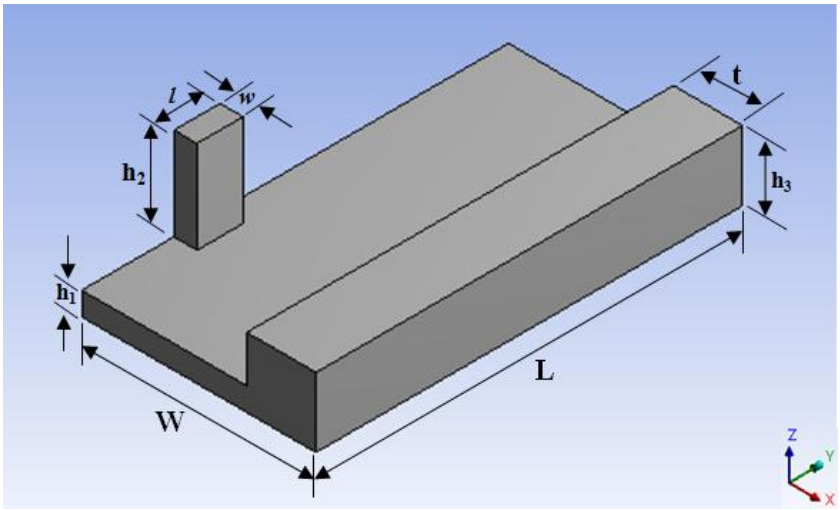

Figure 2.6 Half of Jet and Interaction Zone Model

In the case of a stationary plate (Figure 2.7a), the jet creates a circular spot whereas, in the case of moving plate (Figure 2.7b), the jet spreads over and makes a non-circular shape. Then, the axisymmetric condition is no longer applicable because of the different behavior of the water flow in the upstream and downstream and a three-dimensional model is necessary, not only because the asymmetric condition, but also due to the nature of the turbulent flow particularly in Int-Z. Actually, after the water jets collide, a central pool of water that occurs at

Int-Z depends on the amount of flow rate. In addition, a bulge of water ahead of Int-Z takes place in the case of the moving surface as shown in Figure 2.7b below. This kind of flow structure will be discussed later in more detail. In case of the stationary plate, the water covers all the top surface of the plate but as the plate moves, the top surface is divided into dry and wet regions at upstream and downstream zones, respectively. This affects the uniformity of heat transfer in case of hot plate. The maximum wetting front radii (Y/d) will be based on the amount of flow rate and the moving plate speed. Then, the next array can be placed accordingly and maximize the flow jets interaction (mixing).

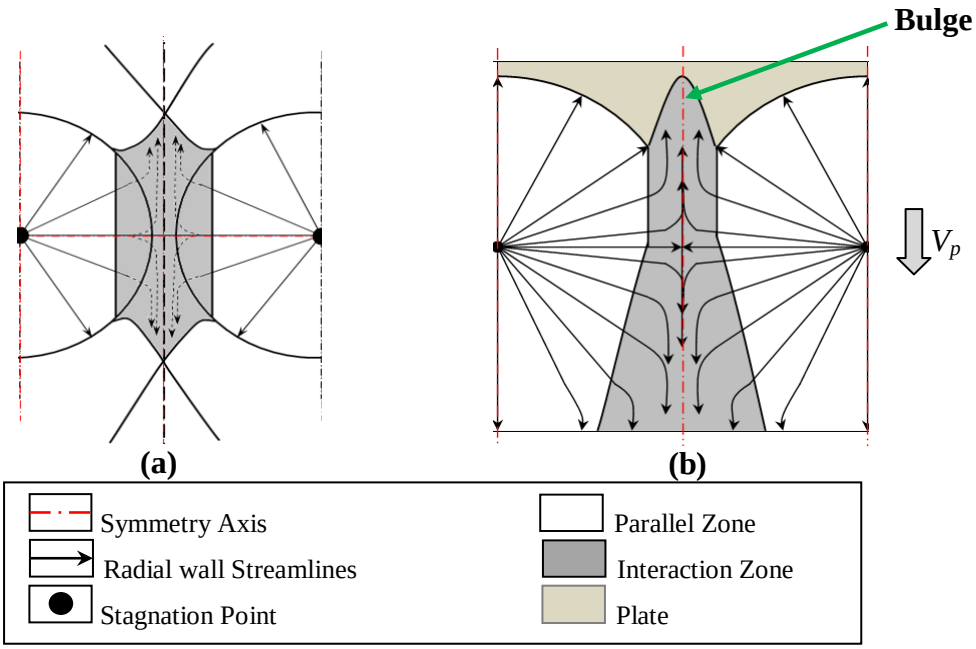

Figure 2.7 Schematic of Two water Jets Impingement, (a) Stationary Case (Modified from [101]) and (b) Moving Case

2.6.1.1 Twin Jets Domain Analysis of Different Flow Rates on a Moving Surface

At the UBC ROT experimental data [101], the flow of the twin jets with different moving plate speeds were captured and recorded by two Sony HD camcorders. The extracted images were utilized to size the domain of twin water jets in our simulations. For instance, Figure 2.8a, shows the image that was taken during the 15 L/min flow rate over the 1.5 m/s plate speed experiments. Each square cell of the mesh at the top of the plate has a 25.4 mm side. Figure 2.8b, illustrates the analysis of the computing domain, especially at the upstream side. The two red

spots indicate the impingement zone of the jets columns, the blue line represents the wetting front or the hydraulic jump which determines the size of the upstream wetting area, the dotted green circles are used to count up the number of square cells away from the impingement zone which is often known as the parallel zone, the vertical dashed-dotted red line defines the center line (somehow stagnation line) of the interaction zone that is defined by the rectangular doted yellow line, and finally the horizontal dotted black line defines the center line between the jets or between the upper and lower zones.

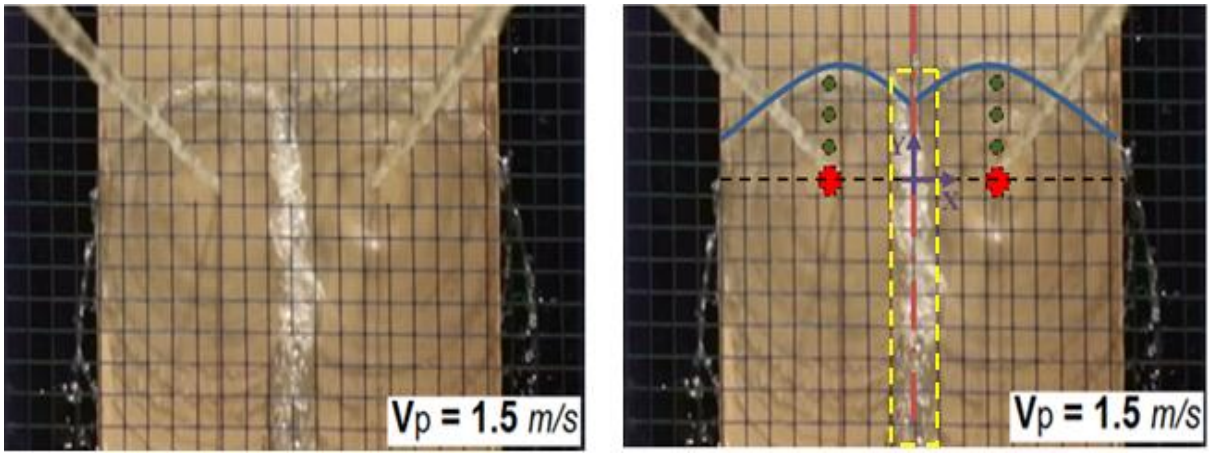

(a) (b)

Figure 2.8 Domain Analysis for Twin Jets of Q = 15 L/min with V_p = 1.5 m/s (Modified from [101])

As seen, the impingement zone is a half cell, the parallel zone is three cells or the upstream wetting zone is 3.5 cells, which equals about 88.9 mm. Also, the interaction zone is equal to approximately one square cell (25.4 mm) up to the mid-line that splits the whole domain into two identical parts. Similarly, the same analysis was performed on the other cases (different jets flow rates and plate speeds) and the results are shown in the following three tables (Tables 2.3, 2.4, and 2.5). The twin jets parameters in the case of 3-D model before impinging on a moving surface are the same as before (Tables 2.1 and 2.2). In some cases, there is a bulge of water ahead of the Int-Z after collision that depends on the plate-to-jet velocity ratio (V_p/V_j).

Table 2.3 Experimental Data Analysis for 15 L/min Flow Rate and Three Plate Speeds

	Experimental Data UBC ROT group (15 L/min) [101]	Upstream Dimensions (Each square cell = 25.4 mm)
V_p	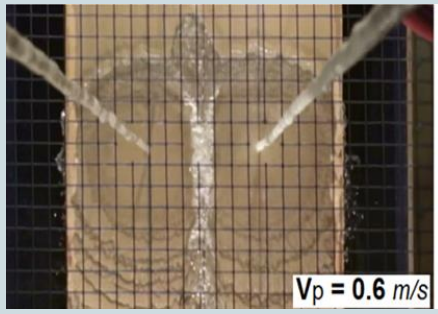 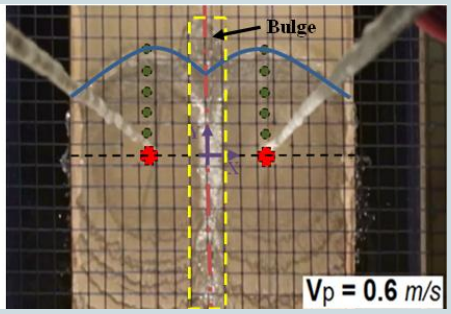	**127 mm**
	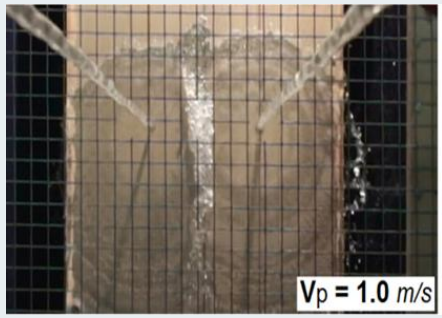 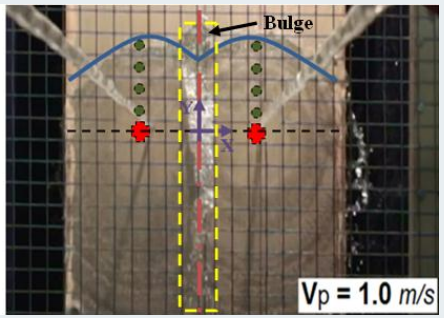	**114.3 mm**
	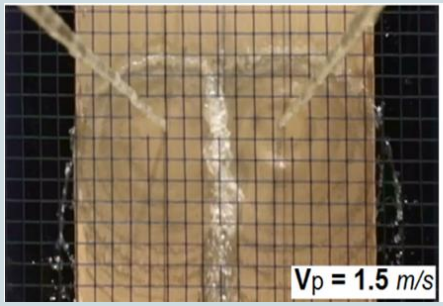 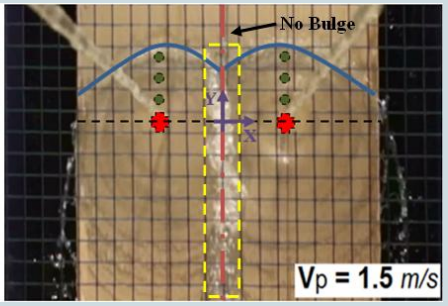	**88.9 mm**

Table 2.4 Experimental Data Analysis for 22 L/min Flow Rate and Three Plate Speeds

	Experimental Data UBC ROT group (22 L/min) [101]	Upstream Dimensions (Each square cell = 25.4 mm)
V_p	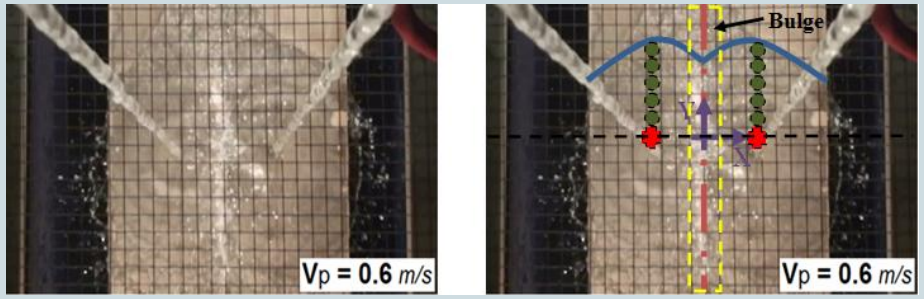	**139.7 mm**
	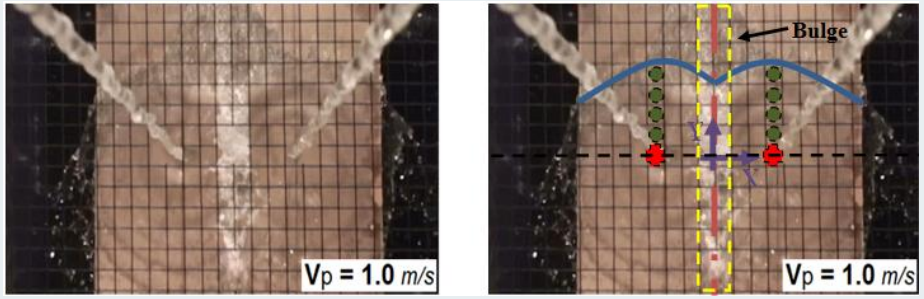	**114.3 mm**
	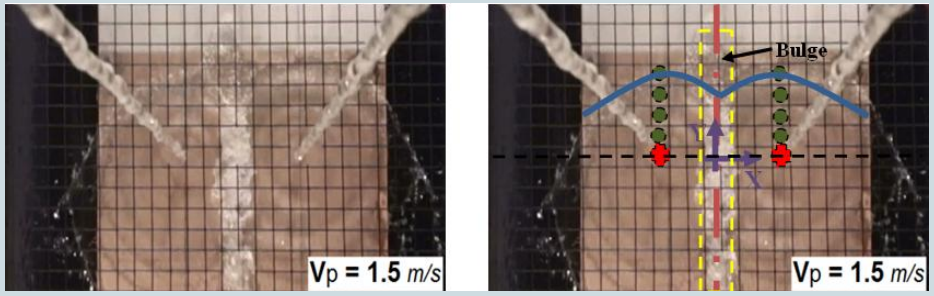	**101.6 mm**

Table 2.5 Experimental Data Analysis for 30 L/min Flow Rate and Three Plate Speeds

	Experimental Data UBC ROT group (30 L/min) [101]	Upstream Dimensions (Each square cell = 25.4 mm)
V_p	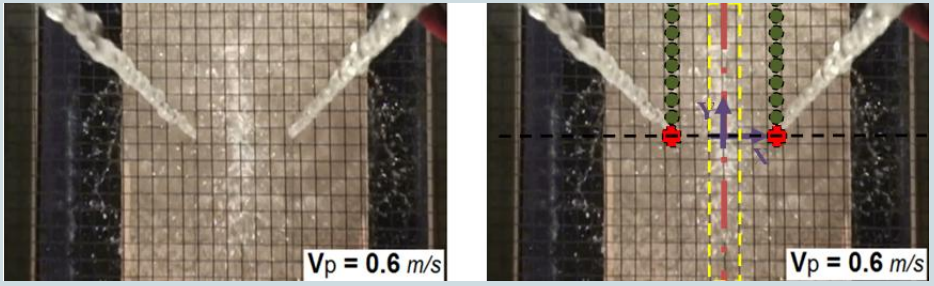	**More than 203.2 mm (Out of frame)**
	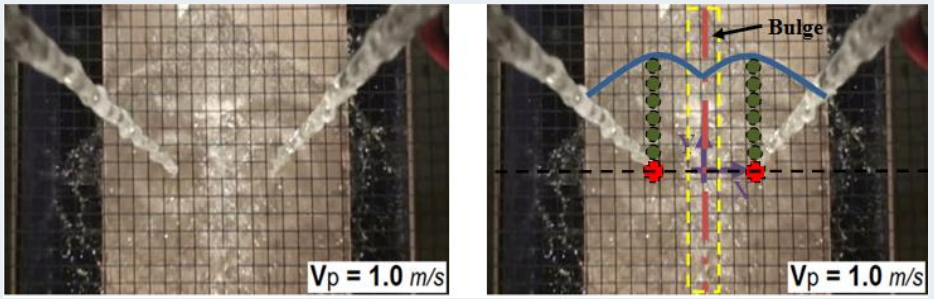	**165.1 mm**
	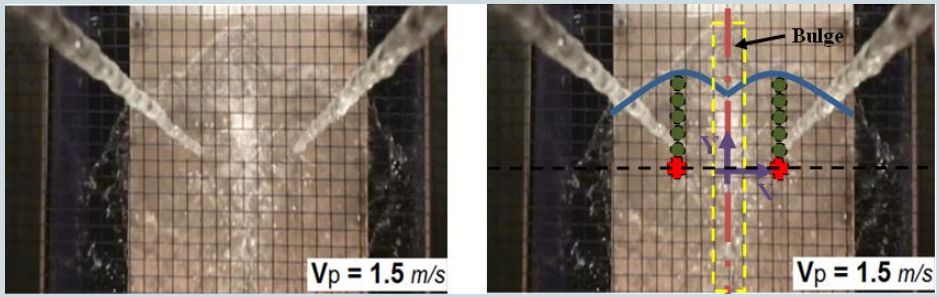	**139.7 mm**

To size the domain adequately, the upper region was modeled with a length of 135 mm and the lower region was designed as 50 mm in the case of 15 L/min, which means 185 mm in total along the Y-axis. However, the dimension of the upper region was considered as 170 mm for 22 L/min jets and 210 mm for 30 L/min jets, with the same downstream region length of 50 mm. In the case of 30 L/min, 0.6 m/s, the wetting front is out of frame, which implies that the upstream zone length is more than 203.2 mm. Thus, in this case, particularly the length of the upper side alone was considered as 260 mm. The main purpose is to minimize the model size so that the total number of cells will be reduced accordingly.

Also, for the interaction zone, a 30 mm length in the X-axis was considered for all cases but the height was modeled as 30 mm in the case of 15 L/min, 40 mm in the cases of 22 L/min and 30 L/min. Note that the two jets were separated by a distance of 203.2 mm which means 101.6 mm up to the midway between them at the interaction zone. Table 2.6 summarizes the dimensions for the computation domain (see Figure 2.6) for all simulations (the three flow rates along with three plate speeds). The plate motion is towards the negative Y-axis.

Table 2.6 Parameters Dimensions for Three Flow Rates and Three Plate Speeds

Flow Rate, Q (L/min)	**Rectangular Inlet**		**Length L (mm)**	**Int-Z Height h_3 (mm)**	**Inlet Height (h_1+h_2) (mm)**	**Width W (mm)**	**Int-Z thickness t (mm)**	**Plate Speed V_p (m/s)**
	l **(mm)**	***w*** **(mm)**						
15	20	10	185	30	50	101.6	30	0.6
22	25	12.5	220	40				1.0
30	30	15	260*	40				1.5

Note: The total height of the jet inlet was considered as 50 mm where h_1=10 mm and h_2= 40 mm. Also, the superscript (*) in the case of 30 L/min indicates the total length (upstream + downstream zones) over only 1.0 and 1.5 m/s moving surfaces.

2.6.1.2 Jet Inlet Profiles

From the two dimensional simulations, we extracted the velocity, VOF (water-air volume-fraction), and turbulent quantities (i.e. *turbulent kinetic energy k* and *turbulent dissipation ε*) to find the profiles for the inlets. To use the two dimensional profiles as input into

the three dimensional simulations, they were transformed to the polar coordinate. This is easily done through the following conversion as revealed below:

$$r^2 = x^2 + y^2 \tag{2.20}$$

where $x = r\,cos\theta$ and $y = r\,sin\theta$

Figure 2.9 illustrates this process, where the dotted black lines represent the angle theta, θ, from the light blue line which stands for the obtained profiles at 50 mm above the plate. Also, the gray line indicates the boundary of the inlet profiles and the red lines correspond to the computed inlet profile after conversion. The light blue line is divided into small segments according to the generated nodes after meshing. Moreover, the boundary line of the inlet profiles (i.e. gray line) is placed at the radius, r, which depends on the amount of flow rate that exits the jet.

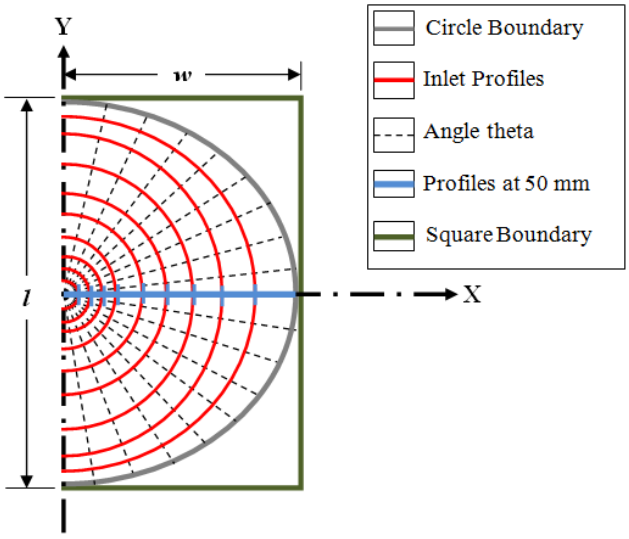

Figure 2.9 Jet Inlet Profiles Transformation

2.6.1.3 Boundary Conditions

Identifying the boundary conditions (B.C.'s) should be carefully specified since it may have an adverse effect on the flow condition within the domain. For the optimal domain that we have here, one should be even more cautious in assigning the appropriate B.C.'s in order to reasonably reflect the real case problem. There are mainly four different B.C.'s defined as: inlet, pressure outlet, symmetry plane, and wall which are numbered in sequence order 1, 2, 3, and 4, respectively, as shown in Figure 2.10.

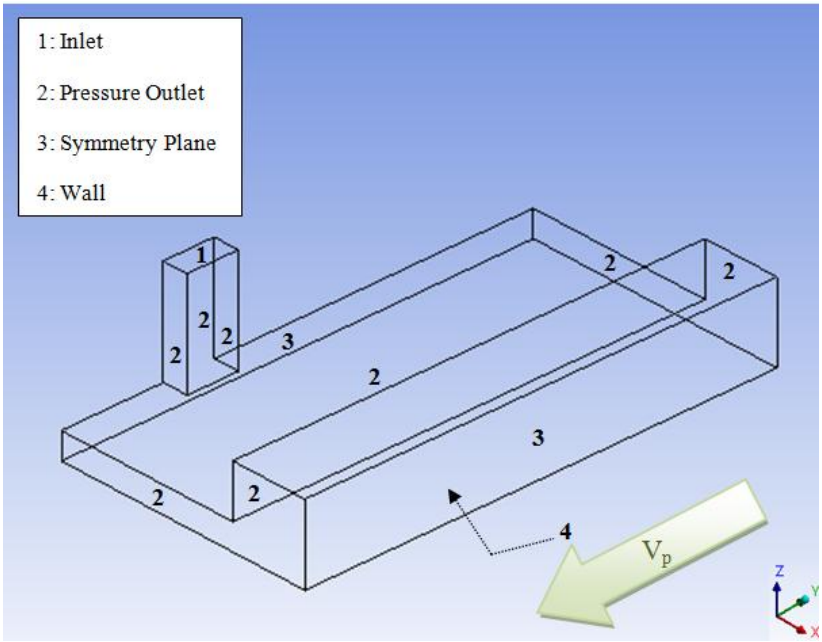

Figure 2.10 Boundary Conditions of Twin Jets Model

At the inlet B.C., all parameters at the jet inlet should be known. As mentioned before, all axial velocity, water jet radius, and the turbulent parameters were obtained from the 2-D simulations at 50 mm vertically above the plate and then implemented in this 3-D models. The profiles of axial velocity and turbulent quantities were assumed as fully developed flow.

At pressure outlet B.C., the specification of a static (gauge) pressure at the outlet domain's boundaries is required. At this kind of B.C., the fluid can exit the solution domain but no backflow is allowed. The value of the gauge pressure is kept as zero in accordance with the default settings that are provided by the FLUENT program (see FLUENT user's guide) [93]. In order to let the program numerically extrapolates the value of the gauge pressure, one should locate a reference point for the pressure or more specifically atmospheric pressure. It can be done by the Operating Condition panel by changing and locating a point (x, y, z) outside the solution domain with a known atmospheric pressure (101,325 Pa). We have to estimate the realistic values for the two turbulent parameters at the outlet boundaries either based on experimental data or analytical calculations. The estimation values for the turbulent quantities were somehow close to the calculated values at the inlet. According to the FLUENT user's guide [93], the turbulent quantities k and ε can be specified based on two different terms. First is the *turbulence length*

scale, l = 0.07 L, where L is the characteristic length. The second term is the *turbulence intensity*, I = 0.16 $Re^{-1/8}$. Generally, when the Re number is about 50,000, the turbulence intensity will be 0.04 or in percentage 4%. After that, those two turbulent parameters are calculated according to the following equations: $k = \frac{3}{2}(VI)^2$, and $\varepsilon = C_\mu{}^{3/4} \frac{k^{3/2}}{l}$ with $C_\mu = 0.09$ [93, 94].

The symmetry B.C. was employed for both half jet and half interaction zone planes. This is done deliberately in order to minimize the domain without affecting the physical reality of the flow. Actually, the vertical water jet hits horizontal plate and creates a circular spot in the case of stationary plate and non-circular shape in the case of the moving plate. If an imaginary plane cut the jet column into half, one would see an identical pattern in the other side. Similar explanation is valid for the interaction zone plane. When the two jets reach to the middle space, hit each other and will rise up in the normal direction creating irregular chaotic shape and maybe splashing. This can be modeled with symmetry condition where it acts as a barrier to the flow spreading. If the two jets have the same amount of kinetic energy, they will transfer to a potential energy after collision by jumping up with the same height in the positive Z-axis against to the gravity. Utilizing the symmetry B.C., the multiple jets (array) is realized, but we will focus on the middle interaction of the flow. Also, we conclude that to study the flow behavior of multiple jets, it may be enough to only consider the case of twin jets with the above numerical model. The wall B.C. was assigned to the bottom of the domain with a specific speed (e.g. 0.6, 1.0, and 1.5 m/s) in the negative Y-direction with no-slip wall condition.

2.6.1.4 Mesh Strategy for All Cases

Generating the mesh is a crucial stage in the numerical method. It requires a high attention since it has great effect on the accuracy of result as well as the stability. As a first attempt, the domain was meshed by sizing each edge and number of segments or dividing the edge line depends on where the water flow is more encountered. However, that procedure did not provide a good meshing pattern. In fact, one of the main priorities in generating the mesh was at least coming up with a coarse mesh and then the refinement will be done later in FLUENT if needed. For that reason, the final mesh for the whole domain was done by using the multi-zone method with structural grid and non-uniform clustering towards the plate surface where the water film is very thin of order 0.1 mm.

Figure 2.11, shows the mesh pattern at the symmetry plane of the jet, for example. It also illustrates the methodology of refinement with FLUENT. The first original mesh was obtained with about (800,000) hexahedral cells with ~25 cells in + Z direction; see Figure 2.11, the first zoomed picture. However during the Q = 15 L/min and 22 L/min simulations, noticeable discontinuities and intermittencies of the water film layer spreading over the moving plate with highest speeds, V_p = 1.0 m/s and 1.5 m/s were observed. Indeed, mesh refinement was necessary to ensure accurate capturing of the water thin film variables that spreads over the moving plate at the two distinct zones: impingement zone and parallel zone. For instant, some those essential variables are water film depth (z), jet diameter (d), radial velocity (V) as well as the stagnation pressure (P).

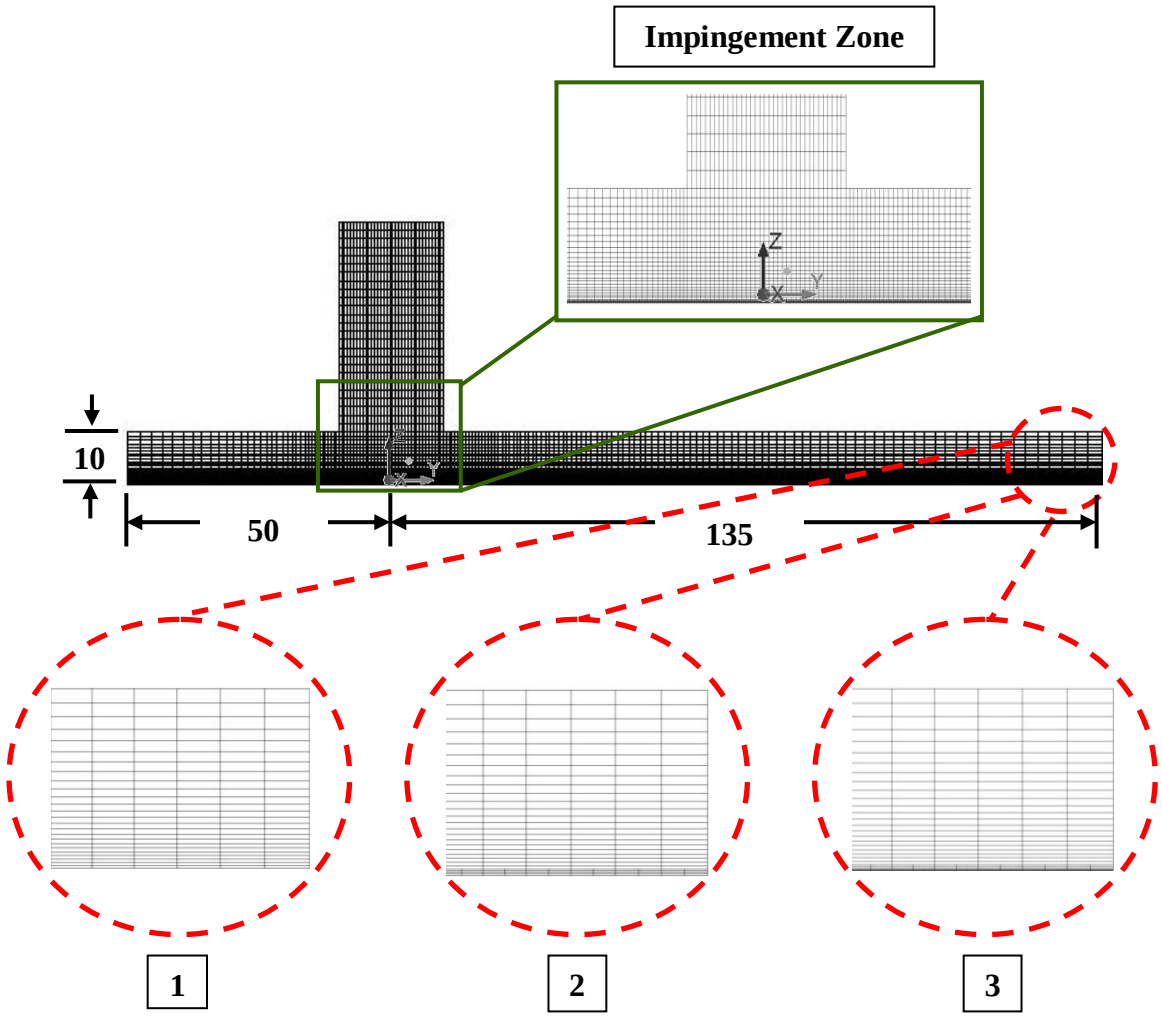

Figure 2.11 Mesh Refinement Progress in Jet Symmetry Plane

In order to resolve discontinuity of the very thin film flows over the moving plate and achieve a good mesh, an appropriate wall y^+ must be obtained. Taking all that in the consideration, for each case the mesh refinement was done in FLUENT by region adaptation method for the whole domain in X, Y directions and at 0.3 mm above the moving plate (wall) in +Z direction. That adaptation increased the number of cells to around (1,200,000) with ~27 cells in + Z direction see the second zoomed picture in Figure 2.11. However, still the intermittency of the spreading flow was not fully resolved especially for 15 L/min and 22 L/min over higher plate speeds. Therefore, the first possible remedy for this problem is to split the z = 0.3 mm above the plate into two (i.e. up to z = 0.15 mm). Unfortunately, that technique leads to dramatic increase in the number of cells (up to 2,500,000 cells) which is considered excessive at this early stage of the simulation. Thus, the domain is re-meshed up to z = 75 μm instead which then generates somehow acceptable number of cells about (1,900,000) cells. Although about 2 million was still a large number of cells, it was not sufficient otherwise to resolve fully the intermittency of the lowest flow rate Q = 15 L/min over 1.0 m/s and 1.5 m/s plate speeds. Once again, the mesh refinement was also required so the same approach was applied as before using adaptation by region but this time with only (0.075/2 mm) above the wall in +Z direction. In other words, half of the first cell row from the bottom of the moving wall was split into two cells and each cell was divided into two cells. This approach provides very huge number of cells about (4,800,000) with ~29 cells in + Z direction see the third zoomed picture in Figure 2.11.

As a result, the final optimal mesh for the whole solution domain should be capable to capture the thin water film in accordance with the plate-to-jet velocity ratio (V_p/V_j). For all cases, the zoomed upper picture that indicates the impingement zone in the Figure 2.11 was carefully clustered towards the target surface since this area has a huge influence on the heat transfer parameters in the case of the heated plate. Table 2.7 summarizes the mesh refinement strategy. This table was used as a guided map after solving for the lowest flow rate 15 L/min over three plate speeds. It is important to note that in the case of high flow rate, Q = 30 L/min the original mesh was sufficient to resolve the problem and no refinement was needed since the water film has a thicker layer in comparison to the case of 15 L/min. Nevertheless, in the case of 22 L/min, the mesh refinement was necessary as the plate speed increases to 1.0 m/s and 1.5 m/s.

Table 2.7 Mesh Refinement Strategy in the Case of Different Flow Rates over Different Plate Speeds

	No. of Cells	+Z (mm)	Explanation (Not to Scale)
Original Mesh	**800,000**	**-----**	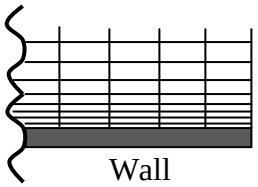 **Non-uniform structural grid using rectangular cells which was clustered towards the moving wall.**
1st Refinement	**1,200,000**	**0.3**	**Each cell was divided into two up to z = 0.3 mm.** 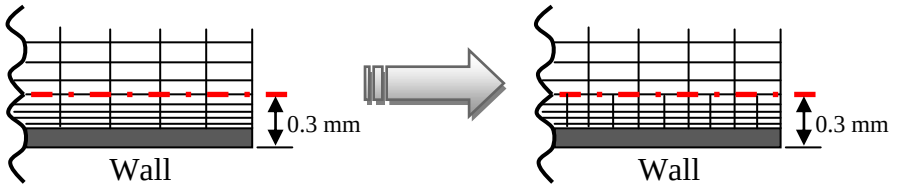
2nd Refinement	**1,900,000**	**0.075**	**Each cell at z = 0.075 mm was further split into two.** 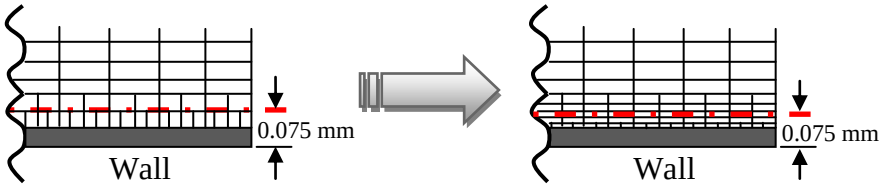
3rd Refinement	**4,800,000**	**0.0375**	**Finally, at z = 0.0375 mm, each cell was divided into two.** 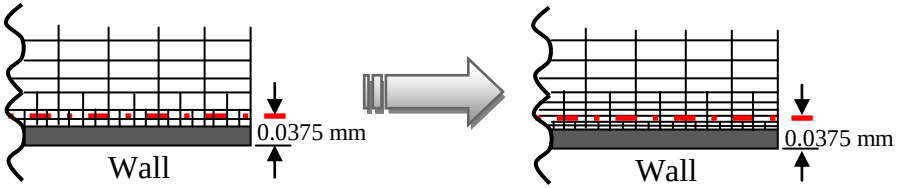

Mesh dependency analysis was performed after ensuring that the impingement water has a continuous development over the moving substrate. As mentioned above that the starting mesh was coarse enough in order to reduce the simulation time and CPU memory consuming. Then, the mesh was refined accordingly inside the fluent if needed. For instance, in the cases of the flow rates Q = 15 and 30 L/min impinging over same moving plate with speed of 0.6 m/s were tested to evaluate if the result is sensitive to mesh adaption. Table 2.8 illustrates the mesh refinement above the moving plate where the above strategy shown in Table 2.7 was used. It is revealed that as the amount of flow rate increases the total number of cells decreases since the impingement water layer becomes thicker.

Table 2.8 Meshes Refinements above the Plate (z = 0.1-0.2 mm)

Flow Rate, Q (L/min)	1st Mesh	2nd Mesh
15	1,200,000	1,900,000
30	800,000	1,200,000

Therefore, the effect of mesh alteration was examined on the normalized flow velocity with respect to the normalized radial displacement above the moving surface. Figure 2.12 represents the sensitivity of the numerical results, normalized radial flow velocity, for example due to the mesh adaption. It is clear that the difference after refinement is very low, so it confirms that the numerical outcome is grid independent. Then, the smallest number of cells was used to reduce the simulation time and CPU memory consuming. The same methodology was applied to check all the cases in order to ensure the independency of the mesh resolution so then assure that the numerical outcomes is accurate enough.

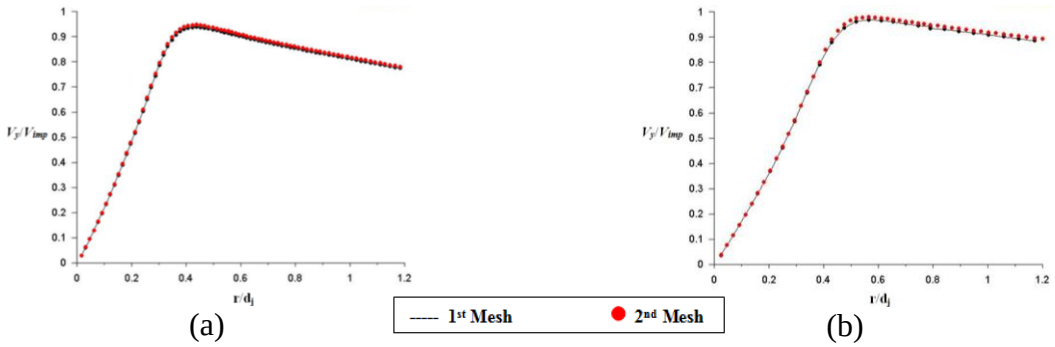

(a) (b)

Figure 2.12 Normalized Velocity near the Moving Plate (V_p = 0.6 m/s) with Different Grids, (a) Q = 15 L/min, (b) Q = 30 L/min

2.7 Conclusion

Initially, a 2-D model was simulated to examine the RKE turbulent model efficiency in regards to the simple case of single jet impinging on a stationary surface. The axial and radial velocities pre-impingement and after impingement were obtained. In order to simulate the multiple jets impinging over a moving plate, a 3-D model is necessary since the flow structure is not symmetric at upstream and downstream regions. Afterwards, the twin jets model was designed accordingly with the optimal size of the solution domain in order to obtain a reasonable number of cells as a good start based on the available computational facilities. Jet inlet profiles were extracted from 2-D simulations and utilized as inputs into 3-D simulations.

In total, nine distinct cases were considered of flow rates as 15, 22, and 30 L/min and systematically change the plate speeds as 0.6, 1.0, and 1.5 m/s. In terms of mesh refinement, it was discovered that, when the plate speed increases, the mesh adaptation is essential especially for the low amount of flow rate to avoid the flow intermittency which in turn dramatically increase the number of cells and makes the simulations so lengthy and CPU memory consuming.

Chapter 3: Results and Discussion

Numerical results of twin water jets of three flow rates (Q = 15, 22, and 30 L/min) simulations impinging over a moving horizontal target surface with three speeds (V_p = 0.6, 1.0, and 1.5 m/s) are discussed. Simulation results are validated with the UBC ROT group experimental data. All simulations were continued until steady state was established.

3.1 Validation of Some Numerical Results

3.1.1 Twin Water Jets Impingement over a Moving Plate

In order to ensure the accuracy of our numerical results, the averaged wetting front measured during the UBC ROT experiments may be compared with the numerical results obtained from the model. The numerical wetting front was measured from the VOF contours on the impingement moving surface (as shown in Table 3.1, top view) for Q = 15, 22, and 30 L/min over V_p = 0.6 m/s (used as examples) using Plot Digitizer program [102]. The same analysis was followed to define the experimental wetting front of the same cases according to the captured frame. Then, the curve-fitted curves of both wetting fronts were compared. Figure 3.1 shows the normalized radial distance (Y/d) along the positive Y-axis (upstream side) with respect to the normalized radial distance (X/d) along X-axis for different flow rates impinging over the same moving surface (V_p = 0.6 m/s). The numerical (Num) wetting fronts for all cases are closer to the impingement point (*0, 0*) making a smaller radius when compared to the experimental (Exp) wetting fronts. This may be attributed to the surface condition which influences the development of the wetting front. As the surface roughness increases, the shear stress between the moving plate top surface and the impingement water increases. Figure 3.1 shows that as the amount of flow rates increases, the water covers much area of the moving surface which indicates more uniform heat transfer. Generally, the computed wetting fronts were smaller than the experimental observations but when the amount of flow rate increased, the numerical simulation provided better correlations.

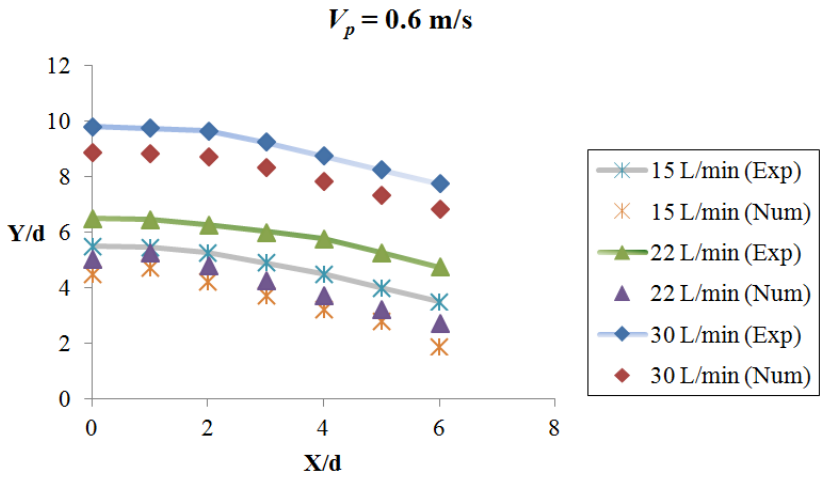

Figure 3.1 Experimental and Numerical Wetting Front Comparison of Different Flow Rates over a Moving Surface

To examine the flow structure and behavior of the numerical results of the above cases, the VOF contours are compared with the experimental data conducted by the UBC ROT group [101] (see Table 3.1). As shown in Table 3.1, the experimental data and numerical results are in good agreement and overall features are properly replicated by the simulations. For instance, in all flow rates, central bumps of water pool ahead of the interaction zone were created of different sizes after the collision took place and established (highlighted by yellow-dotted circle in figures). This kind of water flow structure was successfully captured numerically using VOF contour. Moreover, different interaction types were detected during the experiments that were highly influenced by the jets flow rate and the plate speed. It is noticed that when the *Q* increased the wetting front arrived earlier to the interaction zone and the collision happened sooner which created a thin up-wash splashing fountain (22 and 30 L/min cases). However, another interaction type was shown in low jet flow rate (15 L/min) characterized by a thick dome-shape accumulation of interacting water fluid. Interestingly, when the amount of flow rate was 22 L/min the two interaction types were observed as shown in previous sections depends to the speed of the moving plate.

Generally, the computation outcomes showed a good agreement with the experimental data but no splashing was captured during the numerical simulations. One reason is the surface roughness. The plate in the experiments was Plexiglas with smooth surface but the default

surface in FLUENT is aluminum with certain roughness which most probably is much rougher than smooth Plexiglas surface used in ROT UBC experiments. We know that surface roughness suppresses the splashing (Guo [103] and Sterling [104]). In both studies, they found that splattering occurs on surfaces with lower roughness level. Moreover, the ROT tests on unheated steel plate resulted in much smaller wetting zone respect to the Plexiglas test plate. The Plexiglas roughness is not reported to set it in our simulations.

Figure 3.2 illustrates variations of the normalized distance (Y/d) of the numerical wetting front in accordance with the amount of flow rates (Q = 15, 22, and 30 L/min) impinging over moving surface with three speeds (V_p = 0.6, 1.0, and 1.5 m/s). As shown, when the flow rate increases and the plate speed decreases, the wetting front has the chance to propagate further upstream. In other words, as the plate-to-jet velocity ratio (V_p/V_j) increases, the frictional force becomes higher so that the moving plate restricts the impingement water to freely spread to its upstream destination. Therefore, the water layers accumulated on top of each other creating a thick structure (HJ) and the wetting flow velocity drops with no chance except to flow within the moving plate direction (i.e., reversed flow). This increases the turbulence at HJ.

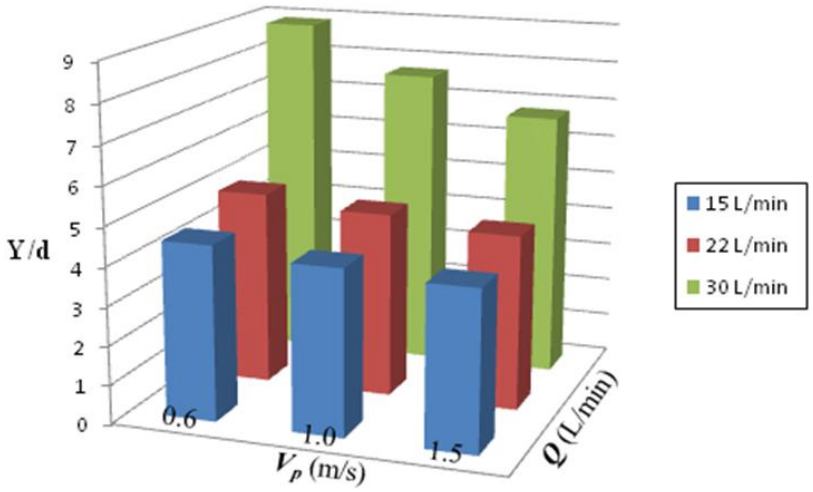

Figure 3.2 Numerical Results of Wetting Front Distance Variation due to Different Flow rates Impingement on Different Plate Speeds

Table 3.1 Validation of the Numerical Results of Different Flow Rates over 0.6 m/s Plate Speed

Experimental Data [101]		Numerical Results	
Top View	**Front View**	**Top View**	**Front View**
Q = 15 L/min			
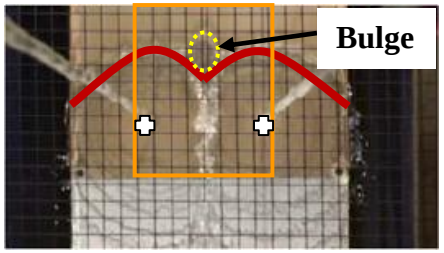		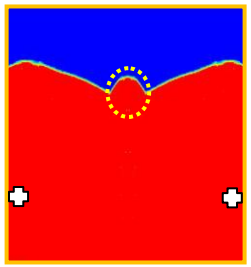	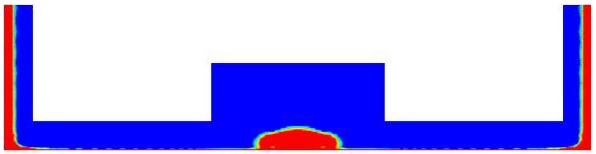 Thick dome-shape interaction type
Q = 22 L/min			
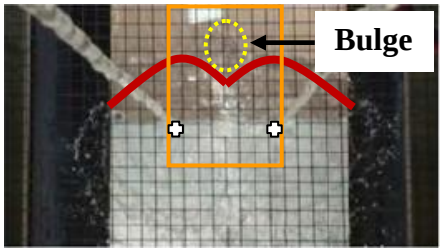		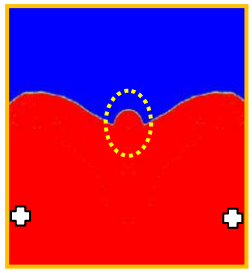	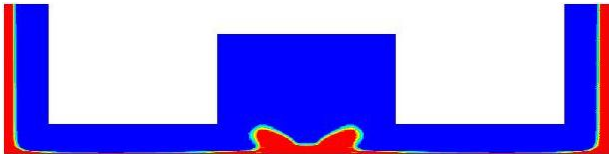 Thin tilted fountain interaction type
Q = 30L/min			
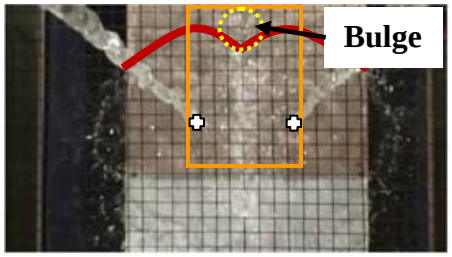		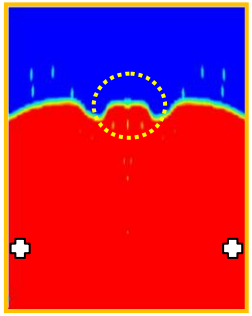	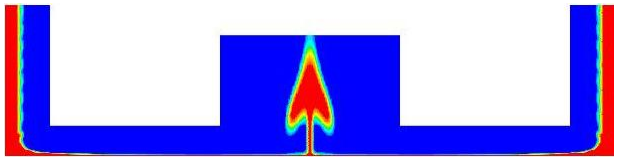 Thin up-wash fountain interaction type
 Stagnation Point.		Wetting Front.		Water (f=1.0)  Air (f=0.0)	

3.1.2 Validation of 22 L/min Impingement Flow over 1.0 m/s Plate Speed

In order to ensure the accuracy of the numerical results, another investigation was done with comparing the computed impingement flow development with experimental data at different time stages; see 22 L/min over 1.0 m/s plate speed, for example. Figure 3.3 represents some sample images extracted from a film recorded by the UBC ROT group by top camera located vertically above the moving plate. Notice that these images are highlighted with times that illustrate the progression of the water impingement and how the wetting front extended over the moving plate along with moderate splashing.

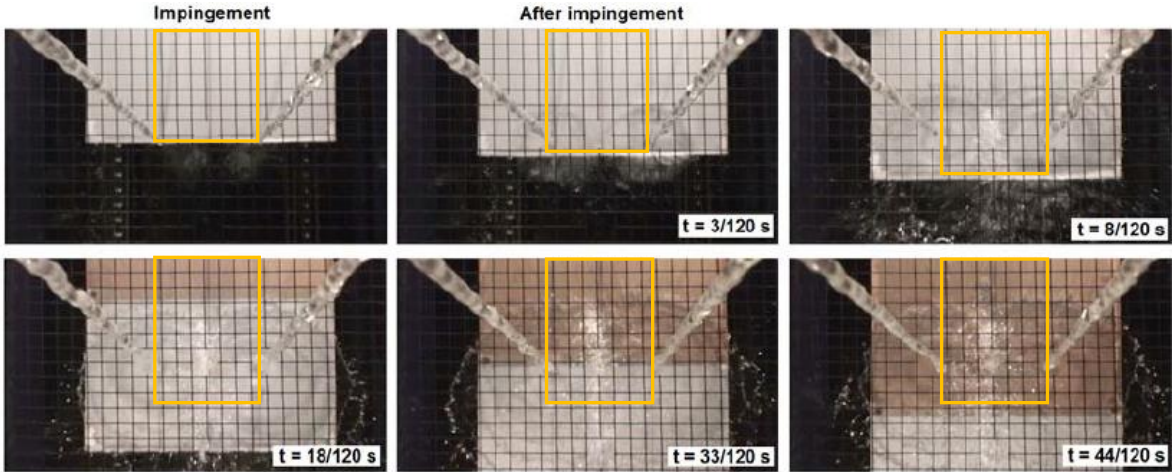

Figure 3.3 Sample of Top View Images for Water Flow Propagation of 22 L/min over 1.0 m/s Plate Speed [101]

The following numerical results for same case in Figure 3.4 show good agreement and similar impingement flow development with the experimental images above. The wetting front took the same characteristics while it readily spreads and then the collision occurred. However, during the experiments the collision occurs earlier than the numerical results which could be attributed to the effect of surface roughness as mentioned above. Also, some splashing of water droplets was sometimes captured in the simulation over the horizontal surface just after the instant of impingement.

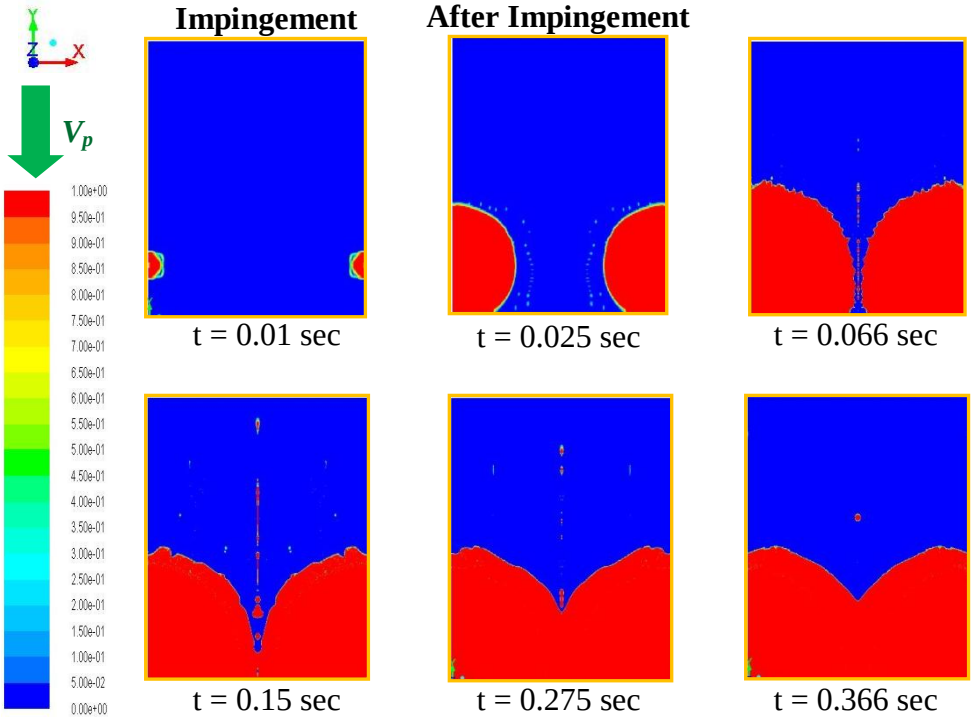

Figure 3.4 Development of Impingement Flow over 1.0 m/s Moving Surface due to 22 L/min Twin Jets

In addition and for next validation, the twin jets interaction during the collision of the same case (Q = 22L/min over V_p = 1.0 m/s) were monitored and analyzed. Figure 3.5 shows the sample images of water flow interaction of the same experiments but captured at different camera that was positioned at the front of the plate in order to provide better observation of the collision and interaction.

Figure 3.5 Sample of Front View Images for Water Jets Interaction of 22 L/min over 1.0 m/s Plate Speed [101]

The following numerical results in Table 3.2 for same case were obtained and could be compared with the above images which showed a reasonable agreement. This table illustrates the flowing of the twin water wall jets before and after the collision along jet-to-jet space. During the experiments, water splashing was observed just after water layers interact within the interaction zone (middle image at t = 0.2 sec in Figure 3.5). However, numerically this kind of flow behavior was not captured at same time and it takes longer time for numerical wall jets to interact (Table 3.2). One compelling reason is that the size of the droplets are so tiny in which the current mesh size is not capable to capture them. If the mesh was refined in order to monitor this feature, the number of cells dramatically increases up to 3 – 4 millions which, in turn, will make the simulation so lengthy and require a very powerful computer. Actually, it is a memory consuming task and not feasible to follow at this stage considering so long time spending for available simulations. Another reason is that the RANS equations were numerically solved which provided an averaged solution to the flow velocity and pressure. Hence, still not possible to capture the small length scale of those water droplet.

Table 3.2 Numerical Results for Water Jets Interaction of 22 L/min over 1.0 m/s

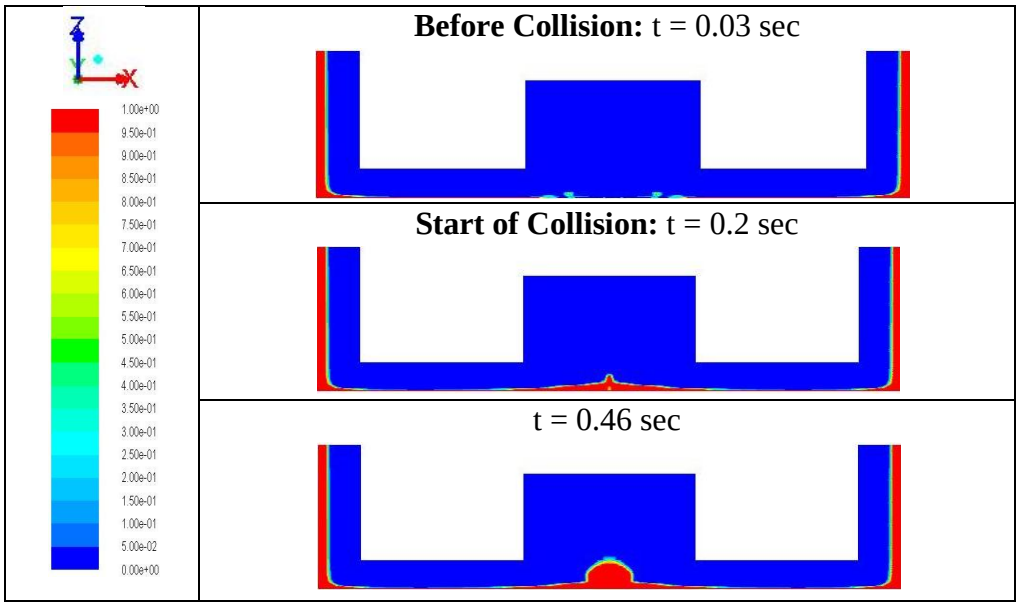

3.1.3 Validation of 30 L/min Impingement Flow over 1.0 m/s Plate Speed

To get more confident of our numerical simulations, another case was considered. The amount of jets flow rate is increased from 22 L/min to 30 L/min but the plate speed (V_p = 1.0 m/s) is kept the same. Figure 3.6 shows the experimental data (top view images) of UBC ROT group after analyzing and extracting the required frames of the reordered film.

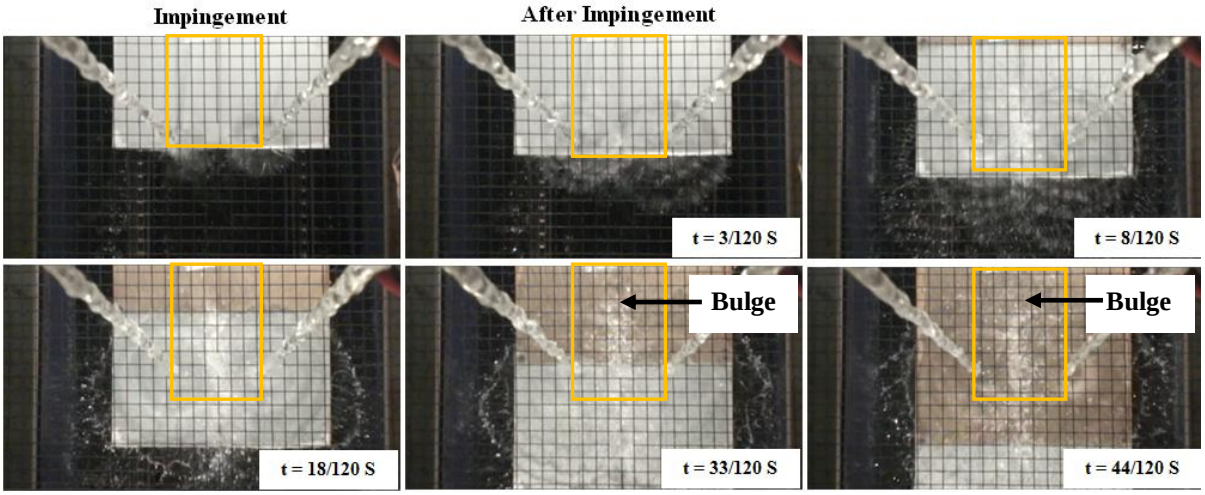

Figure 3.6 Sample of Top View Images for Water Flow Propagation of 30 L/min over 1.0 m/s

The following simulation results in Figure 3.7 show the water flow development. The results are comparable where a similar water flow structure was numerically captured. In fact, after the collision takes place a bulge of water ahead of the interaction zone was observed (see the last two stages in Figure 3.6 and Figure 3.7). Here, the effect of surface roughness diminishes due to the high momentum of the flow wall jets so then a better timing of the water development was obtained.

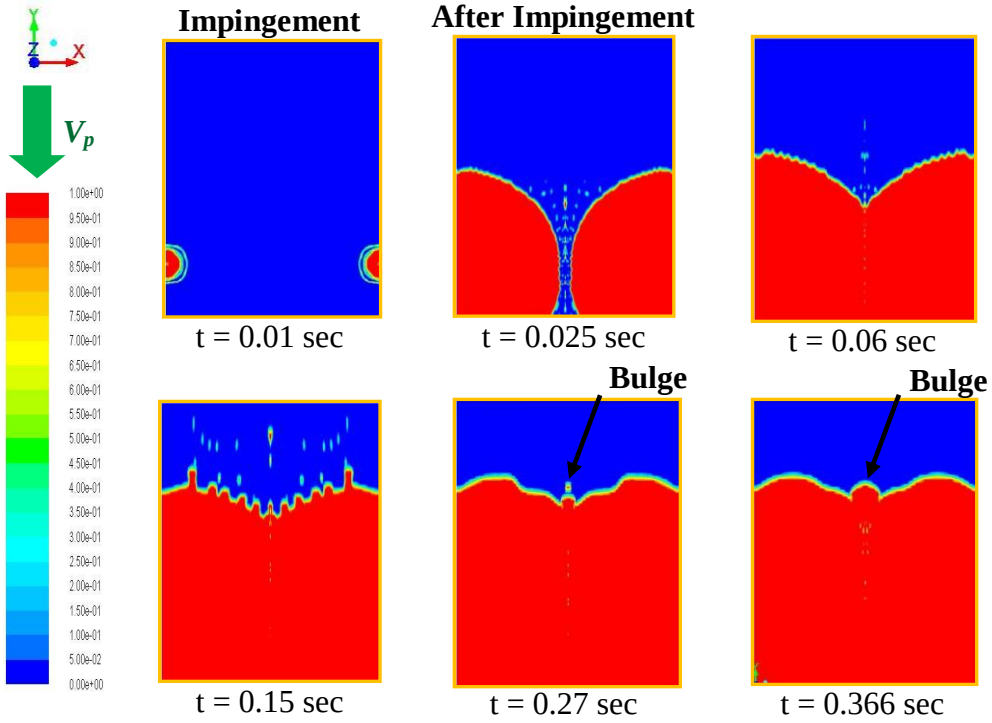

Figure 3.7 Development of Impingement Flow over 1.0 m/s Moving Surface due to 30 L/min Twin Jets

In addition, the interaction between the two 30 L/min adjacent jets was analyzed from the UBC ROT experiments. Figure 3.8 shows the sample images of the front view of the water wall jets collision.

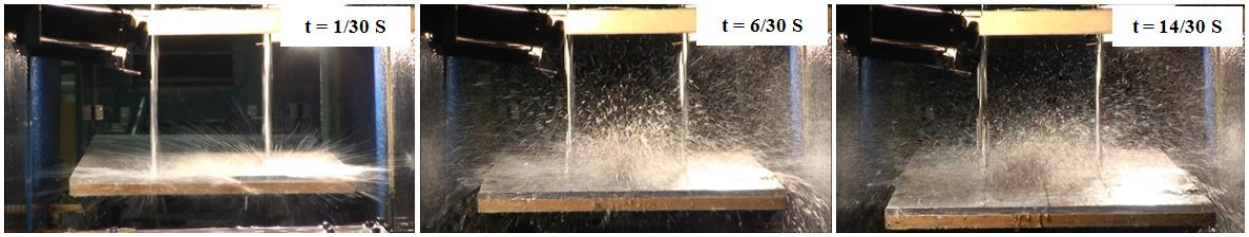

Figure 3.8 Sample of Front View Images for Water Jets Interaction of 30 L/min over 1.0 m/s

The numerical result of the water wall jets development and then the formation of the jets interaction are shown in Table 3.3. These outcomes were showed a good agreement again. However, a huge splashing was observed during the experiments but numerically no water splashing was captured. But, a chaotic and unstable collision obtained in the simulation that

somehow reflects the up-wash fountain interaction occurred experimentally. Overall, the water flow behaves similar to the experiments.

Table 3.3 Numerical Results for Water Jets Interaction of 30 L/min over 1.0 m/s

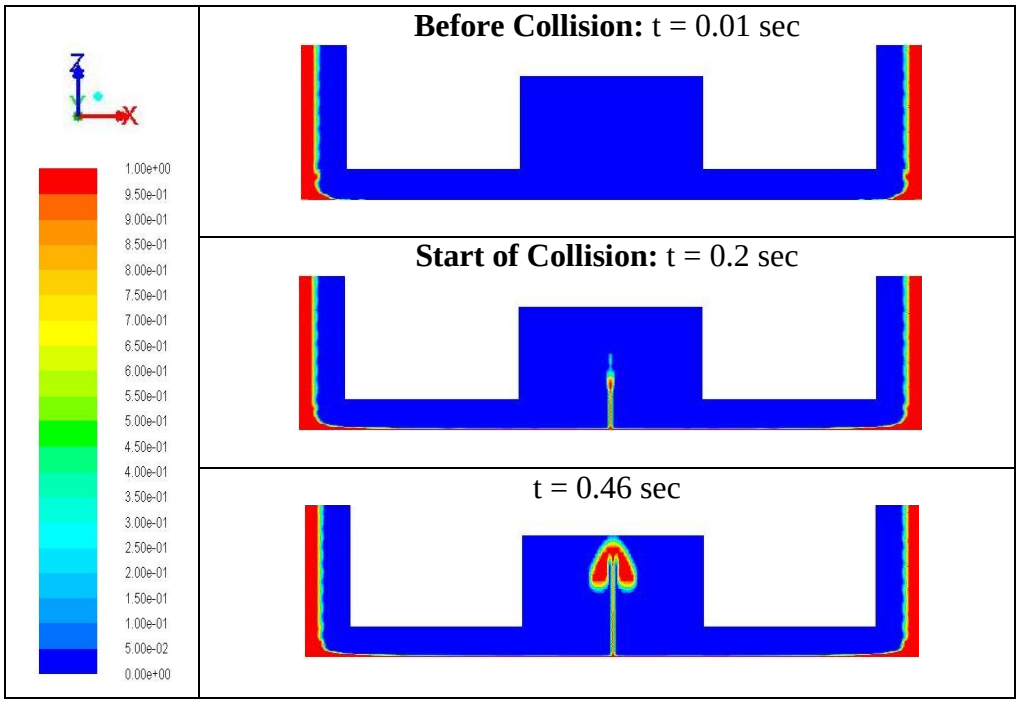

3.2 Three-dimensional Twin Jets over a Moving Impingement Plate

3.2.1 Twin Jets of 15 L/min

3.2.1.1 Wetting Front Development

The wetting front development over the moving plate is the important indication of flow structure at the upfront zone of impingement point which, in turn, identifies the great restrictions exerted by the plate movement. In order to examine the effective confinement of the target horizontal plate on the propagation of the water film layer, the VOF contours was utilized to trace changes that occurs during the simulation time. The simulations were monitored and checked frequently during processing to ensure the right progressing. The mesh efficiency was also crucial; wall y+ was kept in range of $5 < y+ < 10$ to achieve a better resolution of spreading of water film over the moving surface. The VOF method provides very good scheme in capturing the water free-surface as well as in identifying the multiphase system (e.g. air-water mixture) and the interaction between them.

At the jet symmetry plane, there are two related water flow structure properties that can be numerically monitored and investigated: water flow propagation and hydraulic jump configuration. Table 3.4 illustrates the structure of the wetting front of 15 L/min flow rate over the moving plate with different speeds (V_p = 0.6, 1.0, and 1.5 m/s) at time 0.14 second, for example, which represents the best and unchanged results. The red color in the VOF contour illustrates water phase (f = 1) and the blue is for air phase (f = 0) and $0 < f < 1$ depicts the free-surface (interface between water and air).

Table 3.4 Wetting Front and (HJ) Configurations of 15 L/min with Different Plate Speeds

First Case (V_p = 0.6 m/s)	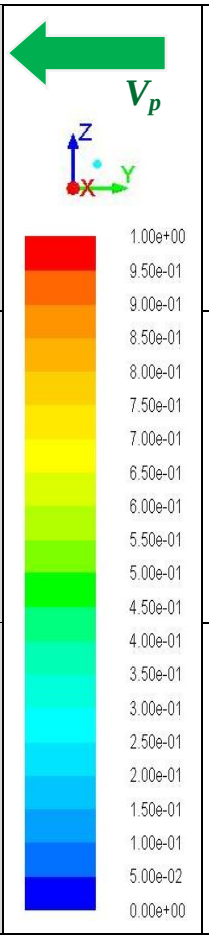	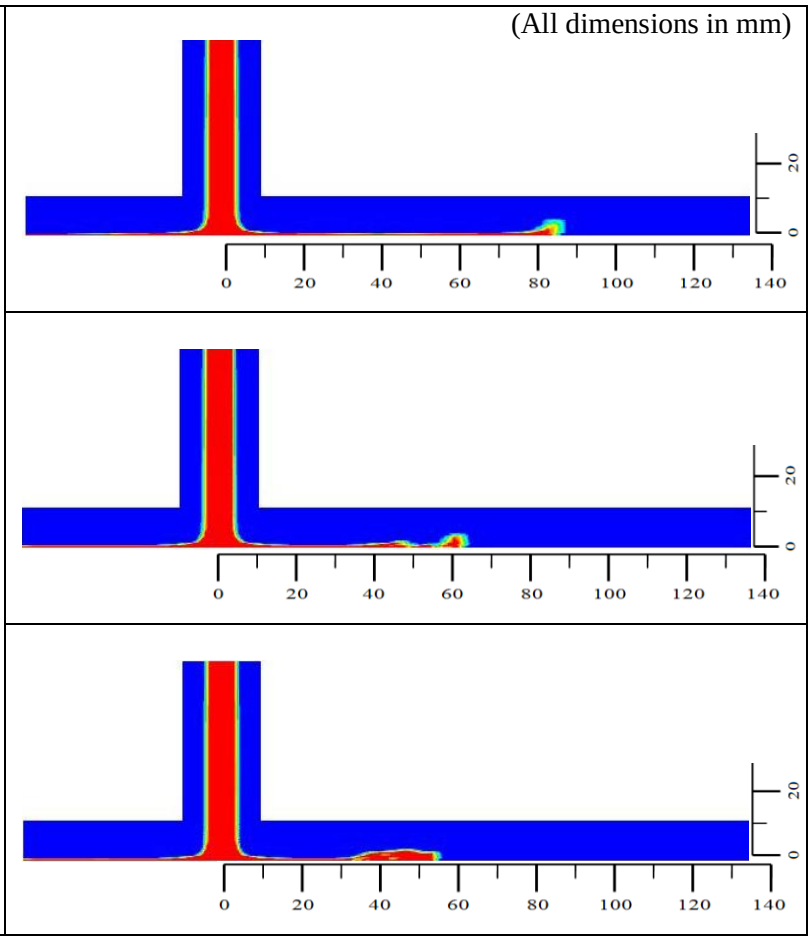
Second Case (V_p = 1.0 m/s)		
Third Case (V_p = 1.5 m/s)		

Furthermore, Table 3.4 shows the height of the wetting front and/or hydraulic jump that change with respect to the speed of the bottom surface. The water film moves against the plate motion which enhances the friction force at the top surface in contact with the water film. Moreover, the water impingement flow does not have enough momentum (issued from only 15 L/min jet) to overcome frictional effect of moving substrate and could freely flow over plate surface. In the case of the lowest plate speed, after the water film settles down (steady state condition), the maximum thickness of HJ is approximately 4 mm height. At the 1.0 m/s case, this propagation looks similar and the only difference is that the impingement water flow was more restricted upstream since the plate-to-jet velocity ratio is a bit higher (V_p/V_j = 1.14). Therefore, the height of the hydraulic jump is also changed. The maximum height of the HJ of the water film is about 4.5 mm. At the highest plate speed case (V_p = 1.5 m/s), the wetting front becomes

even closer to the impingement zone. The water film has a thicker layer compared to the lower speed case, as is clearly shown in Table 3.4. As a result, the height of the HJ is thicker where the maximum is about 5 mm.

Actually, during the water long jet impingement, the hydraulic jump phenomena can also be observed in the case of the fixed plate which is characterized with a circular spot (CHJ); whereas, in the case of the non-stationary plate that moves with a certain speed, the circularity configuration is not valid anymore. For that reason, the asymmetric spreading of the water film can be easily noticed due to the surface motion and that is the key reason behind the complexity of simulating this kind of problem.

3.2.1.2 Axial and Radial Velocities

Table 3.5 illustrates the contours of velocity magnitude for the 15 L/min flow rate impingement over a moving plate with three different speeds (V_p = 0.6, 1.0, and 1.5 m/s) at the jet symmetry plane. From the inlet towards the bottom surface, it mostly represents the axial velocity where the red color contour identifies water jet with velocity of 5.44 m/s (V_{imp}) and it also mostly illustrates the radial velocity after impingement over the moving plate. When the incoming water jet reaches the horizontal plate, it was halted then deflected and became parallel to the surface. Generally, plate motion triggers air to flow much easier than water impingement flow due to the huge difference of densities between air and water. In the velocity contour, blue color identifies mainly air flow which illustrates air backflow in the case of the fastest plate speed, V_p = 1.5 m/s. Also, for the 1.0 m/s case, the flow was slightly constrained from spreading towards the upstream side. However, in the first case, no air backflow was noticed from velocity vectors since the velocities ratio is lower (V_p/V_j = 0.68) compared to the third case (Table 3.5).

Table 3.5 Axial and Radial Velocities of 15 L/min Impingement on Different Plate Speeds

Case	Velocities Contours with Velocity Vector
First Case (V_p = 0.6 m/s)	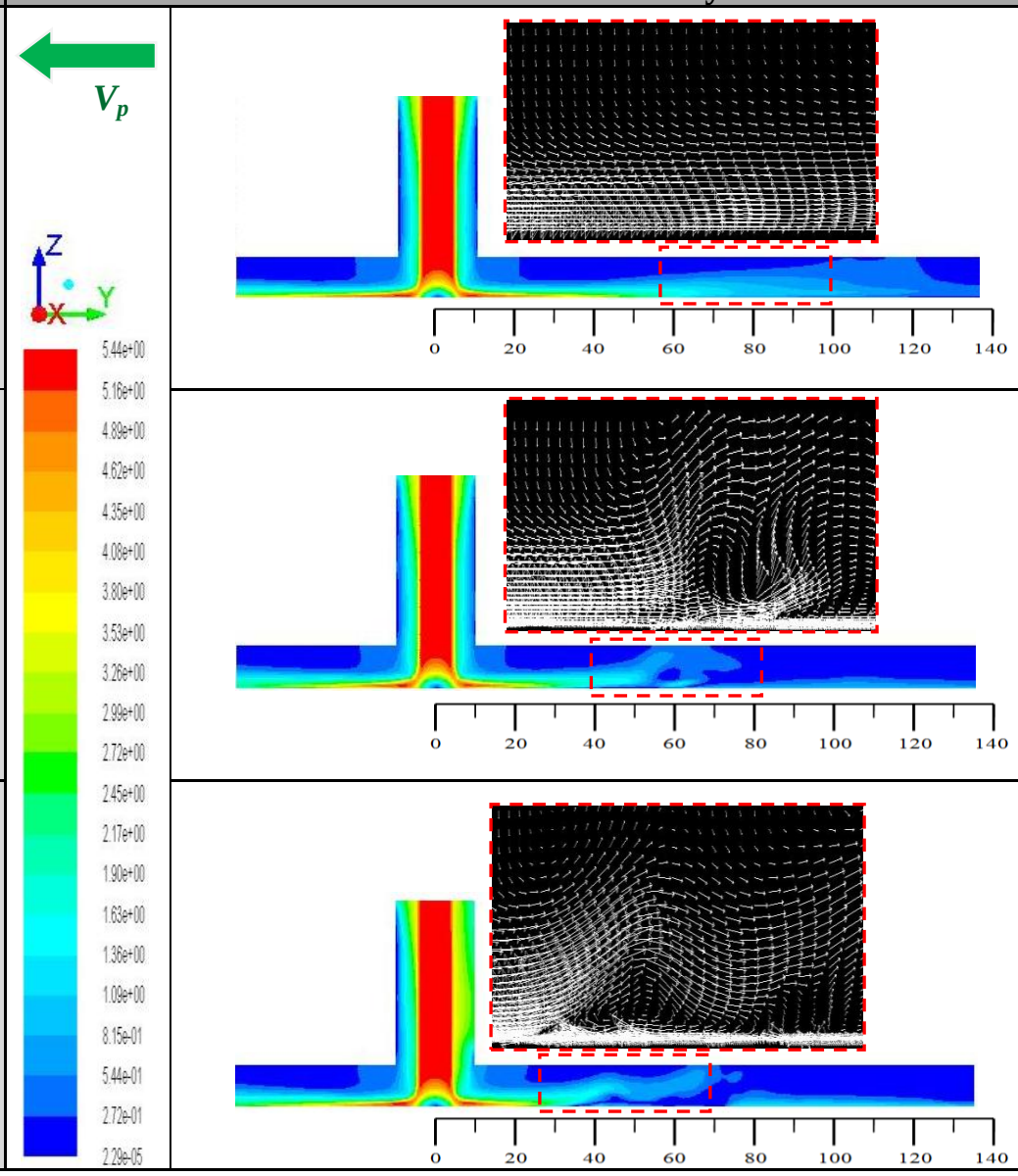
Second Case (V_p = 1.0 m/s)	
Third Case (V_p = 1.5 m/s)	

(All dimensions in mm)

3.2.1.3 Water Flow Impingement Spreading

At V_p = 0.6 m/s case (see Figure 3.9), the impingement water propagates faster than the other plate speed cases because the water film flows with greater velocity than the plate speed so it cannot prevent the water film to reach to its destination upstream. Plate-to-jet velocity ratio (V_p/V_j = 0.68) is very low which means that the water is able to propagate and overcome the plate

motion. At the upstream zone, there is a battle between the solid surface and the fluid layer raises up and the amount of shear stresses increases since they act against each other. As the water propagates over the moving surface, the radial symmetry vanishes. After the collision occurs a bulge of water ahead of the interaction zone appears.

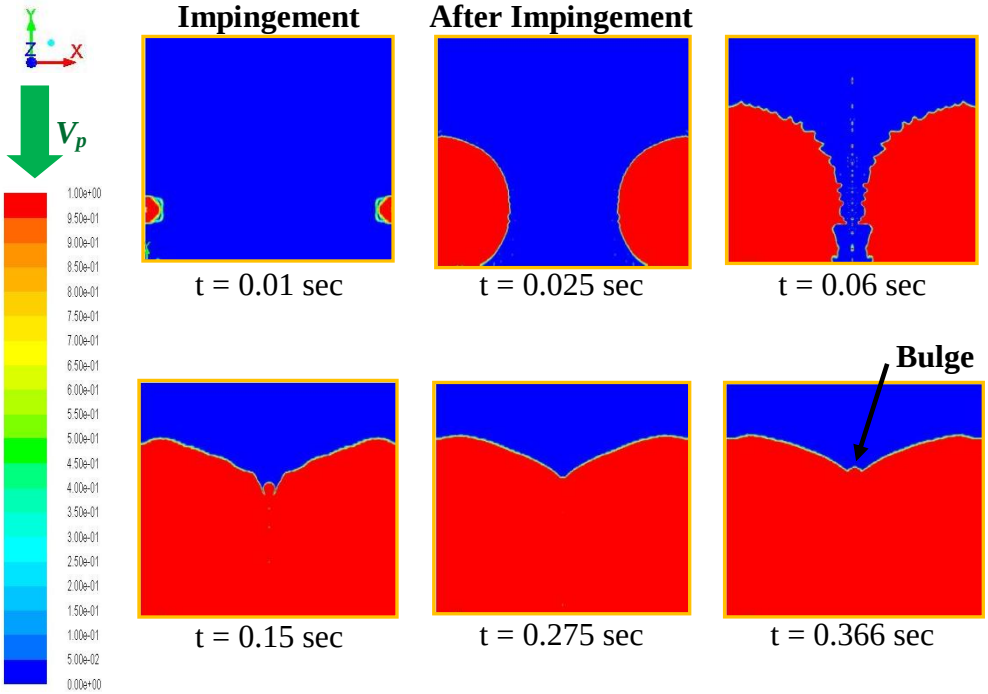

Figure 3.9 Development of Impingement Flow over 0.6 m/s Moving Surface due to 15 L/min Twin Jets

Table 3.6 illustrates the comparison of the water film development over moving plate at time of 0.14 sec, for example, from top view. After the water jet hits the moving plate, it spreads out radially with a symmetric pattern at the impingement region. Thereafter, there are two different water flows that will be observed: a rising and chaotic flow at the front and upstream and a smooth thin layer film at downstream side. At higher speed cases, the water film does not cover too much area upstream and it is restricted by a fast-moving plate which pulls the water layer toward incoming jets and finally drains it out of the solution domain at downstream (negative Y direction). The simulations of faster moving plates took much longer time and memory requirements to reach the collision. Mesh refinement was highly necessary which leads to a dramatic increase in the amount of cells and a much smaller time step. It is worth

highlighting that the water flow spreading over the moving plate for the twin jets is quite similar to the single jet in terms of flow characteristics at the impingement zone and parallel zones in upper and lower regions. The distinction is that the water wall jets interaction in accordance with the three different plate speeds at (Int-Z); it will be discussed later in more detail. Since the velocity ratio is considered a bit higher in the second and third cases compared to the first case (Table 3.6), the collision took place mainly at the lower side of the interaction zone.

Table 3.6 Impingement of Water Flow Rate of 15 L/min over Different Plate Speeds

First Case (V_p = 0.6 m/s)	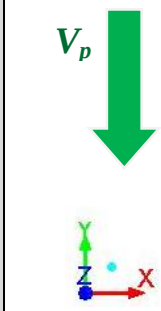	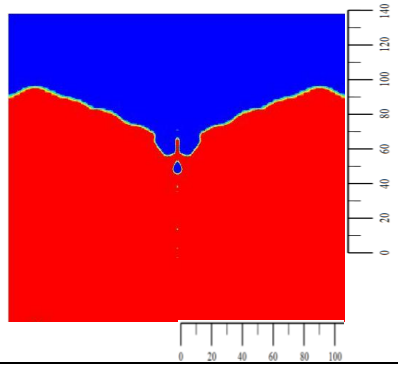
Second Case (V_p = 1.0 m/s)	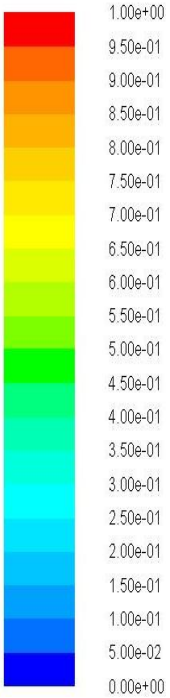	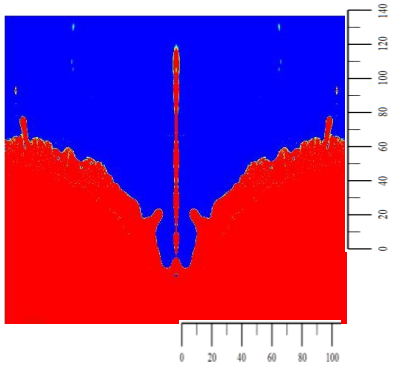
Third Case (V_p = 1.5 m/s)		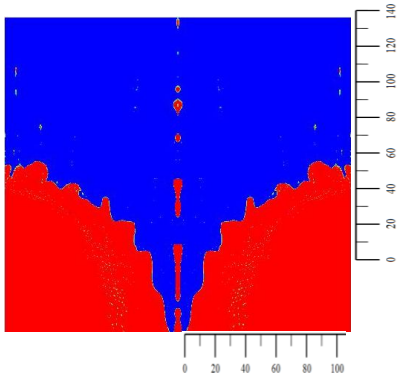

(All dimensions in mm)

The wetting front and the occurrence of the bulge ahead of Int-Z were measured from the VOF contours of 15 L/min impinging on a moving plate with different speeds (V_p = 0.6, 1.0, and 1.5 m/s). The curve-fitted wetting fronts were, then, compared with the experimental data of twin jets impingement as shown in Figure 3.10. It is noticed that we have assumed that the flow is symmetric along the jet and Int-Z planes. In reality, the flow acts chaotically and has unsteadiness behavior. The results of the simulations represent, however, an averaged behavior since we are using RANS simulations. Thus, for simplicity, the fluctuations were neglected to ease the analysis and define the average of the flow. Also, the models have been designed to minimize the solution domain and to reduce the total number of cells and then accordingly decrease the simulation time and CPU memory. The numerical wetting fronts are in good agreement with the averaged experimental observations. As shown, when the plate speed increases, the wetting front becomes closer to the stagnation point with small radius. The occurrence of bulge was experimentally observed during moving plate of speeds V_p = 0.6 and 1.0 m/s and suppressed at the highest speed V_p = 1.5 m/s. Numerically, after the water wall interaction takes place, the bulge of water was only captures during the low plate speed V_p = 0.6 m/s with smaller radius compared to experimental observation. This is attributed to the difference in moving plate surface condition as mentioned before. Interestingly, the numerical wetting front curvature decreases as the plate speed increases due to the increase of the frictional force.

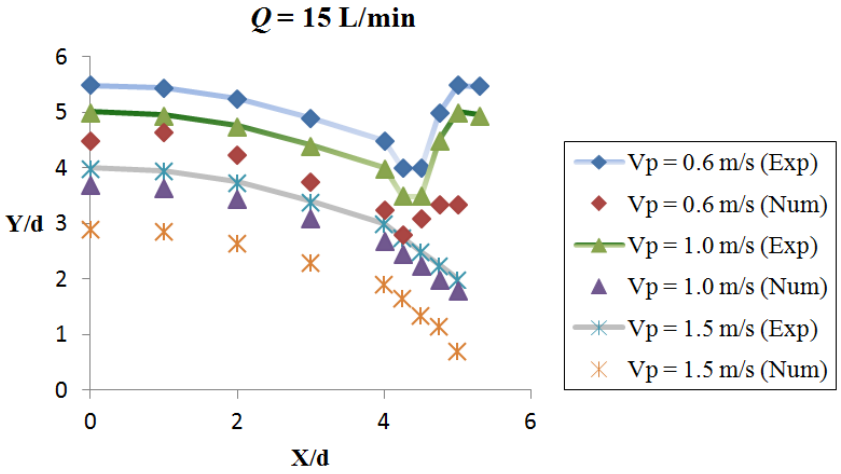

Figure 3.10 Experimental and Numerical Wetting Front with or without Bulge due to Twin Water Jets of 15 L/min Impinging over Different Plate Speeds

3.2.1.4 Pressure Distribution

The pressure distribution over the moving surface varies almost parabolically where it has a very high value at the impingement point and nearby; maximum pressure at center point (stagnant point) and then decrease sharply until it reaches ambient pressure. Table 3.7 shows the pressure contour for the mixture of air-water for 15 L/min jet with respect to different plate speeds. The red color indicates the highest value but then the color varies in accordance with the pressure drop as the water jets flows away from the impingement point. In addition, three pressure plots are represented for each case. In parallel zone, the pressure plots are flat and zero value as expected and the pressure rapidly fluctuates at upstream zone which is for air flow against to the plate movement direction along +Y direction (see Table 3.4).

Interestingly, the pressure beyond the wetting zone became so chaotic in third case of highest plate speed (V_p = 1.5 m/s). Past the wetting front, the pressure fluctuates highly due to the huge air backflow (refer to Table 3.5). In the second case, similar condition was also captured with a bit less pressure fluctuation. However, the first case of lowest plate speed, the pressure does not vary as much as the other cases. Since the amount of flow rate is low and when the plate moves with the highest speed, the stagnation point was slightly shifted towards the upstream zone against the moving plate direction.

Table 3.7 Pressure Contours of Twin Water Jets of 15 L/min Impinging over Different Plate Speeds

Case	Pressure Contour (All dimensions in mm)	Pressure Plot
First Case (V_p = 0.6 m/s)	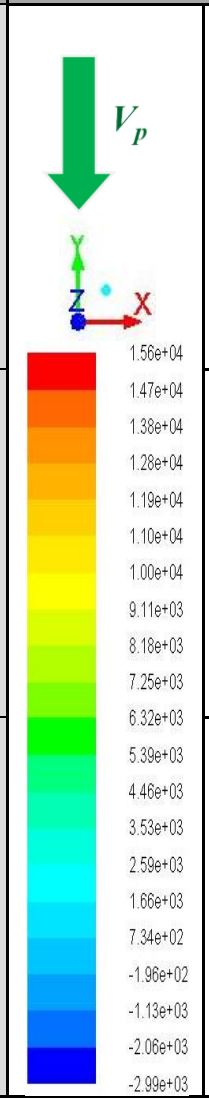 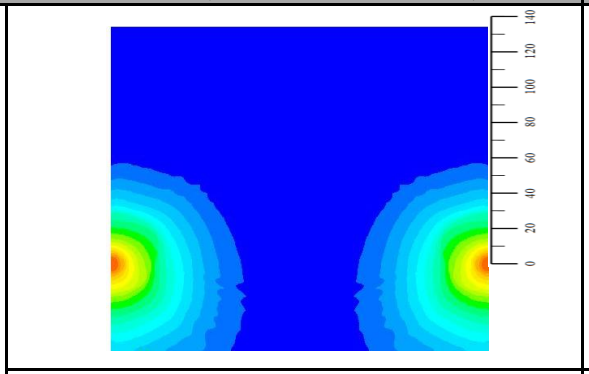	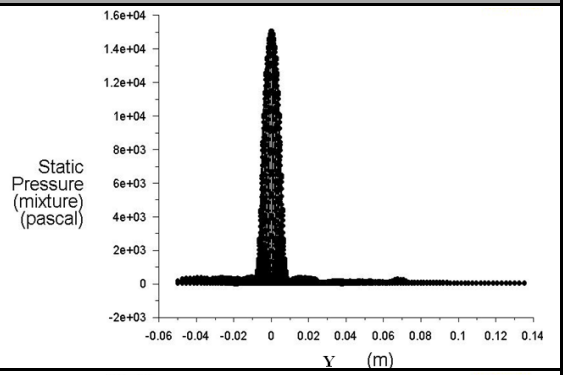
Second Case (V_p = 1.0 m/s)	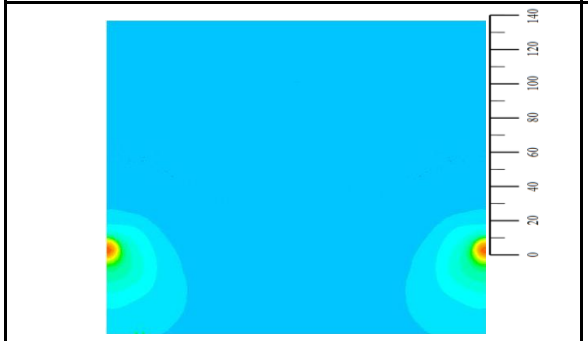	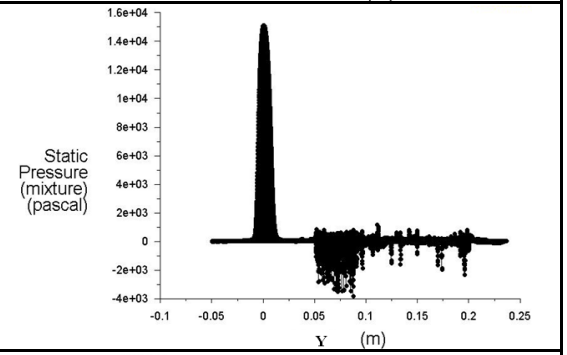
Third Case (V_p = 1.5 m/s)	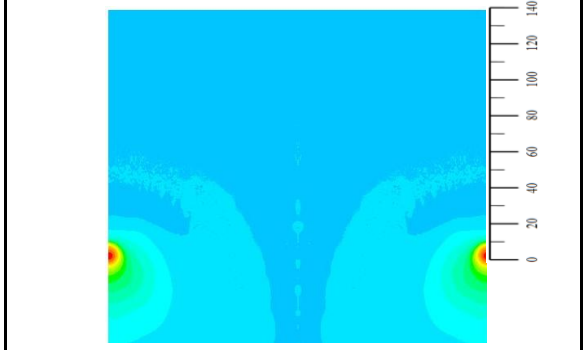	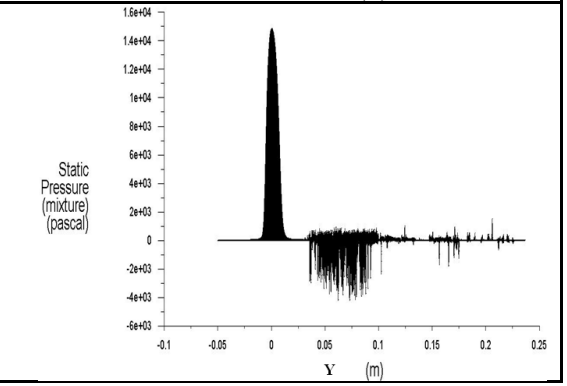

3.2.1.5 Water Flow Collision at Interaction Zone

The collision of water wall jets of 15 L/min over the 0.6 m/s is illustrated in Table 3.8 and shows the development of the water flow along jet-to-jet space at the Int-Z. The water layer creates a thick dome-like shape with non-splashing interaction type as was observed during the experiments.

Table 3.8 Numerical Results for Water Jets Interaction of 15 L/min over 0.6 m/s

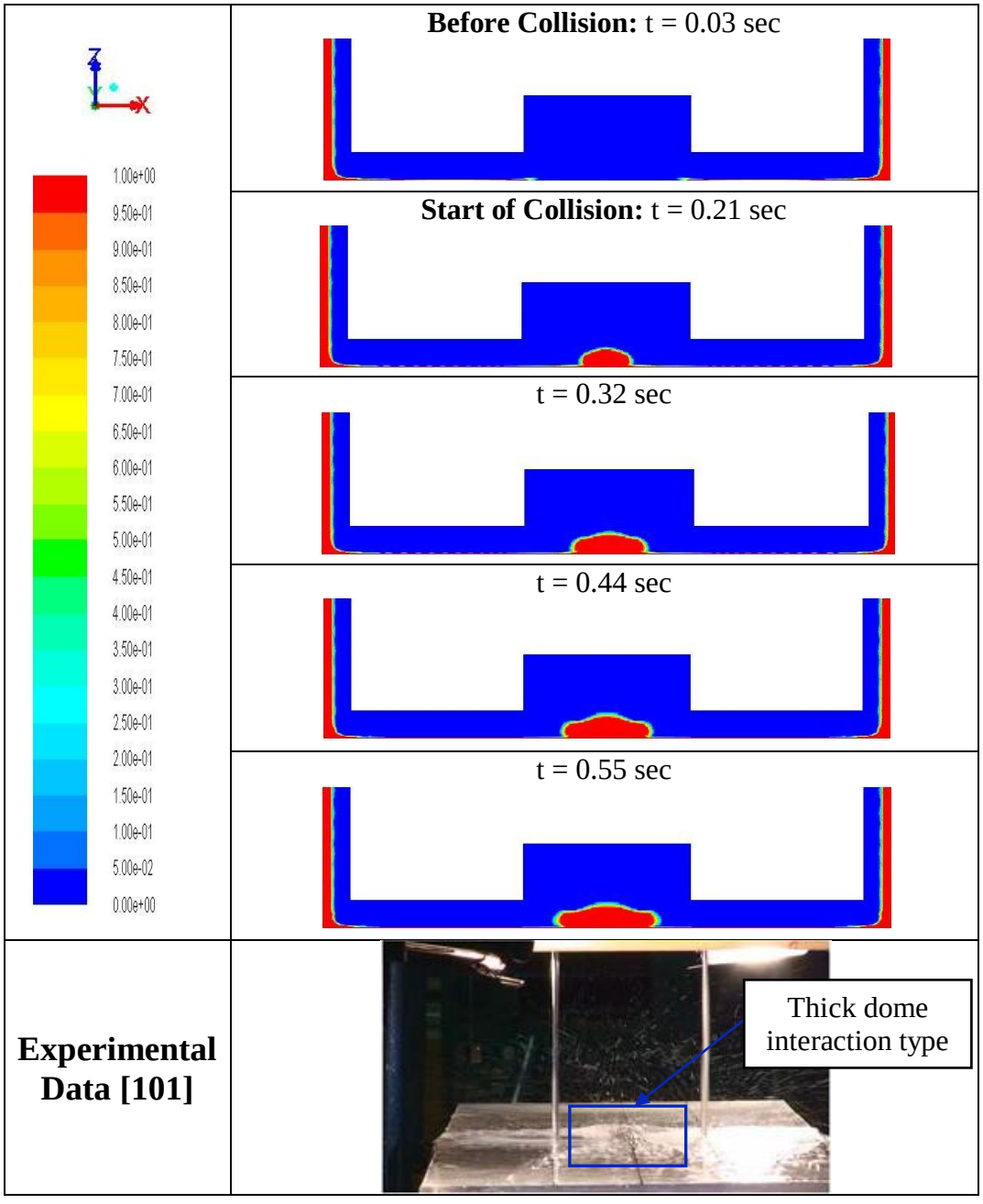

3.2.2 Twin Jets of 22 L/min

3.2.2.1 Wetting Front Development

The wetting front propagation and hydraulic jump formation were depicted and monitored for 22 L/min flow rate jets simulations over moving plate of three different speeds (V_p = 0.6, 1.0, and 1.5 m/s) using VOF contour. Table 3.9 illustrates the effect of plate speed on the impingement flow at the jet symmetry plane at time of 0.30 sec, for example, where different HJ's were captured. According to the plate-to-jet velocity ratio (V_p/V_j), the wetting front has distinct displacements from the impingement point; it gets closer to the impingement point as plate moves faster. In the lowest plate-to-jet velocity ratio (V_p/V_j = 0.6/1.293 = 0.46), the impinging water flow spreads further far from the impingement region. However, the water flow speed decreases gradually and in turn, the plate speed is able to restrict water film from further stretching and the HJ eventually will be established.

Table 3.9 Wetting Front and (HJ) Configurations of 22 L/min with Different Plate Speeds

Forth Case (V_p = 0.6 m/s)	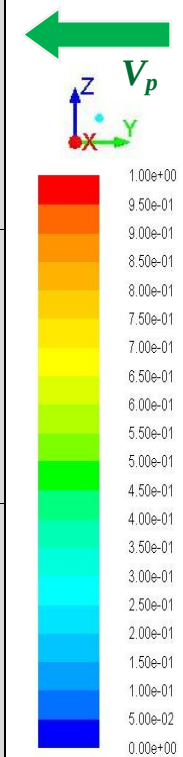	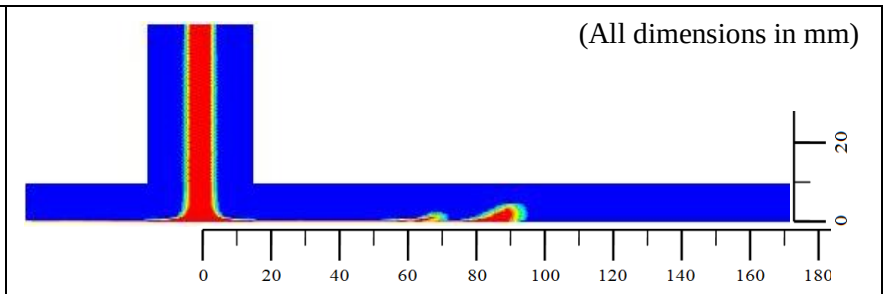
Fifth Case (V_p = 1.0 m/s)		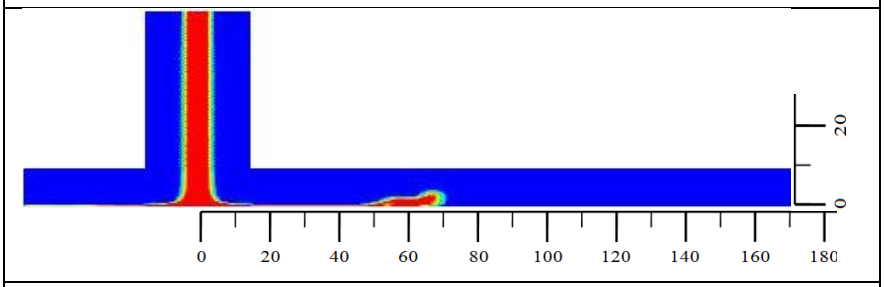
Sixth Case (V_p = 1.5 m/s)		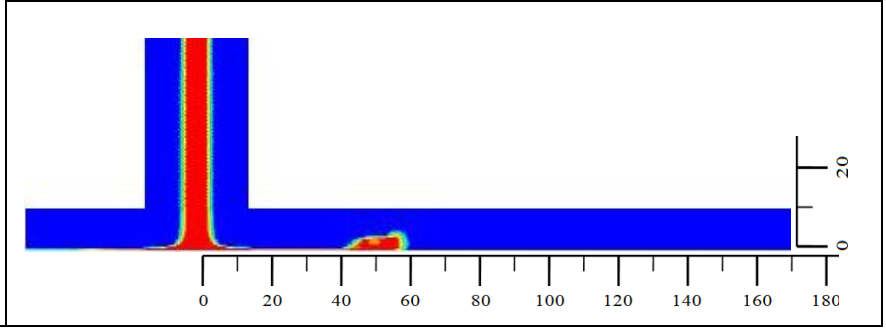

3.2.2.2 Water Flow Impingement Spreading

In order to monitor what happens after the impingement and how the water flow behaves, the top view is considered. This is captured in the 0.6 m/s case in Figure 3.11. At the beginning, the water flow behaves similar to the case of the fixed plate with a circular shape of the impingement but as the water propagates the circularity phenomena disappears due to the influence of the plate movement. When the water reaches the interaction symmetry plane, it becomes stagnant, rises up, and then comes back to the plate which will be added to the left water and creates a central pool of water. As more fresh water comes from wall jets and hits the interaction plane, more water accumulates and then returns back over the moving surface creating a longer wetting front with central bump (bulge) of water a head of Int-Z.

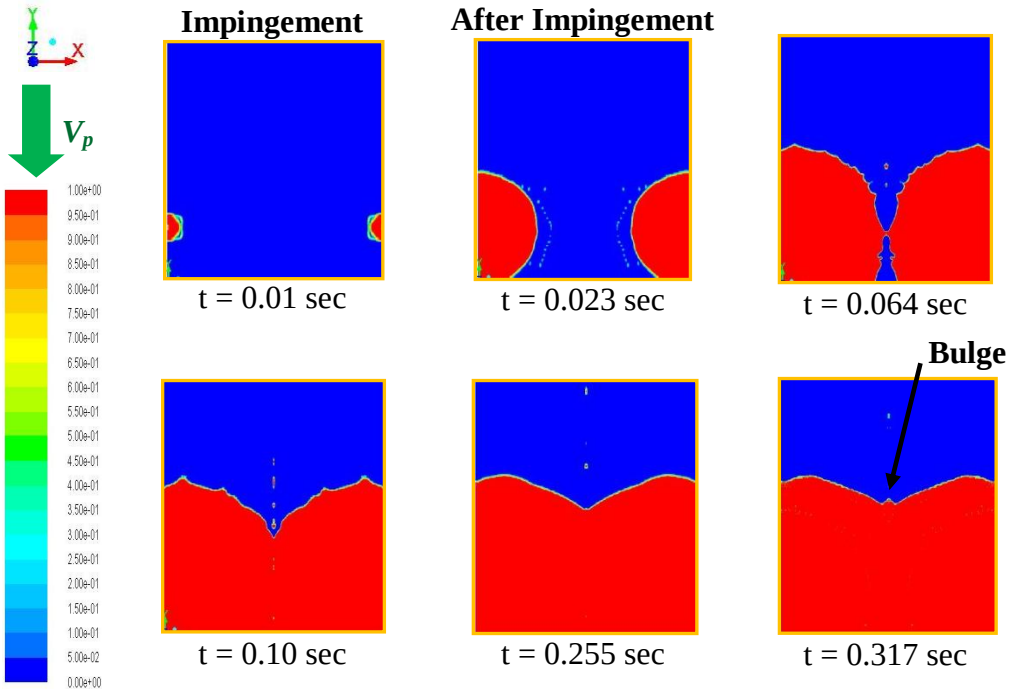

Figure 3.11 Development of Impingement Flow over 0.6 m/s Moving Surface due to 22 L/min Twin Jets

Table 3.10 below represents the comparison of wetting zones of 22 L/min cases at steady conditions. When the plate moves faster (higher velocity ratio V_p/V_j = 0.77 and 1.16), the impingement water does not cover a larger area of the top target surface in comparison to the lowest velocity ratio (V_p/V_j = 0.46). Higher the plate speed is more bent downward the wetting

fronts will be. Moving surface partially washes out the impingement water and drains it from the computation domain at downstream. As the plate moves faster, the chance of the bulge occurrence suppresses. For example, after wall jets interaction took place, a bulge of water a head of Int-Z was noticed only in the case of the lowest plate speed 0.6 m/s as shown in Table 3.10.

Table 3.10 Impingement of Water Flow Rate of 22 L/min over Different Plate Speeds

Forth Case (V_p = 0.6 m/s)	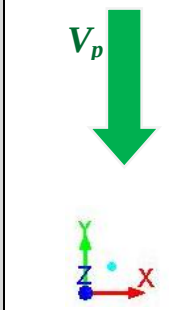	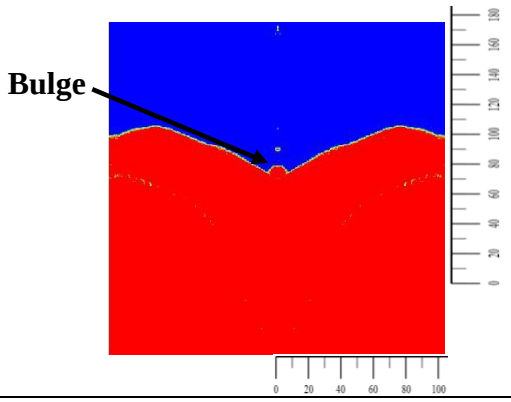
Fifth Case (V_p = 1.0 m/s)	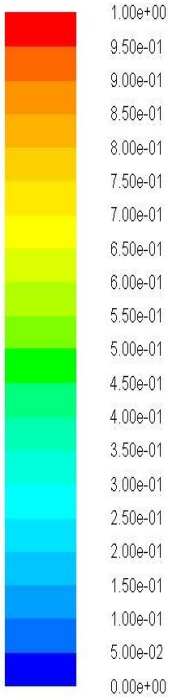	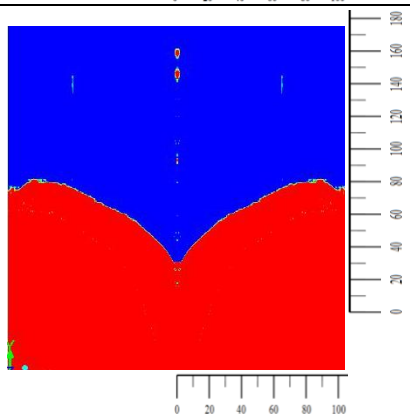
Sixth Case (V_p = 1.5 m/s)		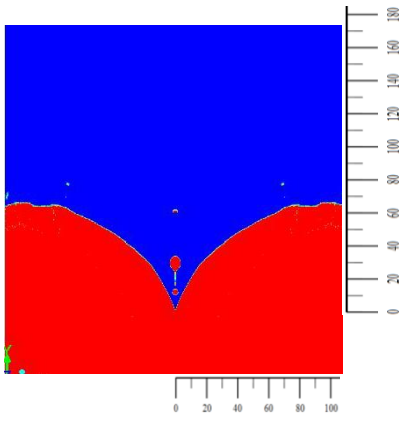

(All dimensions in mm)

In case of twin water jets of 22 L/min impinging on different plate speeds (V_p = 0.6, 1.0, and 1.5 m/s), the wetting fronts radius of the numerical results were compared with the averaged wetting front of the same cases of the UBC ROT experiments. During the experiments, the water impinged over a Plexiglas that has a smooth surface; therefore, the wetting front easily spread on the moving surface whereas in FLUENT, the default material is aluminum that has rougher surface which hinders the spread of the wetting front. Also, this was observed in the amount of the bulge of water that was created ahead of the Int-Z after water wall jets collision. Experimentally, more pool of water was noticed in comparison to the numerical ones. When the plate speed increases, a smaller radius of the numerical wetting front was captured compared to the experimental data as shown in Figure 3.12. During the highest plate speed (V_p = 1.5 m/s), the chance of the bulge of water was suppressed and the wetting front created a small curvature. This flow structure was numerically seen only in case of the lowest plate speed (V_p = 0.6 m/s) with higher slope of wetting front curvature.

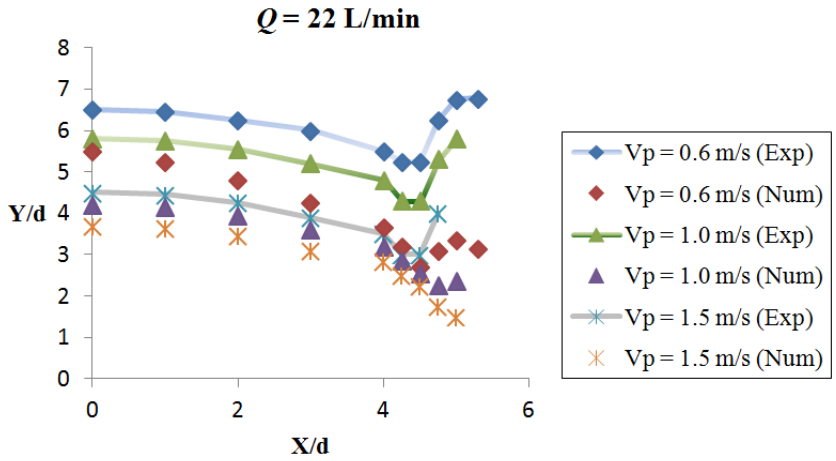

Figure 3.12 Experimental and Numerical Wetting Front with or without Bulge due to Twin Water Jets of 22 L/min Impinging over Different Plate Speeds

3.2.2.3 Water Flow Collision at Interaction Zone

Interestingly, a transition from thin up-wash fountain to somehow thick dome-shape interaction type were observed during UBC ROT 22 L/min experiments due to the promote influence of the moving surface. Actually, these flow behaviors were also numerically captured as shown below in Figure 3.13. When the plate moves with highest speed (V_p = 1.5 m/s), the resulted interaction settles down. As the plate speed increses the interfering water wall jets forms different structures during the collision. Numerically, no splashing was observed, although it was occurred in the experiments; one of the reasons might because of surface condithions (e.g., surface roughness) as disscused before.

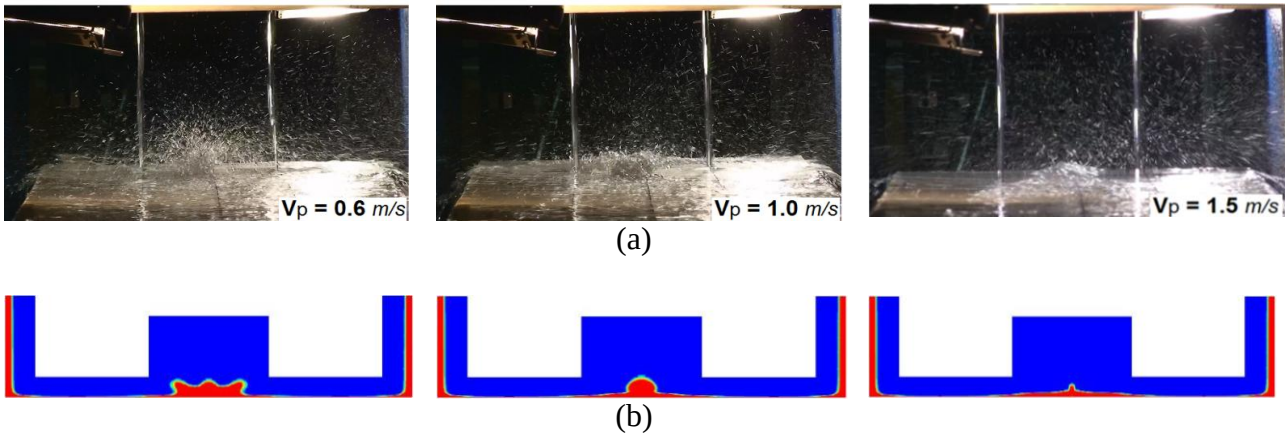

Figure 3.13 Water Wall Jets Interaction Transition of 22 L/min with Different Plate Speeds, (a) Experimental Data [101] (b) Numerical Results

The water flow structure during the collision was observed at the symmetry plane of the interaction zone (Int-Z) by utilizing the VOF contour. Table 3.11 shows the influence of the plate movement on the formation of the interaction of water wall jets after collision. During the fastest plate speeds (V_p = 1.0 and 1.5 m/s), the water takes longer time to reach to the Int-Z plane and the collision happens later. In addition, most of the water accumulation occurs at the downstream side towards the exit of the domain.

However, in the case of the lowest plate speed (V_p = 0.6 m/s), the water layer covers more area at the Int-Z plane and it creates an up-wash fountain compared to a thick film of a dome shapes as were already noticed in the faster moving cases. It is worth mentioning that as the plate speed increases, water jets collision occurs at the downstream zone instead at the middle along the plate direction as in the case of a non-moving impingement surface.

Table 3.11 Water Flow Structures of 22 L/min at Int-Z Symmetry Plane According to Different Plate Speeds

Forth Case (V_p = 0.6 m/s)	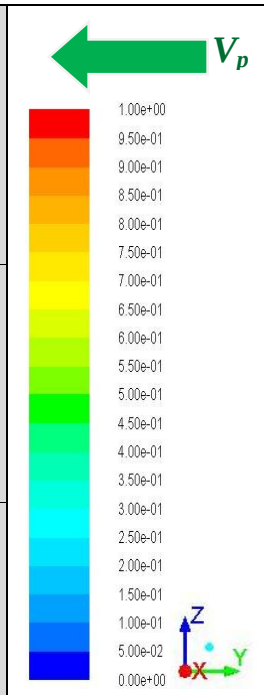	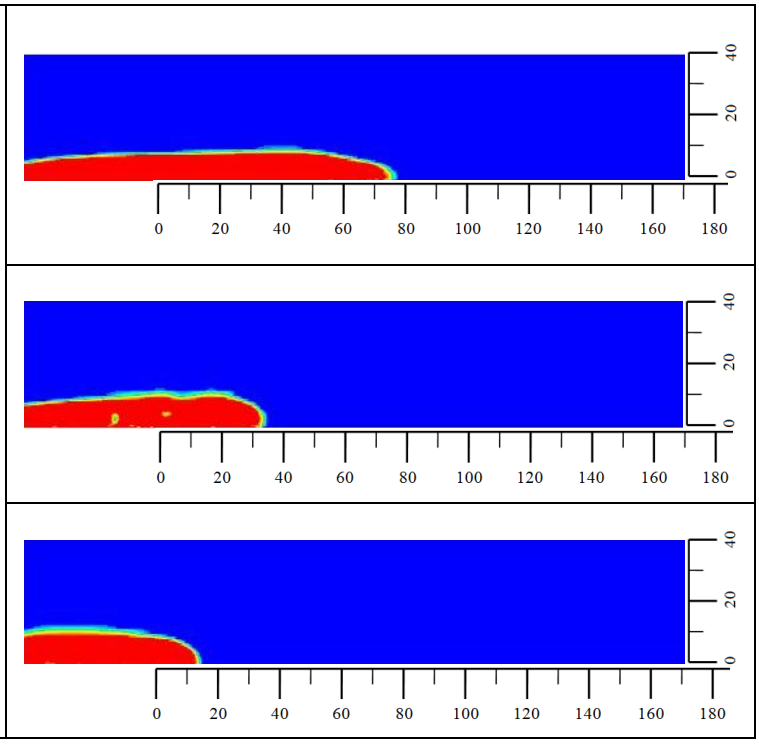
Fifth Case (V_p = 1.0 m/s)		
Sixth Case (V_p = 1.5 m/s)		

(All dimensions in mm)

The plate movement also influences the jet interaction type as shown in Table 3.12 in the case of the highest plate speed 1.5 m/s. From 0.41 sec and after, the water flow structure in Int-Z remains similar until reaches a steady state condition at t = 0.61 sec. In the experiments, the interaction type was settled to upright thick dome-shape and the simulation successfully reproduces this flow behavior even though no splashing was captured.

Table 3.12 Numerical Results for Water Jets Interaction of 22 L/min over 1.5 m/s

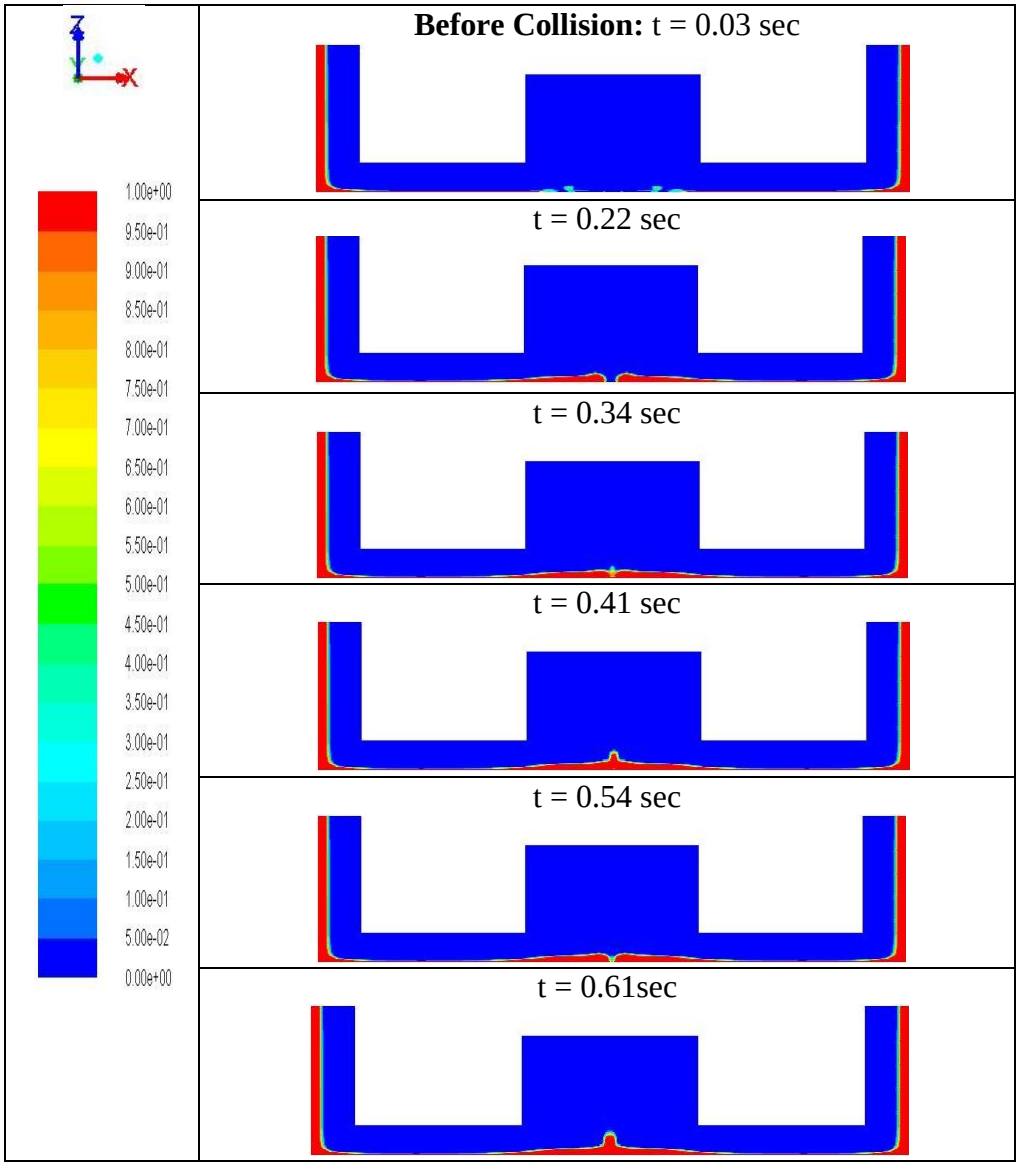

3.2.3 Twin Jets of 30 L/min

3.2.3.1 Wetting Front Development

Increasing the amount of flow rate from 15 L/min to 30 L/min implies that double amount of water poured on the moving substrate and so thicker water film covers the surface quicker. Actually, the increment of flow rate is one of the trial and error methods done by steel making industries in order to ensure that the water layer largely covers area of the steel plate surface as much as possible so that a uniform cooling of the heated steel strip occurred. Table 3.13 illustrates the simulated wetting front configuration and hydraulic jump formation in the case of 30 L/min flow rate impingement at symmetry jet plane. It was revealed that the wetting front propagation of the water film behaves similar to the previous cases of lower flow rate (15 L/min).

However, the distance of the wetting front from the impingement point is bigger than before since the amount of water increases to double or the wall jets has much higher momentum. Even in the case of the lowest plate speed (V_p = 0.6 m/s), the impingement water film has the velocity to flow further radially far from the impingement point at the upper region in +Y direction due to huge amount of water. Also, the wetting zone is enlarged more and more along the jet symmetry plane but the hydraulic jump at the wetting front is low height in comparison to the other plate speeds. In contrast, the faster moving plate (velocity ratios V_p/V_j = 0.57 and 0.85) contracts the wetting front closer to the impingement point.

Table 3.13 Wetting Front and (HJ) Configurations of 30 L/min with Different Plate Speeds

Seventh Case (V_p = 0.6 m/s)	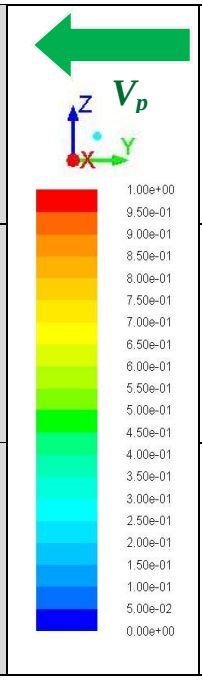	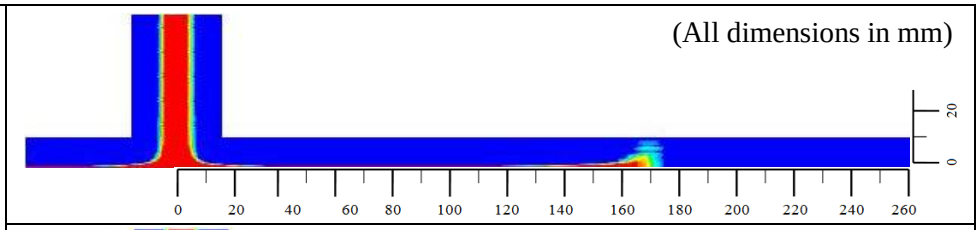
Eighth Case (V_p = 1.0 m/s)		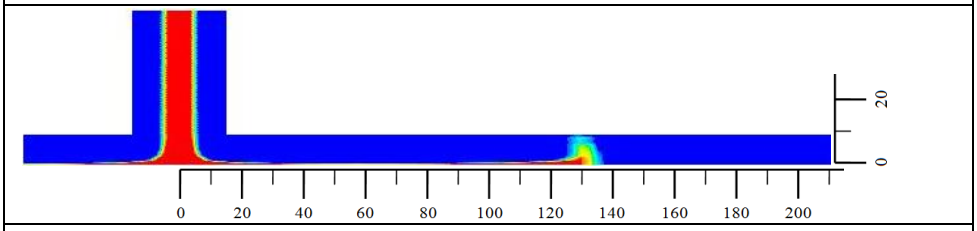
Ninth Case (V_p = 1.5 m/s)		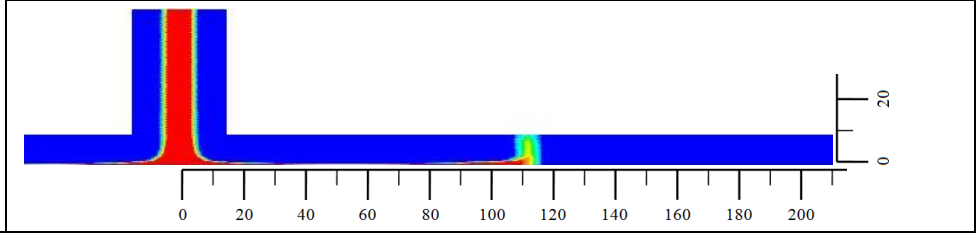

In all of the above cases, very little air backflow was observed. Figure 3.14 illustrates the velocity magnitude contour in the case of the 30 L/min over the highest plate speed 1.5 m/s with the backflow vector highlighted by velocity vector around wetting front. In fact, the water film has high momentum and could push forward against moving wall and less chance is remained for huge air backflow to occur and accelerate. In the 15 L/min respect to 30 L/min (Table 3.5 and Figure 3.14), there is much more air, therefore, air flow is easily detected for the 15 L/min case over the plate surface.

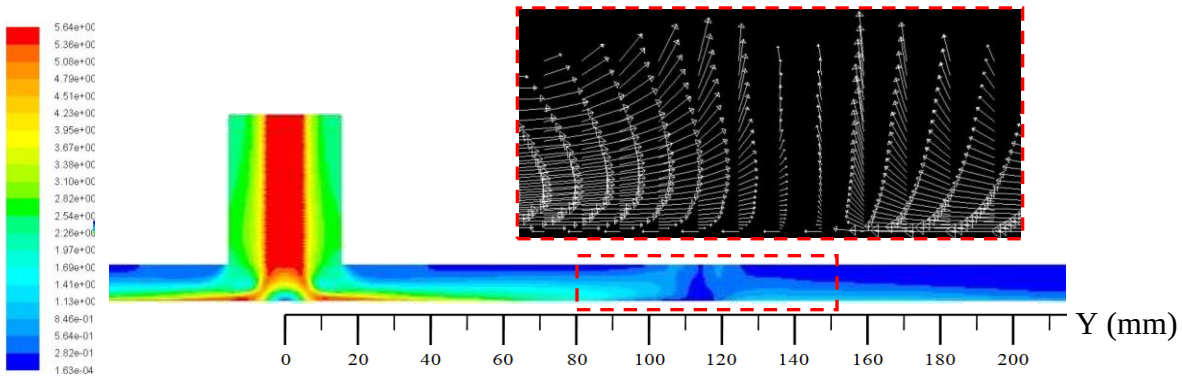

Figure 3.14 Velocity Magnitude Contour in the Case of 30 L/min over 1.5 m/s Plate Speed

3.2.3.2 Water Flow Impingement Spreading

Basically, the impingement water covers larger area of the plate surface in 30 L/min cases compared to 15 and 22 L/min jets impinging on same plate speed. Also, the water spreads much quicker over the surface since the water flow has high momentum (more water amount and higher velocity) and, in turn, could counteract easier the frictional drag from plate surface and develop more. Figure 3.15 shows the water flow propagation of 30 L/min over 0.6 m/s plate speed. As seen in the previous flow rate cases impinging on same plate speed, the water behaves similar to the fixed plate (circular impingement) at the beginning but as the water film propagates further, the moving plate deforms the wetting front and curves it to noncircular shape. Interestingly, an intensified splattering happened during the experiments and this kind of flow was also captured numerically as shown in Figure 3.15.

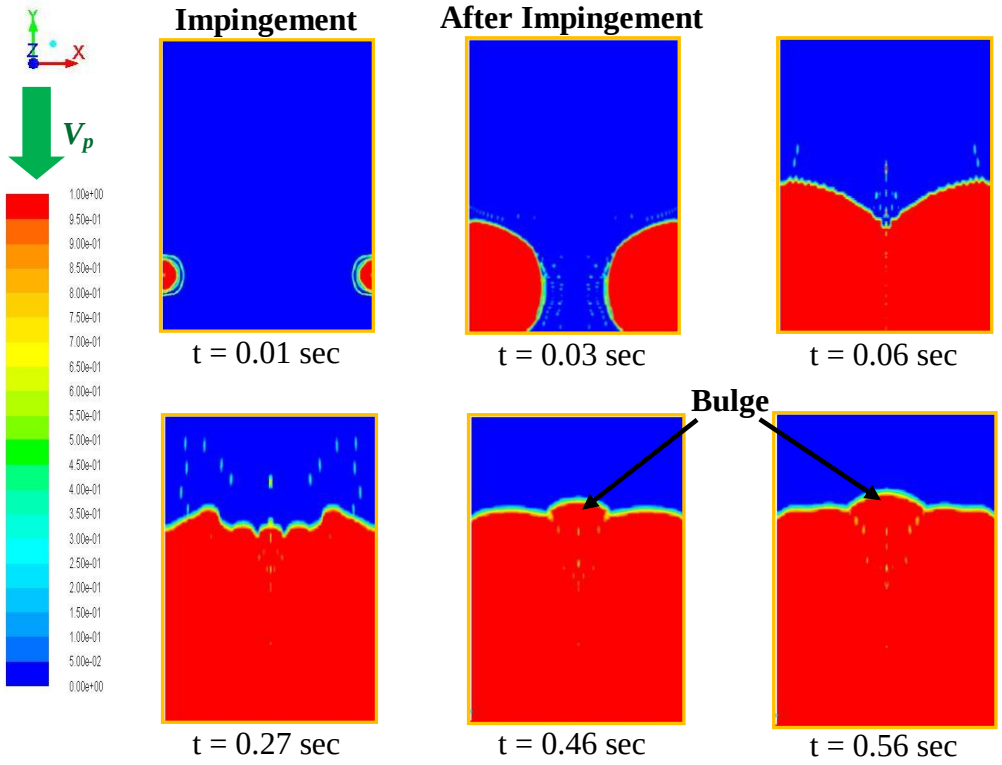

Figure 3.15 Development of Impingement Flow over 0.6 m/s Moving Surface due to 30 L/min Twin Jets

Table 3.14 represents numerical predictions of the water impingement film on top of the moving surface at the three cases of the 30 L/min jets. When the plate speed increases to 1.0 m/s, the flow structure is smoother at early stage of the simulation and later a bulge of water ahead of Int-Z occurs. But, the impingement water does not cover as much area as the lowest plate speed case. Likewise, the water film behaves similarly in the case of the highest plate speed 1.5 m/s, with smaller distance from the stagnation point up to the wetting front location and the bulge. The pool of water at the bulge is chaotic and air mixing into the water is evident as observed in the experiments. Here, the effect of plate motion reduces since the amount of flow rate increases so then the chance to observe the bulge of water is higher. In fact, the wall jets interaction occurs earlier which implies that the bulge will be created at early stage of simulation compared to the other Q = 15 and 22 L/min (Figures 3.7, 3.8 and 3.11).

Table 3.14 Impingement of Water Flow Rate of 30 L/min over Different Plate Speeds

Seventh Case (V_p = 0.6 m/s)	V_p 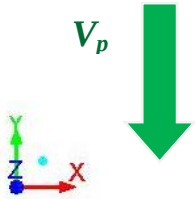	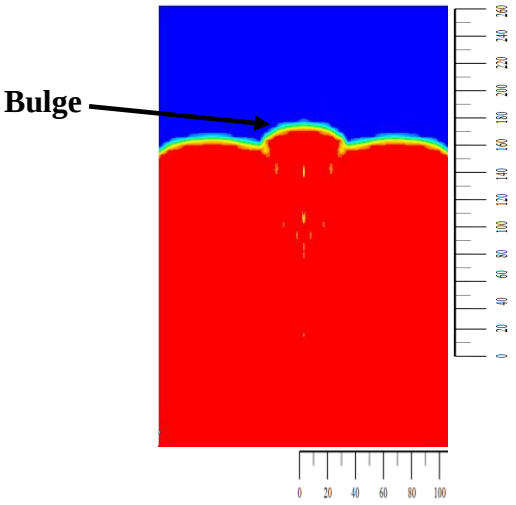
Eighth Case (V_p = 1.0 m/s)	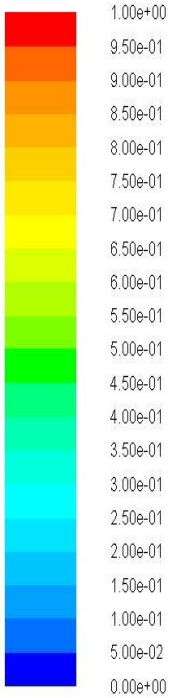	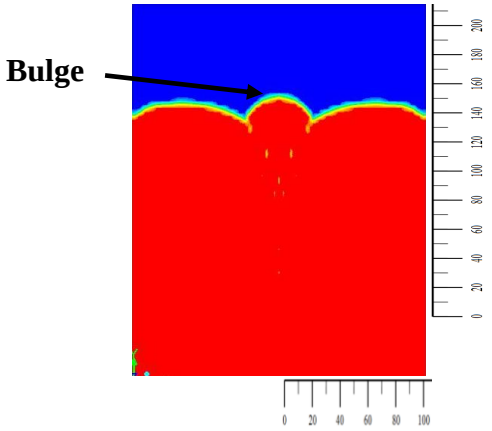
Ninth Case (V_p = 1.5 m/s)		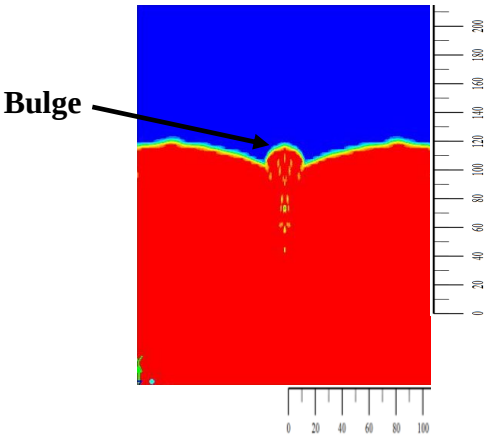

(All dimensions in mm)

Figure 3.16 shows the comparison between the numerical and experimental wetting fronts in case of 30 L/min twin water jets impinging on a moving surface with three speeds (V_p = 0.6, 1.0, and 1.5 m/s). Here, the effect of the moving plate on the wetting front propagation decreases as the amount of flow rate increases (high momentum). The numerical wetting front has a similar radius size to the experimental ones in comparison to the previous cases of Q = 15 and 22 L/min. The occurrence of the bulge of the water ahead of Int-Z was observed experimentally and numerically for all plate speeds. Note that, in case of the lowest plate speed (V_p = 0.6 m/s), the bulge was not shown in the Figure 3.16 because during the experiments, it occurred out of the captured frame of the recorded film. Therefore, the wetting front was measured from the single jet experiments of 30 L/min on 0.6 m/s plate speed which had better captured frame [105]. After collision, the amount of the pool of water has more chance to spread over the Plexiglas test plate during the experiments and creating a higher bulge compared to the numerical solutions. Overall, the numerical outcomes have a better matching with the UBC ROT experimental observations especially when the amount of flow rate increases and the plate speed decreases.

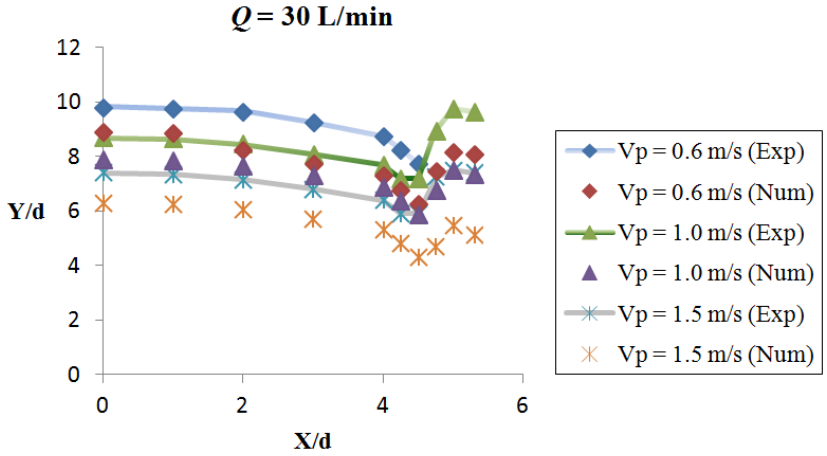

Figure 3.16 Experimental and Numerical Wetting Front with or without Bulge due to Twin Water Jets of 30 L/min Impinging over Different Plate Speeds

3.2.3.3 Water Flow Collision at Interaction Zone

After the water wall jets from impinging 30 L/min parent jets spread and reach the interaction zone and meet each other, the resulted interaction flow rises up highly and makes different interaction type due to the amount of flow and speed of the inflows. Table 3.15 illustrates the formation of the interaction flow during the collision over the fastest moving plate (V_p = 1.5 m/s). The water flow behaves chaotically and is fully unstable. This is not seen in the cases of the 22 L/min due to much less powerful water wall jets inflow to the interaction zone even though the plate speed is preserved (Figure 3.9). Therefore, up-wash fountain like interaction is produced where is in parallel to fountain interaction type observed in the ROT UBC experiments.

Table 3.15 Numerical Results for Water Jets Interaction of 30 L/min over 1.5 m/s

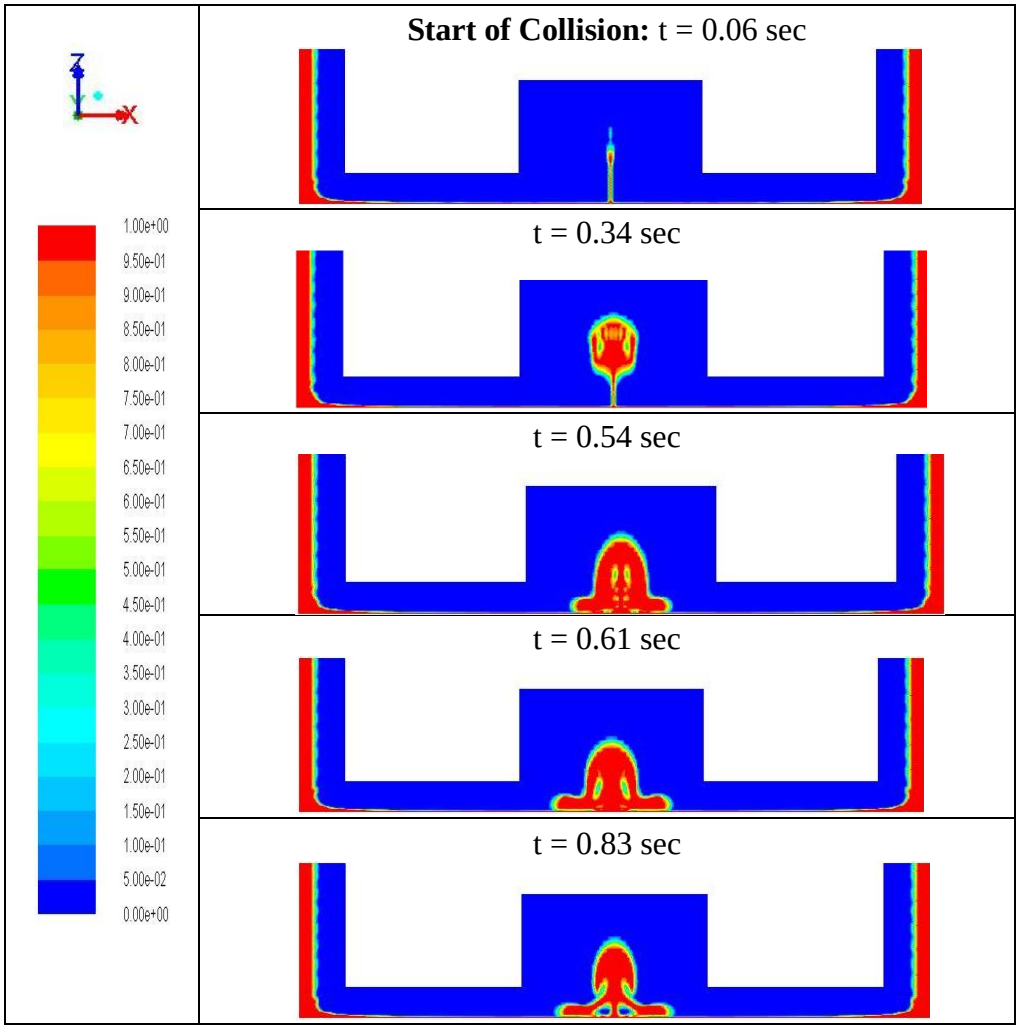

3.3 Velocity in Symmetry Planes

3.3.1 Along Jet Symmetry Plane

In order to adequately investigate the flow velocity profiles of this very thin impingement water film over a moving surface within different speeds, one can draw a chart showing its relationship with respect to its position. At jet symmetry plane, the velocity Y-components (V_y) of 15, 22 and 30 L/min twin water jets were found at different distances (z) above the moving surface with speed of 0.6 m/s, for example. Figure 3.17 illustrates the normalized V_y/V_{imp} velocity profiles with respect to the normalized radial displacement r/d_j along Y-direction. After impingement, at the stagnation point the flow velocity becomes stagnant (zero velocity). Then, at impingement zone, it linearly increases while spreads out radially in both directions (e.g. positive and negative Y directions). This kind of linear variations were also observed during the Stevens and Webb experimental study [17] and compared with 15 L/min, for example. Equation (1.3) can be used to get the linear profile with dimensionless radial velocity gradient $B \approx 1.83$ and $-0.5 \leq r/d \leq 0.5$. Note that, the impingement zone size is smaller in the case of the short jet impinging on a fixed plate. Also, in our cases (long jet), the dimensionless radial velocity gradient B was almost double. After that, at parallel zone, it decreases until reaches to the impingement velocity value. However, due to the wall moving, the velocity variation is not the same at upstream (+Y direction) and downstream (-Y direction). The velocity gradient is smaller at the upstream region compared to downstream region since the water is flowing against to the moving plate direction. Consequently, this kind of variation may cause non-uniform heat dissipation at the impingement zone in case of cooling of moving heated surface. Therefore, it is always important to accurately size the impingement zone since it has a direct effect on the amount of heat that needs to be removed. The influence of the horizontal moving target on the wetting front development is more pronounced at z = 0.1 mm especially for low flow rate 15 L/min. But, as the amount of flow rate increases, the effect of moving plate becomes much lesser since the water wall jet has higher momentum. As seen before in Tables 3.4, 3.9 and 3.13, the wetting front (HJ) configuration was captured by VOF contours. For each different plate-to-jet velocity ratio, the wetting front and HJ were changed accordingly in terms of position and structure. The hydraulic jump of a round shape front tip was commonly observed in all cases due to the surface tension. In addition, after the hydraulic jump takes place a negative velocity (air backflow) was seen

since the plate moves opposite to the flow streamline direction. As the jet velocity decreases, the plate has the ability to push the flow more back within its direction along the negative Y-axis. In case of 15 L/min, the water has a very thin layer and the free-surface stands almost at z = 0.2-0.5 mm. Also, in case of 22 L/min, the water film has a moderate thickness where the free-surface as high as about 0.5-1.0 mm. In contrast, when the water has flow rate of 30 L/min, a thick layer was generated and the free-surface becomes higher in between z = 1.0-3.0 mm.

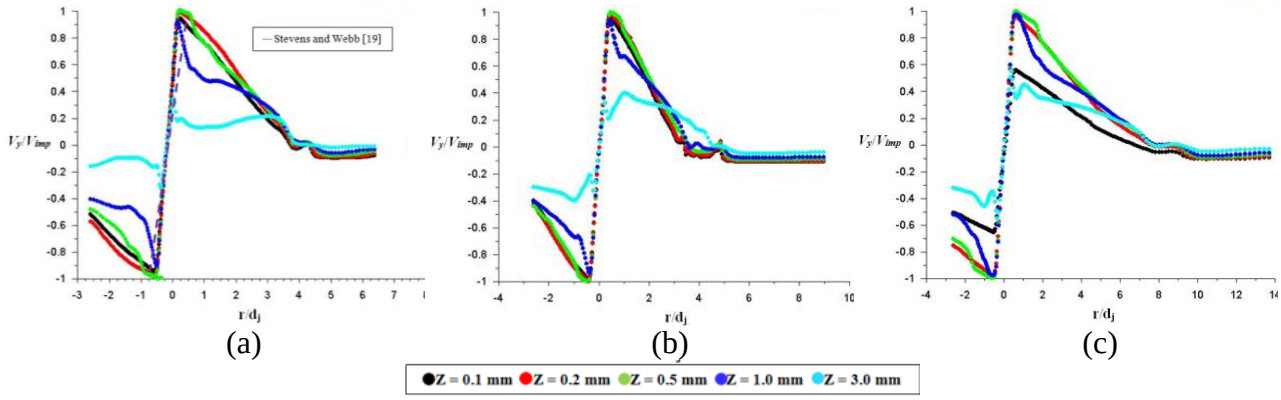

Figure 3.17 Velocity at Y-direction along Jet Symmetry Plane on Moving Plate V_p = 0.6m/s, (a) Q = 15 L/min (b) Q = 22 L/min (c) Q = 30 L/min

After observing the alterations of wetting front (WF) due to the effect of different flow rates impingement on a moving plate of same speed, we shall discuss the influence of plate motion with different speeds (V_p = 1.0 and 1.5 m/s) with a fixed flow rate 22 L/min. The velocity Y-component of 22 L/min twin water jets impingement is found along jet and Int-Z symmetry planes at different distances (z) above the moving surface with various speeds. Figure 3.18 represents plots of the normalized V_y velocity at jet symmetry plane at different z elevations. The flow velocity behaves similarly as seen before at the impingement and parallel zones with some difference in the HJ location and structure. As the plate speed increases, the wetting front becomes closer to the impingement point (e.g. smaller radius r/d_j such as: ~$3.5d_j$ and ~$3d_j$ for V_p = 1.0 and 1.5 m/s, respectively) see Table 3.9. Also, a thicker HJ was established with a reverse velocity in case of moving plate with speed of 1.5 m/s. In other words, due to the frictional force initiated by the moving plate that overcomes the impingement water flow momentum, a negative velocity occurs at the elevated wetting front known as HJ. At the parallel zone, the water layer is

very thin respect to the sudden jump of thicker layer where the free-surface in both cases looks similar as high as in range of 0.5-1.0 mm.

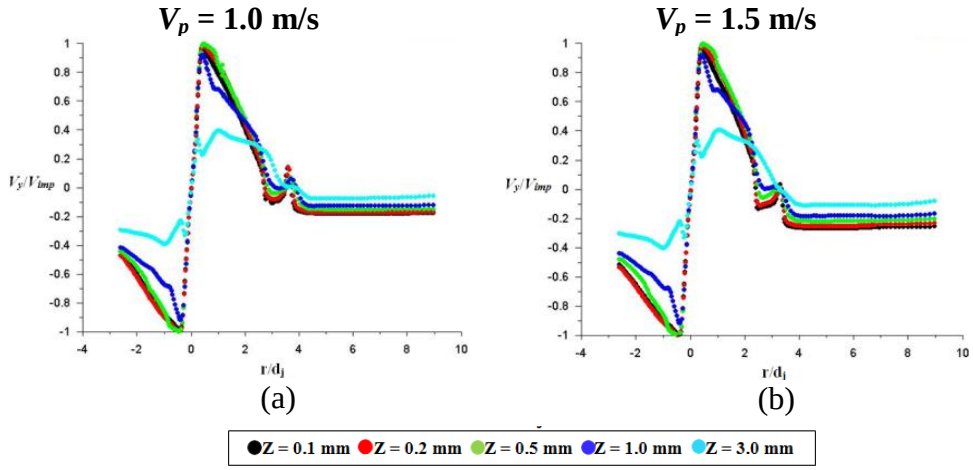

Figure 3.18 Velocity at Y-direction along Jet Symmetry Plane of 22 L/min Twin Jets on Moving Plates

3.3.2 Along Interaction Zone Symmetry Plane

At Int-Z symmetry plane, the velocity Y-components (V_y) at different elevation of the previous cases were plotted in order to examine the effect of moving plate on the formation of wall jets interaction. In all cases, the velocity increases with negative values (-Y direction) at downstream zone and then continues to increase at upstream zone until about $2d_j$. In cases of 22 and 30 L/min, the velocity was fluctuating at the downstream zone as assign of chaotic flow structure but it was very calm in case of low flow rate. Beyond $2d_j$, the flow velocity jumps up in case of 15 L/min and then sharply drops corresponding to the dome-shape interaction type (Figure 3.19a) but in case of 30 L/min, a higher jump was noticed due to the up-wash fountain kind of interaction (Figure 3.19c). Then a sharp drop occurs in case of 15 L/min respect to 30 L/min. However, in case of 22 L/min, the velocity variation behaves somehow similar to 15 L/min (Figure 3.19b). The only difference is that the flow velocity is unstable downstream after the wall jets of higher momentum start colliding and result a transient kind of flow.

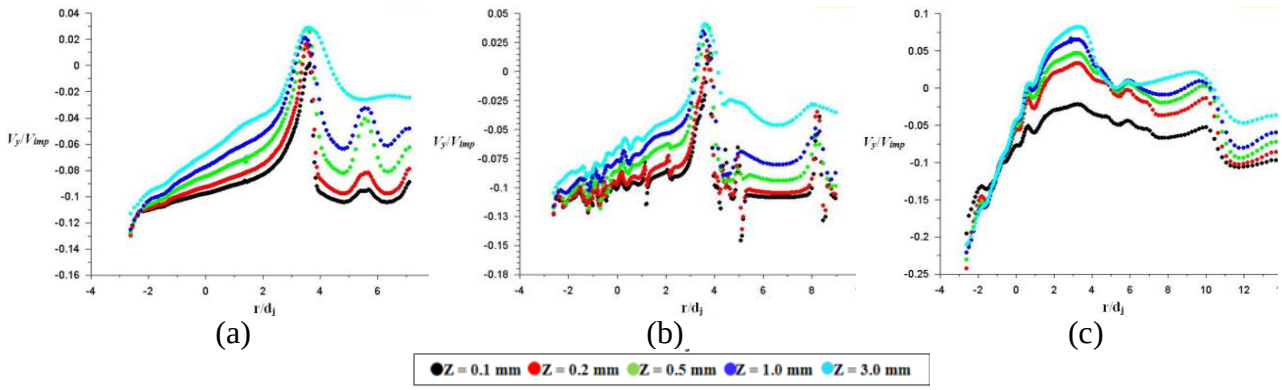

Figure 3.19 Velocity at Y-direction along Int-Z Symmetry Plane on Moving Plate V_p = 0.6m/s, (a) Q = 15 L/min (b) Q = 22 L/min (c) Q = 30 L/min

According to this variation, different flow velocity V_y profiles at the Int-Z symmetry plane was observed as shown by VOF contours in Figure 3.20. The accumulated water at Int-Z becomes thicker as the amount of flow rate increases. The water flow wetting front upstream distance at the Int-Z symmetry plane is a bit smaller in both cases of 15 and 22 L/min respect to the WF location at the jet symmetry plane. This is due to the motion of plate that alters the circular shape and curves it to non-circular spot. Nevertheless, in case of higher amount of water as 30 L/min, different scenario was seen, where the WF has longer upstream distance at Int-Z symmetry plane compared to jet symmetry plane. Actually after wall jets interaction takes place, a bulge of water a head of Int-Z is created so then it pushes the WF even further towards the upstream zone.

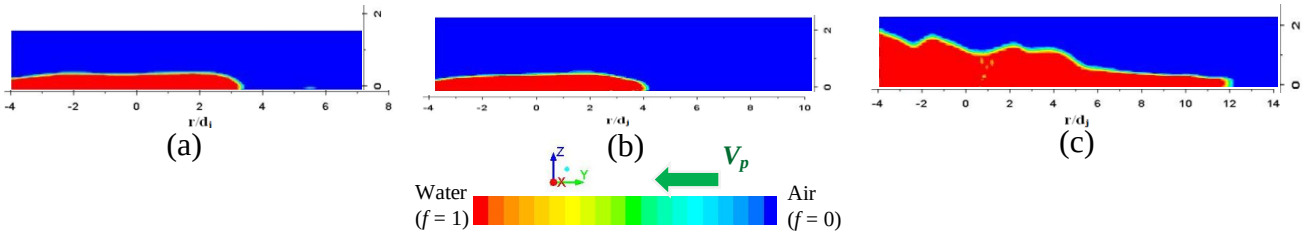

Figure 3.20 VOF Contours at Int-Z Symmetry Plane on Moving Plate V_p = 0.6m/s, (a) Q = 15 L/min (b) Q = 22 L/min (c) Q = 30 L/min

Generally, as the amount of flow rate changes, different interaction types were captured after the water wall collide with the Int-Z plane. For example, a thick dome-shape interaction type was observed in case of 15 L/min; however, a thin tilted fountain when the amount of flow

rate was changed to 22 L/min and a thin up-wash fountain interaction type was captured in case of the high flow rate of 30 L/min (Figure 3.21a). Actually, this is in a good agreement with the UBC ROT experimental observations. In order to evaluate the behavior of resulted interaction, different velocity vectors were plotted for each case as shown in Figure 3.21b. These velocity vectors clearly illustrate the water flow circulation (highlighted by a dotted-green rectangular) as an indication of its chaotic behavior. When the amount of flow rate was low as 15 L/min, the resulted interaction was not strongly fluctuating as much as seen in cases of 22 and 30 L/min. As the amount of water increases, the water flow momentum increases accordingly. Thus, when wall jets reach to the interaction zone, they still have enough energy even though the moving plate exerts a frictional force. On the other hand, as the flow rate decreases so then the impingement water has thin layer and low momentum. Therefore, the wall jets are not able to survive the drag force caused by the moving plate and they become almost tired when they reach to their destination (Int-Z).

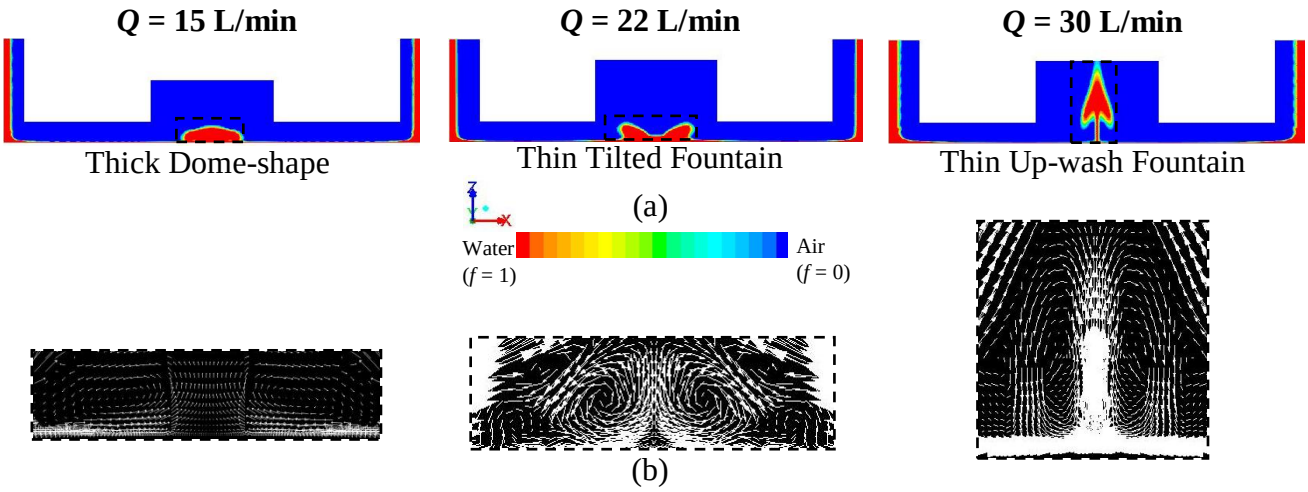

Figure 3.21 Different Interaction Type of Twin Water Wall Jets on a Moving Plate V_p = 0.6m/s, (a) VOF Contours (b) Velocity Vectors

Interestingly, the plate motion also controls the wall jets interaction type in case of 22 L/min as shown in Figure 3.22. In both cases, the normalized velocity highly fluctuates downstream and part of upstream regions. The portion of downstream zone is shorter in case of faster plate speed 1.5 m/s that forces the water film layer to flow within its direction and drains it out the solution domain (Figure 3.22b). Moreover, the height of the resulted wall jets interaction

is a bit higher in case of moderate plate speed 1.0 m/s at the middle (at around $0d_j$). For instance, when the plate moves with speed of 1.5 m/s, less amount of water layer reaches to the Int-Z plane and it is forced and drained out towards the downstream zone with the moving surface direction (Table 3.11). According to this alteration, the wall jets interaction transfers from type to other. For example, a thin tilted fountain was seen in case of low plate speed (refer to Figure 3.21a); but, as the plate speed increases a thick dome-shape interaction type was captured (Figure 3.13). This kind of transformation was also observed experimentally by the UBC ROT group. The depth of the dome-shape interaction type is a bit lower in case of fastest plate speed respect to the experimental observations due to the insert of the Int-Z symmetry plane. During the experiments the collision happened between fluid-fluid wall jets; however, in case of simulation and according to the minimized model, the water wall jet interacts with the vertical dry wall. Overall, the numerical outcomes are in good qualitative agreement with the UBC ROT experimental data.

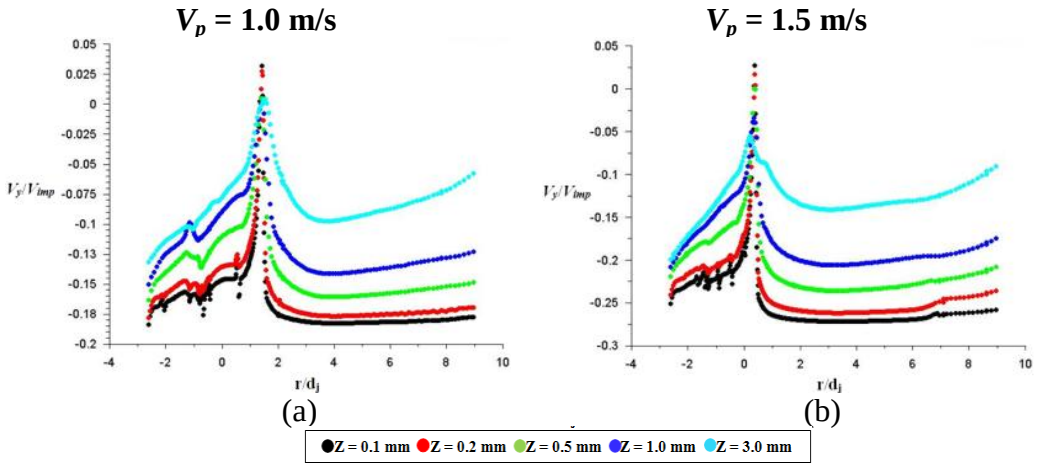

Figure 3.22 Velocity at Y-direction along Int-Z Symmetry Plane of 22 L/min Twin Jets on Moving Plates

3.4 Pressure Profiles at Impingement Region

After the water jet impinges the moving surface, it becomes stagnant and the high pressure value takes place at the stagnation pressure (P_{stagn}) and then the pressure monotonically drops as the water spreads out radially. Figure 3.23 shows the normalized pressure with respect the normalized radial distance for different flow rates Q = 15, 22, and 30 L/min at z = 0.1 mm

above a moving plate of speed V_p = 0.6 m/s, for example. For all flow rates, at the impingement zone the numerical pressure profiles are similar with slightly high value at the stagnation point as the flow rate increases.

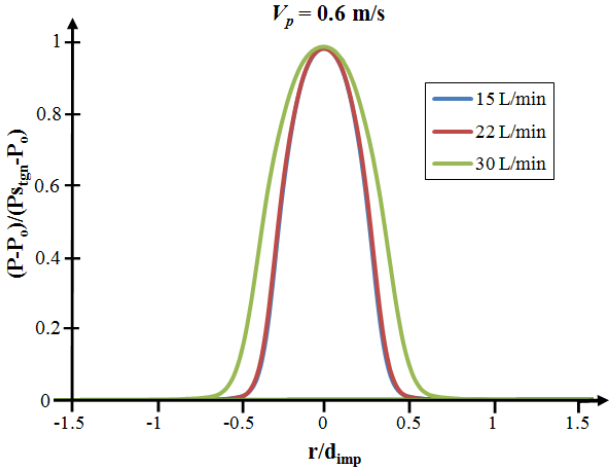

Figure 3.23 Pressure Distribution above a Moving Plate (V_p = 0.6 m/s) of Different Flow Rates

Table 3.16 represents a comparison between analytical and numerical results of different flow rates at the stagnation point. The analytical solution can be found based on Bernoulli's equation (1.4) at the center of the plate (r = 0). The stagnation pressure (P_{stagn}) has great influence on the local saturation temperature (T_{sat}) of water in case of heated plate. The T_{sat} is usually assumed to be about 100^{o}C in case of ambient pressure (P_o = 101,325 Pa). In our numerical simulations, for all different flow rates, the stagnation pressure was at least 85% higher than the atmospheric pressure. Although the size of the impingement zone is smaller than the parallel zone, it has more impact on the overall dissipated heat and the highest heat transfer coefficient would be expected at the impingement zone that is characterized by high stagnation pressure value and high velocity gradient *B*.

Table 3.16 Analytical and Numerical Comparison of Velocity and Pressure at Stagnation Point

		Analytical Calculations		**Numerical Results**	
Q (L/min)	**V_j (m/s)**	**V_{imp} (m/s)**	**P_{stgn} (Pa)**	**V_{imp} (m/s)**	**P_{stgn} (Pa)**
15	0.88	5.49	116367.9	5.44	116325
22	1.29	5.58	116848.5	5.54	116825
30	1.76	5.70	117540.8	5.64	117425

3.5 Conclusion

The nine cases of the 15, 22, and 30 L/min flow rates and three plate speeds (0.6, 1.0, and 1.5 m/s) were discussed and compared based on the numerical results of the wetting front propagation and hydraulic jump configuration over the plate surface, water impingement flow development at the jet symmetry plane, and the water wall jets collision at the symmetry interaction plane as well as the interaction zone. Remarkably, significant air backflow was observed in the case of the lowest flow rate 15 L/min over higher plate speeds 1.0 and 1.5 m/s. Also, a very strong pressure fluctuation was depicted outside the wetting zone along the +Y direction. As the plate speed increases, the wetting front becomes closer to the impingement zone. When the amount of flow rate increases, a better correlation between numerical WF and experimental WF was obtained.

At the impingement zone, the velocity profile was linear for all flow rates and the dimensionless radial velocity gradient B was almost double the value in case of short jet. The highest pressure took place at the stagnation point and was at least 85% higher than the ambient pressure. Validation of numerical results with the experimental data conducted by the UBC ROT group showed good qualitative agreement in terms of water jets interaction. The two types of interaction: thick dome-shape and thin up-wash fountain were numerically captured. Interestingly, during the cases of 22 L/min over the three different plate speeds, the interaction type transfers from thin up-wash structure to calm dome-shape one due to the influence of the horizontal moving surface which is in-line with the experimental observations.

Chapter 4: Summary, Conclusion and Future Works

ROT cooling is a crucial stage in steel making industries since it affects the quality of the final product in terms of mechanical and metallurgical properties. This process has been extensively studied by many researchers experimentally and numerically but usually in laboratories conditions and not with industrial scale parameters. However, the UBC ROT group has conducted series of experiments at a ROT facility which is relevant to the industrial scale. The main contribution of this work is to numerically investigate the impingement of twin circular long free-surface water jets on a moving plate. Nine different cases were simulated including three flow rates (Q = 15, 22, and 30 L/min) and three plate speeds (V_p = 0.6, 1.0, and 1.5 m/s) in order to examine systematically the influence of plate motion on the wetting front propagation, HJ configuration, and the wall jets interaction type.

4.1 Summary of the Numerical Results

4.1.1 2-D Model of Single Jet Impinging over a Fixed Plate

A 2-D model was first constructed to gain some insights into the problem, to examine the power of the numerical simulation, and to test the limits of the available computer facilities. Accordingly, the 2-D simulations of hydrodynamics of the long circular water jet impinging on a stationary plate (axisymmetric condition) were the first attempt in this study. The realizable k-ε model (RKE) turbulent model was utilized with non-equilibrium wall treatment function. The numerical results were analytically validated using equation of free-falling particle and showed a good agreement. In addition, the Volume of Fluid method (VOF) method was used to capture the water film development before and after impingement and following wetting front (HJ) over the target horizontal plate. Mesh refinement was necessary especially near the wall where the water film thickness of order (0.1) mm forced an increase in the number of cells and required much higher CPU time. The corresponding inlet profiles (axial velocity, VOF flow fraction, k and ε turbulent quantities) were obtained from the 2-D simulations and used in the final 3-D simulations.

4.1.2 3-D Model of Twin Jets Impingement over a Moving Plate

In the case of the moving plate, only three-dimensional model will sufficiently represent the problem since the water film flows asymmetrically upstream and downstream of impingement point and due to the non-wetting and wetting areas over the moving surface. The computation domain for the 3-D model has been chosen and dimensioned carefully to have optimum size and number of cells. For instance, the jet exit was considered at H = 50 mm above the plate and the input from a 2-D analysis was used as a boundary condition for the inlet velocities. Furthermore, the two nozzles are assumed to have same flow rates and so the wall jets have equal momentum as they meet at midway distance along jet-to-jet space (S). Accordingly, the domain was reduced to half of the full 3-D model which significantly reduced the number of cells. These assumptions practically reflect an array of jets perpendicular to the plate moving direction and satisfy equation (1.4) due to equal jets momentum [49].

Finally, the mesh was created, tested and refined in accordance with each case of flow rate and plate speed (Q, V_p) separately. It was observed that more cells were required as the plate speed increases especially near the moving wall to avoid intermittency of the water impingement flow and to smoothly capture the thinning film of order less than 0.1 mm. This led to significant increase in CPU time and memory requirements. Actually, the fluid flow has different conditions upstream and downstream which leads to separate and local mesh adaption rather than same overall adaption for the whole domain. Moreover, mesh refinement for such kind of transient simulation requires monitoring and checking intermittent results frequently as the impingement flow spreads over the moving surface. The mesh refinement was achieved gradually with the objective of coming up with the optimized number of cells that would be capable to resolve the discontinuity issue at impingement flow which was seen in low jets Q (15 and 22L/min) and high V_p (1.0 and1.5 m/s). At each time the value of y^+ was monitored to be $5 < y^+ < 10$. However, this range for y^+ implies a very fine mesh near that wall which led to more demands and constraints with the available computation facilities.

The k-ε turbulent model (RKE) may provide reasonably accurate results for the above problem. This model was verified by monitoring the spreading of water impingement film from different perspectives (jet symmetry plane, plate surface, and the symmetry interaction zone) and by investigating wetting front as well as hydraulic jump configuration and the interaction types.

Overall, the plate motion clearly influences the flow impingement structures and development at all over the domain and also the height of the HJ.

For the nine cases considered, different water layer develop at the Int-Z symmetry plane which give more insights about the interaction location as well as the flow structure after collision. The final results are in good agreement with the experimental data. In the case of low flow rates (Q = 15 L/min and 22 L/min) and higher plate speeds (V_p = 1.0 m/s and 1.5 m/s), some splattering was detected at the early stage after impingement. Water layers form gradually at the interaction plane and become thicker creating a shape like a dome. This kind of results does not, however, indicate that we may be able to capture the experimental splatter realized in our experiments. When the jets flow rates increase to 30 L/min, the formation of interaction water was accelerated much earlier with a very intensive splashing regardless of plate speed. Next, a thin up-wash fountain with reduced height occurred at downstream side (along –Y direction).

Interestingly, in experiments of 22 L/min over faster moving plate, the interaction water film was observed that the type of interaction transfers from up-wash shape to another in accordance with the plate speed. In the numerical simulations, this transfer behavior was also reproduced and depicted using the VOF contours and showed a good agreement with those experimental observations. As the plate speed increases the wetting front is restricted much closer to the impingement point and, in turn, distorted excessively the wetting zone. The moving plate elongates the wetting zone along moving direction (i.e. +Y direction) as much as possible at the downstream zone and contracts it on other direction and shapes it noncircular. This affects the heat transfer in the case of the heated plate. In fact, the water film temperature rises up after spreads over the heated plate (in parallel zone in both upstream and downstream) and then the hot water is pulled more toward the incoming jet and interacts with the fresh incoming water. On the other hand, the plate movement makes the free-surface of thin impingement film in upstream wavy and promote the recirculation and turbulence which can increase the convection heat transfer. It should be noted that the location of the next jets array should be adjusted accordingly in order to ensure that the impingement water can cover all the plate surface area between the two successive jets array. In addition, the simulations of high velocity ratio of plate-to-jet (15 and 22 L/min jets on 1.0 and 1.5 m/s plate speeds) cases indicate that collisions were delayed and most of water impingement film is transferred to downstream region and exits the solution

domain faster. So, the nozzle space along the jets array should be adjusted accordingly to ensure that the water covers all the plate width so then a uniform heat transfer is properly achieved.

When the plate-to-jet velocity ratio decreases the impingement water flows easier over the moving surface as seen in the case of the highest flow rate 30 L/min with lowest plate speed of 6.0 m/s. The impingement water creates unsteady irregular shape over the moving plate at early stage of the simulation and, then, it took time to form the noncircular shape. The wetting front was not pulled as much (as other cases) towards the stagnation zone since the water wall jets has much more momentum and the impingement water film covers larger area of the upstream region. This is a desired phenomenon since it enhances extraction of more heat flux from the plate surface.

4.2 Conclusions

The main outcomes of this may be summarized in the following points:

- The realizable k-ε turbulent (RKE) model showed a good performance with the aid of non-equilibrium wall treatment function to model jet impingement and interaction hydrodynamics.
- The volume of fluid method (VOF) is capable of tracing the wetting front and/or hydraulic jump (HJ) contours and jet interaction hydrodynamics. Careful attention should be paid to the mesh refinement to aid in getting reliable results.
- Even with careful consideration of model reductions and simplifying assumptions, the 3-D simulations are very lengthy (some take more than a month) with parallel processing capability and FLUENT license on a 32-core, 96 MB RAM workstation.
- During this kind of transient simulations, tangible and smart control on mesh refinement is required gradually and regionally to minimize the total number of cells. For instance, the mesh was clustered towards the target plate to provide appropriate wall y^+ value to maintain continuity of spreading thin impingement flow in wetting zone and nearby. Wetting zones covers different portions of moving surface and each case needs unique mesh refinement.
- As the plate speed increases, the mesh refinement near to the wall based on the y^+ value (5 to 10) is necessary to avoid discontinuity in the spreading impingement water film; the

intermittency occurred frequently in the cases of low flow rates (15 L/min) over highest plate speeds (V_p = 1.0 and 1.5 m/s).

- The plate motion and flow rate have noticeable impact on the averaged velocity and pressure profiles especially with low flow rate (Q = 15 L/min). Also, a large air backflow and pressure fluctuation were captured with higher plate speed (V_p = 1.5 m/s).
- At the impingement zone, the velocity profile was linear for all flow rates regardless the plate speed. Also, the dimensionless radial velocity gradient (B) was twice the value of short jet (nozzle exist close to the plate).
- The highest pressure value was captured at the stagnation point. This value sharply drops to ambient pressure as the water spreads out radially. It was found that, this local pressure is at least 85% higher than the ambient pressure which enhances the local saturation temperature of water and maximizes the cooling rate at the impingent zone. Many existing correlations assume ambient pressure at stagnation point.
- As the plate speed increases, the wetting front forced to create a noncircular shape. When the amount of flow rate decreases and the plate speed increases, the wetting front has a smaller radius and becomes closer to the impingement zone.
- The type of water wall jets interaction is highly influenced by the amount of flow rate and the plate speed. Two different interaction types namely, thick dome-shape and thin up-wash fountain were successfully captured numerically through VOF contours. Also, after the collision, the wall water jets create a central pool of water and then a bulge of water film grows ahead of Int-Z. In the case of 22 L/min, the moving plate triggers the transition of jets interaction type to thick dome-shape and reduces the splashing. Overall, the numerical results are in a good agreement with the experimental data of the UBC ROT experiments.

4.3 Recommendations and Future Works

The main contributions of this study are to evaluate the water flow structure at two particular zones namely: the parallel zone and the interaction zone. Studying the multiple water jets impinging on moving plate in industrial scale is valuable due to its relevance to the industrial

applications. In order to assist for better understanding of this complex problem, the following points are suggested for the future works:

- In this thesis, the available computational domains were simplified as much as possible as though large number of cells is inevitable. The main assumption was based on the fact that the water wall jets meet at the midway jet-to-jet distance, and interacting flows at instant of collision becomes stagnant and then, the joint accumulated flow rises up which is similar to the collision at the interaction symmetry plane (flow with wall). A full three-dimensional computational model for twin jets is recommended if a powerful computational facility (e.g. a cluster with tens of cores which is equipped with FLUENT parallel processing) is available for considerable time in order to better capturing the real water jets interaction. This allows simulation of more real conditions at the collision happened between two wall jets. In addition, full 3-D numerical modeling can handle collision of wall jets with different momentum which occurs if the parent jets have unequal flow rate, either different ones or fluctuating jets Q.
- The mesh refinement is vital particularly in the cases of high V_p and low jets Q to avoid the intermittency in thin impingement water film but in expenses of excessive computation cost (CPU memory and time). So, investigating different turbulent modeling and different mesh treatment is important.
- The realizable k-ε turbulent model (RKE) was utilized due to its low computational cost in comparison to other turbulent models. The k-ω turbulent model (shear-stress transport SST version) is also a candidate. It is more accurate than the RKE model for flow investigation near the wall but it is more demanding on mesh and computational resources.
- The majority of the previous studies were either mostly focused on the heat transfer alone or less on the associated hydrodynamics of jet impingement separately. Hence, the first step in studying these two aspects together is to numerically simulate single jet impinging on the stationary and moving high-temperature plate. This is currently being investigated by a PhD candidate in our group.
- During the simulations some splattering and splashing were captured. This is not an indication of being able to fully capture this behavior since RANS analysis is used. The

splattering should be investigated in more detail since it has adverse impact on the heat transfer process due to the wasted water. Different discretization schemes, turbulent models and the associated grid refinements are required to be adapted accordingly and in a systematic manner to treat this issue and obtain better understanding.

- It is worth finding the material surface roughness for Plexiglas and using this data in the FLUENT to examine its effect on the wetting front propagation, hydraulic jump configuration, and the wall jet interaction including the splashing during the impingement and after the jet collision.

Bibliography

[1] World Steel in Figures, "*World Steel Association*," 2014.

[2] SSAB. (25 July 2003). *Steel Making Process, Processing, Sheet Steel*. Available: http://www.ssab.com/en/Products--Services/About-SSAB/Steel-making-process/Processing/Sheet-steel/.

[3] Tacke, G., Litzke, H., Raquet, E.,. Investigations into the efficiency of cooling systems for wide-strip hot rolling mills and computer-aided control of strip cooling, accelerated cooling of steel, P.D. southwick (ed), pp. 35-54. 1986.

[4] Filipovic, J., Viskanta, R.,Incropera, F. P., "Cooling of Moving Steel Strip by an Array of Round Jets, ," vol. Steel research, 65, pp. 541-547, 1994.

[5] Filipovic, J., Viskanta, R., Incropera, F. P., Veslocki, T. A., "Thermal Behaviour of a Moving Steel Strip Cooled by an Array of Planar Jets, *Steel research*, ," vol. 63, pp. 438-446, 1992.

[6] Viskanta, R., Incropera, F. P., "Quenching with Liquid Jet Impingement, In: Tanasawa I, Lior N (eds) *Heat and Mass Transfer in Materials Processing*, Hemisphere Publishing New York," pp. 455-476, 1992.

[7] Wolf, D. H., Incropera, F. P., Viskanta, R., "Jet Impingement Boiling, *Advances in Heat Transfer* ," vol. 23, pp. 1-132, 1993.

[8] Bohr, T., Dimon, P., and Putkaradze, V., "Shallow-Water Approach to the Circular Hydraulic Jump, *J. Fluid Mech.* ," vol. 254, pp. 635-648, 1993.

[9] R. Godwin, "The Hydraulic Jump Shocks and Viscous Flow in the Kitchen Sink, *Am. J. Phys*. ," vol. 61, pp. 829-832, 1993.

[10] Brechet, Y., and Néda, Z., "On the Circular Hydraulic Jump, *Am. J. Phys*." vol. 67, pp. 723-731, 1999.

[11] F. C. Kohring, "Water all Water-cooling Systems, *Iron and Steel Engineer* ," pp. 30-36, 1985.

[12] Liu, X., Gabour, L.A., Lienhard V, J.H., "Stagnation-Point Heat Transfer during Impingement of Laminar Liquid Jets: Analysis Including Surface Tension, *J. Heat Transfer* ," vol. 115, pp. 99-105, 1993.

[13] Stevens, J., Pan, Y., and Webb, B. W., "Effect of Nozzle Configuration onTransport in the Stagnation Zone of Axisymmetric Impinging Free-surface Liquid Jets, Part 1: Turbulent flow structure, *J. Heat Transfer* ," vol. 114, pp. 874-879, 1992.

[14] Liu, X., Lienhard, J. H. V., and Lombara, J. S., "Convective Heat Transfer by Impingement of Circular Liquid Jets, *J. Heat Transfer* ," vol. 113, pp. 571-582, 1991.

[15] Ma, C. F., Zhao, H. Y., Sun, M., and Gomi, T., "Analytical and Experimental Study on Impingement Heat Transfer with Single-phase Free-surface Liquid Jets, *J. Thermal Science*," 1995.

[16] Yonehara, N., Ito, I., "Cooling Characteristics of Impinging Multiple Water Jets on a Horizontal Plane, *Tech. Rep. Kansai Univ.* ," vol. 24, pp. 267-281, 1982.

[17] Stevens, J., Webb, B. W., "Measurements of Flow Structure in the Stagnation Zone of Impinging Free-surface Liquid Jets, *Int. J. Heat Mass Transfer*," vol. 36, pp. 4283-4286, 1993.

[18] Whelan, B. P. and Robinson, A. J., "Nozzle Geometry Effects in Liquid Jet Array Impingement, *Applied Thermal Eng* ," vol. 29, pp. 2211-2221, 2009.

[19] Barata, J. M. M., Sousa, N. M. S., Silva, A. R. R., Meireles, P. M. S., "Flow Characteristics of Twin Impinging Jets, *47th AIAA Aerospace Sciences Meeting* ," 2009.

[20] A. Abdel-Fattah, "Numerical and Experimental Study of Turbulent Impinging Twinjet Flow, *Exp Thermal Fluid Science* ," vol. 31, pp. 1061-1072, 2007.

[21] B. J. Watson, "The Radial Spread of a Liquid Jet over a Horizontal Plane, *J. Fluid Mech.*," vol. 20, pp. 48-99, 1964.

[22] Webb, B., Ma, C.F., "Single-phase Liquid Jet Impingement Heat transfer, *Advances in Heat Transfer* ," vol. 26, pp. 105-217, 1995.

[23] Xu, F., Gadala, M. S., "Heat Transfer Behavior in the Impingement Zone Under Circular Water Jet, *Int. J Heat and Mass Transfer* ," vol. 49, pp. 3785-3799, 2006.

[24] Prodanovic, V., Wells, M., "Propagation of the Wetting Front during Jet Impingement Boiling on a Horizontal Flat Surface, ECI, *6th Int. Conference on Boiling Heat Transfer*, Spoleto Italy," 2006.

[25] Wells, M.A., Militzer, M., Prodanovic, V., "Heat Transfer during Run-out Table Cooling Effect of Jet Configuration, *Materials Science and Technology* ," vol. 6, pp. 3680-3690, 2007.

[26] Franco, G.A., Wells, M.A., Militzer, M., "Effect of Nozzle Configuration on Cooling of a Hot Moving Steel Plate, *Canadian Metallurgical Quarterly* ," vol. 48, pp. 197-206, 2009.

[27] Sung, M.K., Mudawar, I., "Single-phase and two-phase heat transfer characteristics of low temperature hybrid microchannel/micro-jet impingement cooling module, *Int Heat Mass Transfer* ," vol. 51, pp. 3882-3895, 2008.

[28] Narumanchi, S., Troshko, A., Bharathan, D., and Hassani, V., "Numerical simulations of nucleate boiling in impinging jets: Applications in power electronics cooling, *Int Heat Mass Transfer* ," vol. 51, pp. 1-12, 2008.

[29] Molana, M., Banooni, S., "Investigation of heat transfer processes involved liquid impingement jets: a review, *Brazilian Journal of Chemical Engineering* ," vol. 30.3, pp. 413-435, 2013.

[30] Stevens, J., Pan, Y., Webb, B. W., "Effect of Nozzle Configuration on Transport the Stagnation Zone of Axisymmetric, Impinging Free-surface Liquid Jets, Part 2 Local Heat Transfer, *J. Heat Transfer* ," vol. 114, pp. 880-886, 1992.

[31] Ochi, T., Nakanishi, S., Kaji, M. and Ishigai, S., "Cooling of a Hot Plate with Impinging of Circular Water Jet, *Multiple Flow and Heat Transfer III*, Part A: Fundamentals, ed. By T.N. Veziroglu, Elsevier Science Publishers B. V., Amsterdam ," pp. 681-761, 1984.

[32] Stevens, J., Webb, B. W., "Local Heat Transfer Coefficients Under an Axisymmetric Single-Phase Liquid Jet, *J. Heat Transfer* ," vol. 113, pp. 71-78, 1991.

[33] Craik, A., Lathman, R., Fawkes, M., Gibbon, P., "The Circular Hydraulic Jump, *J. Fluid Mech.* ," vol. 112, pp. 347-362, 1981.

[34] Bush, J.W., Aristoff, J. M., "The Influence of Surface Tension on the Circular Hydraulic Jump, *J. Fluid Mech.*," vol. 489, pp. 229-238, 2003.

[35] Bush, J.W., Aristoff, J. M., Hosoi, A.E., "An Experimental Investigation on the Stability of the Circular Hydraulic Jump, *J. Fluid Mech*." vol. 588, pp. 33-52, 2006.

[36] Ellegaard, C., Hansen, A. E., Haaning, A., Bohr, T., "Experimental Results on Flow Separation and Transitions in the Circular Hydraulic Jump, *Phys. Scr.*," vol. 67, pp. 105-110, 1996.

[37] Olsson, R. G., Turkdogan, E. T., "Radial Spread of a Liquid Stream on a Horizontal Plate, *Nature (London)* ," vol. 211 (5051), pp. 831-816, 1966.

[38] Yokoi, K., Xiao, F., "Mechanism of Structure Formation in Circular Hydraulic Jumps: numerical studies of strongly deformed free-surface shallow flows, *Physica D* ," vol. 161, pp. 202-219, 2002.

[39] H. Fujimoto, Y. Suzuki, T. Hama and H. Takuda. Flow characteristics of circular liquid jet impinging on a moving surface covered with a water film. *ISIJ Int 51(9)*, pp. 1497-1505. 2011.

[40] Seraj, M. M., Gadala, M. S., "Hydrodynamics of Long Jet Impingement, *Proc. 5th Int. Conference on Advances in Fluid Mechanics*, Italy," vol. VII, pp. 361-370, 2007.

[41] Seraj, M.M., Frigaard, I., Gadala, M.S., " An Investigation of the Hydrodynamics of a Long Water Jet, Submitted to *J Exp Thermal fluid Science*," 2010.

[42] Seraj, M. M., Gadala, M. S., "Experimental Investigation of Wetted Zone of an Impinging Circular Water Jet on a Moving Surface, *ASME Int. Mech. Eng Cong Exposition*, IMECE-39399, Canada," 2010.

[43] Seraj, M. M., Gadala, M. S., "Noncircular Hydraulic Jump on a Moving Surface due to an Impinging Circular Free Surface Jet of Water, *Steel Research Int.* ," 2012.

[44] Kate, R.P., Das, P.K., and Chakraborty, S., "An Experimental Investigation on the Interaction of Hydraulic Jumps Formed by Two Normal Impinging Circular Liquid Jets, *J. Fluid Mech.* ," vol. 590, pp. 355-380, 2007.

[45] Kate, R.P., Das, P.K., and Chakraborty, S., "Effect of Jet Obliquity on Hydraulic Jumps Formed by Impinging Circular Liquid Jet on a Moving Horizontal Plate, *J. Fluids Engineering* ," vol. 131, pp. 034502, 2009.

[46] Ishigai, S., Nakanishi, S., Mizuno, M., Imamura, T., "Heat Transfer of the Impinging Round Water Jet in the Interference Zone of Film Flow along the Wall, Bull. *JSME*," vol. 20, pp. 85-92, 1977.

[47] J. M. M. Barata, "Fountain Flows Produced by Multiple Impinging Jets in a Crossflow, *AIAA J.* ," vol. 34, pp. 2523-2530, 1996.

[48] K. R. Saripalli, "Laser Doppler Velocimeter Measurements in a 3-D Impinging Twin-jet Fountain Flow, *AIAA, AHS, and ASEE, Aircraft Design Systems and Operations Meeting*, Colorado, USA," 1985.

[49] Siclari, M. J., Hill Jr., W. G. Jenkins, R. C., "Stagnation Line and Upwash Formation of Two Impinging Jets, *AIAA J.* ," vol. 19, pp. 1286-1293, 1981.

[50] Cabrita, P. M., Saddington, A. J., Knowles, K., "PIV Measurements in a Twin-Jet STOVL Fountain Flow, *Aeronaut. J.* ," vol. 109, pp. 439-449, 2005.

[51] Pan, Y., Webb, B. W., "Heat Transfer Characteristics of Arrays of Free-Surface Liquid Jets, *J. Heat Transfer*," vol. 117, pp. 878-884, 1995.

[52] Womac, D.J., Incropera, F.P., Ramadhyani, S., "Correlating Equations for Impingement Cooling of Small Heat Sources with Multiple Circular Liquid Jets, *J. Heat Transfer* ," vol. 116, pp. 482-486, 1994.

[53] Slayzak, S. J., Viskanta, R., Incropera, F. P., "Effect of Interactions between adjacent Free Surface Planar Jets on Local Heat Transfer from the Impingement surface, *Int. J. Heat Mass Trans*," vol. 37, pp. 269-282, 1994.

[54] Slayzak, S. J., Viskanta, R., Incropera, F. P., "Effect of Interactions between Adjoining Rows of Circular, Free Surface Jets on Local Heat Transfer from the Impingement surface, *Int. J. Heat Mass Trans*," vol. 116, pp. 88-95, 1994.

[55] Chen, S., Kothari, J., Tseng, A. A., "Cooling of a Moving plate with an Impinging Circular Water Jet, *Exp. Thermal Fluid Science* ," vol. 4, pp. 343-353, 1991.

[56] Han, F., Chen, S.J., Chang, C.C., "Effect of Surface Motion on Liquid Jet Impingement Heat Transfer, *Fundamentals of forced and Mixed convection and transport Phenomena, ASME* ," vol. 180, pp. 73-81, 1991.

[57] Hatta, N., Osakabe, H., "Numerical Modeling for Cooling Process of a Moving Hot Plate by a Laminar Water Curtain, *ISIJ International* ," vol. 29, pp. 919-925, 1989.

[58] Chan P., "Jet Impingement Boiling Heat Transfer at Low Coiling Temperatures, MA. Sc. Thesis, University of British Columbia, BC," 2007.

[59] Jondhale, K., Wells, M.A., Militzer M., Prodanovic, V., "Heat Transfer during Multiple Jet Impingement on the Top Surface of Hot Rolled Steel Strip, *Steel Research Int.* ," vol. 79, pp. 938-946, 2008.

[60] G. Franco, "Boiling Heat Transfer during Cooling of a Hot Moving Steel Plate by Multiple Top Jets, M.A.Sc. Thesis, University of British Columbia, BC," 2008.

[61] H. Maghzian, ""Simulation of hydrodynamics of the jet impingement using arbitrary lagrangian eulerian formulation." PhD Thesis., University of British Columbia, Canada," 2007.

[62] Á T. Hauksson, "Experimental Study of Boiling Heat Transfer during Water Jet Impingement on a Hot Steel Plate, PhD Thesis, University of British Columbia, Canada," 2001.

[63] Q. Meng, ""Experimental study of transient cooling of a hot steel plate by an impinging circular jet" PhD Thesis, University of British Columbia, Canada," 2002.

[64] Fujimoto, H., Lee, Y., Kato, R., Hama, T., and Takuda, H., "Experimental and Numerical Study of Twin Circular Water Jets Impinging on a Moving Thin Film. *ISIJ international*, ," vol. 53, No. 8, pp. 1427-1435, 2013.

[65] P. Phutthavong and I. L. Hassan T., "Unsteady Numerical Investigation of Blade Tip Leakage, Part 1: Time-Averaged Results, *J. Thermophysics Heat Transfer* ," vol. 22, pp. 464-473, 2008.

[66] P. Phutthavong and I. L. Hassan T., "Unsteady Numerical Investigation of Blade Tip Leakage, Part 2: Time-Dependent Parametric Study, *J. Thermophysics Heat Transfer*," vol. 22, pp. 474-484, 2008.

[67] Craft, T.J., Graham, L.J.W., Launder, B.E., "Impinging Jet Studies for Turbulence Model Assessment, Part II: An Examination of the Performance of Four Turbulence Models, *Int. J. Heat Mass Transfer* ," vol. 36, pp. 2685-2697, 1993.

[68] Craft, T.J., Gant, S.E., Gerasimov, A.V., Iacovides, H., Launder, B.E., "Development and Application of Wall-function Treatments for Turbulent Forced and Mixed Convection Flows, *Fluid Dynamics Research*," vol. 38, pp. 127-144, 2006.

[69] Fujimoto, H., Takuda, H, Hatta, N., Viskanta, R., "Numerical Simulation of Transient Cooling of a Hot Solid by an Impinging Free Surface Jet, *Numerical Heat Transfer, Part A*," vol. 36, pp. 767-780, 1999.

[70] Fujimoto, H.,, Dejima, S., "Numerical Analysis and Heat transfer of a Free Surface Circular Jet Impinging onto a Substrate, *ASME Int. Mech. Eng. Cong. Exp.(IMECE2007),* Seattle, USA," vol. 8, pp. 1117-1124, 2007.

[71] A. T. Tong, "A Numerical Study on the Hydrodynamics and Heat Transfer of a Circular Liquid Jet Impinging onto a Substrate, *Numerical Heat Transfer Part A* ," vol. 44, pp. 1-19, 2003.

[72] J. H. Lienhard V, "Heat Transfer by Impingement of Free Surface Liquid Jets, Invited Keynote Paper, *8th National and 7th ISHMT-ASME Heat and Mass Transfer Conf.*, IIT Guwahati, India," 2006.

[73] Sharif, M.A.R., Banerjee, A., "Numerical Analysis of Heat Transfer due to Confined Slot-jet Impingement on a Moving Plate, *Applied Thermal Engineering*," vol. 29, pp. 532-540, 2009.

[74] Huang, P.G., Mujumdar, A.S., Douglas, W.J.M., "Numerical Prediction of Fluid Flow and Heat Transfer Under a Turbulent Impinging Slot Jet with Surface Motion and Crossflow, *ASME Paper 84-WA/HT-33*," 1984.

[75] L. Aldabbagh and A. Mohamad. A three-dimensional numerical simulation of impinging jet arrays on a moving plate. *Int. J. Heat Mass Transfer 52(21),* pp. 4894-4900. 2009.

[76] B. Prasad. Computational flow and heat transfer of multiple circular jets impinging on a flat surface with effusion. *Heat and Mass Transfer 47(9),* pp. 1121-1132. 2011.

[77] H. Chattopadhyay and A. C. Benim. Turbulent heat transfer over a moving surface due to impinging slot jets. *Journal of Heat Transfer 133(10),* pp. 104502. 2011.

[78] Hosseinalipour, S.M., Mujumdar, A.S., "Comparative Evaluation of Different Turbulence Models for Confined Impinging and Opposing Jet Flows, *Numerical Heat Transfer, Part A*," vol. 28, pp. 647-666, 1995.

[79] Wang, S.J., Mujumdar, A.S., "A Comparative Study of Five Low Reynolds Number k-ε Models for Impingement Heat Transfer, *Applied Thermal Engineering*," vol. 25, pp. 31-44, 2005.

[80] Sagot, B., Antonini, G., Christgena, A., Burona, F., "Jet Impingement Heat Transfer on a Flat Plate at a Constant Wall Temperature, *Int. J. of Thermal Sciences*," vol. 47, pp. 1610-1619, 2008.

[81] Xing, Y., Spring, S., Weigand, B., "Experimental and Numerical Investigation of Heat Transfer Characteristics of Inline and Staggered Arrays of Impinging Jets, *J. Heat Transfer* ," vol. 132, pp. 092201, 2010.

[82] Kubacki, S., Dick, E., "Convective Heat Transfer Predictions in an Axisymmetric Jet Impinging onto a Flat Plate using an Improved k-ω Model, *J. Computational Applied Mathematics* ," vol. 234, pp. 2327-2335, 2010.

[83] Tzeng, P.Y., Soong, C.Y., Hsieh, C.D., "Numerical Investigation of Heat Transfer under Confined Impinging Turbulent Slot Jets, *Numerical Heat Transfer, Part A*," vol. 35, pp. 903-924, 1999.

[84] Gradeck, M., Kouachi, A., Dani, A., Arnoult, D., Borean, J.L., "Experimental and Numerical Study of the Hydraulic Jump of an Impinging Jet on a Moving Surface, *Experimental Thermal and Fluid Science* ," vol. 30, pp. 193-201, 2006.

[85] Cho, M.J., Thomas, B.G., Lee, P.J., "Three-dimensional Numerical Study of Impinging Water Jets in Run-out Table Cooling Processes, *Metallurgical and Materials Transactions B* ," vol. 39, pp. 593-602, 2008.

[86] M. Passandideh-Fard, A. R. Teymourtash and M. Khavari. Numerical study of circular hydraulic jump using volume-of-fluid method. *Journal of Fluids Engineering 133(1),* pp. 011401. 2011.

[87] Stark, P., & Fritsching, U., "Simulation of the impinging liquid jet cooling process of a flat plate. *International Journal of Numerical Methods for Heat & Fluid Flow*, ," vol. 25, No. 1, 2015.

[88] Aghahani, M., Eslami, G., & Hadidi, A., "Heat transfer in a turbulent jet impinging on a moving plate considering high plate-to-jet velocity ratios. *Journal of Mechanical Science and Technology*, ," vol. 28, No. 11, pp. 4509-4516, 2014.

[89] Seraj, M. M., Gadala, M. S., "Numerical investigation of impingement flow due to a long axisymmetric water jet, *ASME Int. Mech. Eng Cong Exposition*, IMECE2011-63185, Denver, USA," 2011.

[90] Seraj, M. M., Mahdi, E., Gadala, M. S., "Numerical Assessments of Impingement Flow over Flat Surface due to Single and Twin Circular Long Water Jets. *Transaction on Control and Mechanical Systems
*," vol. 1, No. 7, pp. 290-299, 2013.

[91] ANSYS FLUENT, "12.0 Theory Guide, Chapter 1: Basic Fluid Flow," 2009.

[92] F. M. White, *Fluid Mechanics, Ch. 5.* USA: McGraw-Hill, 1998.

[93] ANSYS FLUENT, "6.3 User's Guide, Chapter 12: Modeling Turbulence," 2006.

[94] D. C. Wilcox, *Turbulence Modeling for CFD.* DCW Industries Inc.: 2004.

[95] Launder, B. E. and Spalding, D. B., "The Numerical Computation of Turbulent Flows, Computer Methods in Applied Mechanics and Engineering," vol. 3, pp. 269-289, 1974.

[96] F. M. White, *Viscous Fluid Flow, Ch. 6.* USA: McGraw-Hill, 1991.

[97] Shih, T.H., Liou, W.W., Shabbir, A., Yang, Z., Zhu, J., "A New k-ε Eddy-viscosity Model for High Reynolds Number Turbulent Flows - Model Development and Validation, *Computers Fluids*," vol. 24, pp. 227-238, 1995.

[98] (7 September 2011). *Law of the Wall*. Available: http://www.cfd-online.com/Wiki/Law_of_the_wall.

[99] Kim, S.-E., Choudhury, D., "A Near-wall Treatment using Wall Functions Sensitized to Pressure Gradient, ASME FED Separated and Complex Flows, ASME 217," pp. 273-279, 1995.

[100] Hirt, C.W., Nichols, B.D., "Volume of Fluid (VOF) Method for the Dynamics of Free Boundaries, *J. of Computational Physics*," vol. 39, pp. 201-225, 1981.

[101] M. M. Seraj, "Hydrodynamics of circular free-surface long water jets in industrial metal cooling, PhD Thesis, University of British Columbia, Canada," 2011.

[102] Ankit Rohatgi, "WebPlotDigitizer, Website: http://arohatgi.info/WebPlotDigitizer," vol. 3.8, May, 2015.

[103] Y. Guo, "Newtonian and viscoelastic liquid jet impingement on a moving surface, MASc. Thesis, University of British Columbia, Canada," 2014.

[104] G. E. G. Sterling, "An experimental study on jet impingement on a very high speed moving surface, MASc Thesis, University of British Columbia, Canada," 2012.

[105] M. M. Seraj and M. S. Gadala. Non-Circular hydraulic jump on a moving surface due to an impinging circular free surface jet of water. *Steel Research International 83(7),* pp. 653-670. 2012.

Appendix A

This appendix includes the main apparatus that were utilized during all the experiments that conducted with a relative industrial scale at a very unique lab (a pilot-scale ROT facility) at the University of British Columbia. The main parts are labeled and described in the same schematic as shown in Figure A.1. Table A.1 illustrates the operating conditions and geometry.

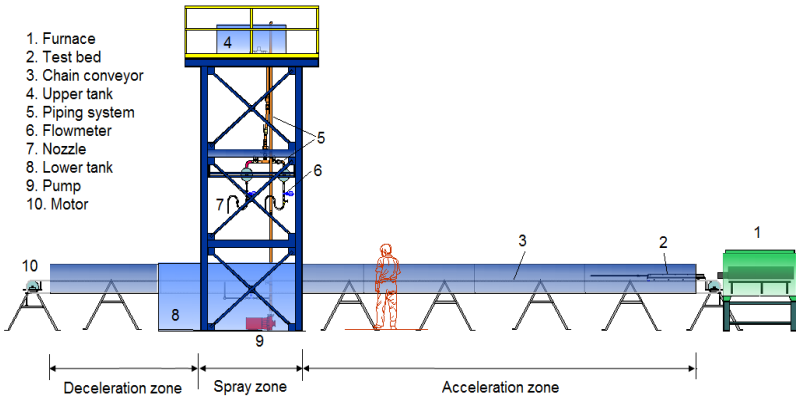

(a) Run-out-Table Layout

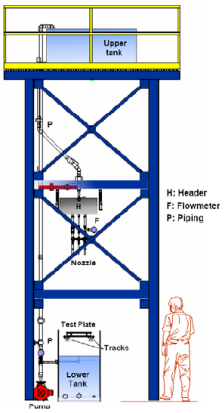

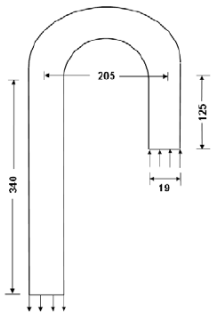

(b) Spray Zone (c) Nozzle Dimensions (mm)

Figure A.1 Schematics of UBC Pilot Scale Apparatus

Table A.1 Geometry and Experimental Operating Parameters

Maximum Flow Rate, *Q* (L/min)	90
Maximum Number of Nozzles	6
Nozzles Configuration	In-line
Type of Nozzle	Round nozzle with 19 mm inner diameter
Nozzle Exit Elevation, *H* (m)	0.5 – 2.0
Plate Velocity, V_p (m/s)	0.3 – 1.5